A WIDEBAND CHANNEL SOUNDER

A Thesis

Presented in Partial Fulfillment of the Requirements for

the Degree Master of Science in the

Graduate School of The Ohio State University

By

José Manuel Albornoz, Ing.

* * * * *

The Ohio State University

2007

Master's Examination Committee:

Dr. Michael P. Fitz, Adviser

Dr. Philip Schniter

Approved by

Adviser

Department of Electrical Engineering

ABSTRACT

The development of wideband mobile communications systems require a better knowledge of the characteristics of the mobile channel as described by its impulse response. Such impulse response can be modelled as a tapped delay line with unknown delays, amplitudes and phases associated with each tap. In order to obtain satisfactory estimates of these parameters a wideband channel sounder is required. In this thesis we examine the factors that determine the performance of such a system and develop a channel estimation algorithm that provides multipath resolution capabilities that are significantly better than the reciprocal of the transmission bandwidth. An experimental sounding system operating in the ISM band with a bandwidth of 1.56 MHz was built and tested; this system was used to conduct channel soundings on OSU's central campus.

A WIDEBAND CHANNEL SOUNDER

By

José Manuel Albornoz, M.S.

The Ohio State University, 2007

Dr. Michael P. Fitz, Adviser

The development of wideband mobile communications systems require a better knowledge of the characteristics of the mobile channel as described by its impulse response. Such impulse response can be modelled as a tapped delay line with unknown delays, amplitudes and phases associated with each tap. In order to obtain satisfactory estimates of these parameters a wideband channel sounder is required. In this thesis we examine the factors that determine the performance of such a system and develop a channel estimation algorithm that provides multipath resolution capabilities that are significantly better than the reciprocal of the transmission bandwidth. An experimental sounding system operating in the ISM band with a bandwidth of 1.56 MHz was built and tested; this system was used to conduct channel soundings on OSU's central campus.

In memory of Lola

...lege, lege, relege, ora, labora et invenies...

ACKNOWLEDGMENTS

I want to express my gratitude to my adviser, Dr. Michael P. Fitz for his support and guidance through my stay at the I.P.S. Wireless Laboratory. I also want to thank Dr. Philip Schniter for the many valuable observations and suggestions provided throughout the course of my research. Thanks also to Mr. Karthik Balasubramanian, Mr. Siddarth D'Silva, Mr. Shengchao Li and Mr. David Browne for their kind help with hardware issues.

VITA

May 23, 1962	Born - Caracas, Venezuela
1980-1984	Ensign, Venezuelan Navy Venezuelan Naval Academy, Vargas, Venezuela
1985-1990	B.S. Electronic Engineering, Universidad Simón Bolivar, Caracas, Venezuela
1991-present	Lecturer, Escuela de Ingenieria Eléctrica, Universidad de Los Andes, Mérida, Venezuela
1999-2001	Fulbright Fellow, The Ohio State University, Columbus, Ohio, USA

FIELDS OF STUDY

Major Field: Electrical Engineering

Studies in Wireless Communications: Dr. Michael P. Fitz

TABLE OF CONTENTS

Page

LIST OF FIGURES

CHAPTER 1

INTRODUCTION

1.1 Multipath Radio Channels

A major requisite in the design of any wideband digital mobile radio system is an adequate characterization of the radio channel. Due to obstructions such as ground irregularities, buildings, vehicles or vegetation we seldom have a direct line of sight between receiver and transmitter, and in this situation the propagation of electromagnetic waves is dominated by mechanisms such as diffraction, scattering and reflection. In this scenario the transmitted wave interacts with obstructions and surface irregularities creating a continuum of scattered partial waves. Therefore the received signal is the superposition of many copies of the original transmitted signal with different time delays, amplitudes and phases. In addition, due to relative motion between transmitter and receiver, each received wave experiences a Doppler shift ν, thereby generating random frequency modulation of the total received signal. All this phenomena give rise to a highly complex, time varying *multipath transmission channel* which depends on the specific properties of the transmission environment.

A multipath radio channel can be modelled as a time-varying linear filter, and thus it is formally described by its impulse response. The received signal $y(t)$ is thus given by the convolution of the transmitted signal $x(t)$ with the time-varying channel

impulse response $h(t, \tau)$

$$y(t) = \int_{-\infty}^{t} x(t)h(t, \tau)d\tau \tag{1.1}$$

The time variation of $h(t, \tau)$ depends on the relative motion between transmitter and receiver, the wavelength of the carrier and the nature of the scattering process. The time-varying impulse response $h(t, \tau)$ provides a completely general model for a mobile wireless channel, synthesizing the relation between a specific propagation environment and its influence on the received signal. However several simplifications of this general model are possible. If the maximum Doppler shift ν_{max} is much less than the inverse of the maximum delay τ_{max} in the channel (which is normally the case), then the channel is said to be *separable* [1], and $h(t, \tau) \approx h_t(\tau)$. If we further assume that signals in different paths are uncorrelated, we can express the channel impulse response as $h(t, \tau) \approx \sum_p h_p(t)\delta(t - \tau_p)$. For most purposes the response of the channel outside a certain signal bandwidth is irrelevant, and thus the channel can be sampled leading to the *tapped delay line model* [2]:

$$h_b(t, \tau) = \sum_{p=0}^{P-1} a_p(t) \exp\left\{j[2\pi f_c \tau_p(t) + \phi(t, \tau_p(t))]\right\} \delta(\tau - \tau_p(t)) \tag{1.2}$$

In this particular model $h_b(t, \tau)$ represents the equivalent baseband impulse response of the channel, $a_p(t)$ represents the real amplitudes associated with each multipath component and $\tau_p(t)$ represents the relative delay or *excess delay* of each component as compared to that of the first arriving one. The phase term $2\pi f_c \tau_p(t) + \phi(t, \tau_p)$ represents phase shift due to free space propagation of the p^{th} multipath component, plus any additional phase shifts that may be encountered in the channel. P is the total number of multipath components and $\delta(\cdot)$ is the unit impulse function. Notice that the amplitude, phase and delay of each multipath component can experience

temporal variations due to the motion of the receiver, and that there are only P possible values of the excess delay $\tau_p(t)$. This particular model implies discrete scatterers and a geometrical optics approximation.

It is convenient to discretize the range of possible multipath delays into $P-1$ *delay bins*, each bin having a delay width equal to $\tau_{p+1} - \tau_p$. If we define $\tau_0 = 0$ for the first signal arriving at the receiver, $\tau_1 = \Delta\tau$ and $\tau_p = p\Delta\tau$ we will have P equally spaced multipath components, and any number of signals received within the pth delay bin will be represented by a single multipath component with excess delay τ_p. The delay bin width $\Delta\tau$ determines the resolution of the model, and it can be shown that the useful frequency span of the model is $\frac{1}{2\Delta\tau}$. Under this assumption The available transmission bandwidth B sets an upper bound for the resolution of structures in the impulse response of the channel. Due to this limited bandwidth each of the arriving multipath components represented as $c_p\delta(\tau - \tau_p(t))$ are smeared and superposed, and therefore it is not possible to resolve each single path in the impulse response (notice that here we have used c_p to represent the complex amplitude associated to each channel tap). In this situation the inverse of the transmission bandwidth B is greater than the minimum time delay difference between paths, and the channel is referred to as a narrowband channel. If, on the other hand B^{-1} is comparable or smaller than the time delay differences between paths, the achievable resolution is far better and detailed structures in the channel impulse response can be observed; we are then dealing with a wideband channel.

1.2 The Need for Channel Sounding

In order to have a satisfactory channel characterization, the amplitudes, phase shifts and delays associated with each multipath component in the channel model represented by (1.2) must be determined. In view of the multitude of possible propagation environments, a deterministic modelling of these parameters is not feasible. The observed characteristics of mobile radio channels lead to the conclusion that their behavior is non-stationary [3], and in practice characterization proves extremely difficult unless stationarity is assumed over short distances of travel or short intervals of time. Assuming stationarity over a small time or distance interval, the channel impulse response described by (1.2) can be simplified to yield

$$h_b(\tau) = \sum_{p=0}^{P-1} a_p \exp(j\theta_p)\delta(\tau - \tau_p) \tag{1.3}$$

In the above expression we have used θ_p to represent $2\pi f_c \tau_p + \phi(\tau_p)$. Our objective is then to obtain estimates of the amplitudes, phases and delays in this simplified model; once we have several "snapshots" of these estimates they can be averaged to derive a statistical description of the radio channel in parametrized form [4]. In this way all possible channel configurations can be reduced into a small number of classes described by a few parameters. From a systems engineering standpoint, this information allows the evaluation of modulation schemes, allowable data rates, diversity techniques, coding strategies and equalization techniques; whereas from the standpoint of radio propagation modelling such information allows to relate multipath phenomena to local conditions, making possible a classification in terms of several propagation environments (rural, urban, suburban, hilly, etc.).

In view of the preceding discussion, it is clear that field surveys are essential to determine the parameters that describe the wireless channel impulse response. Such surveys require a channel measurement system or *channel sounder*. In this thesis we examine the factors that determine the performance of such a system, suggest channel estimation strategies, and present the results of the design and construction of a channel sounder.

1.3 Outline of the Thesis

After this introductory presentation, the architecture of a channel sounder and the factors that affect its performance are discussed in Chapter 2. In Chapter 3 we examine estimation strategies for channel sounding in the presence of noise and present simulation results for a channel estimation algorithm. Chapter 4 documents the development of an experimental wideband channel sounder, presents an evaluation of its performance and shows results of actual channel soundings performed on OSU's central campus. Chapter 5 offers conclusions, suggests improvements and analyzes future trends.

CHAPTER 2

CHANNEL SOUNDING ARCHITECTURES

2.1 A Basic Channel Sounder

As mentioned in the preceding Chapter, a channel sounder is a device that allows estimation of the parameters associated with the impulse response of a radio channel, namely the number of multipath components and their associated amplitudes, phases and delays. In its simplest form a channel sounder can be nothing more that a bistatic pulsed radar that transmits a repetitive pulse of width T_{bb} seconds and uses a receiver with a wide bandpass filter, as shown in Fig. 2.1. The received signal is then amplified, detected with an envelope detector, acquired and stored. The minimum resolvable delay between multipath components is equal to the probing pulse width T_{bb}, while the repetition rate T_{REP} determines the maximum unambiguous excess delay that can be resolved [3]. The pulse repetition rate must be fast enough to allow observation of the time-varying response of individual propagation paths, while the time interval between pulses must be long enough to ensure that all multipath signals have decayed between successive pulses. This type of system gives an immediate measurement of the square of the channel impulse response convolved with the probing pulse; however it is subject to interference and noise due to the wide bandpass filter required for

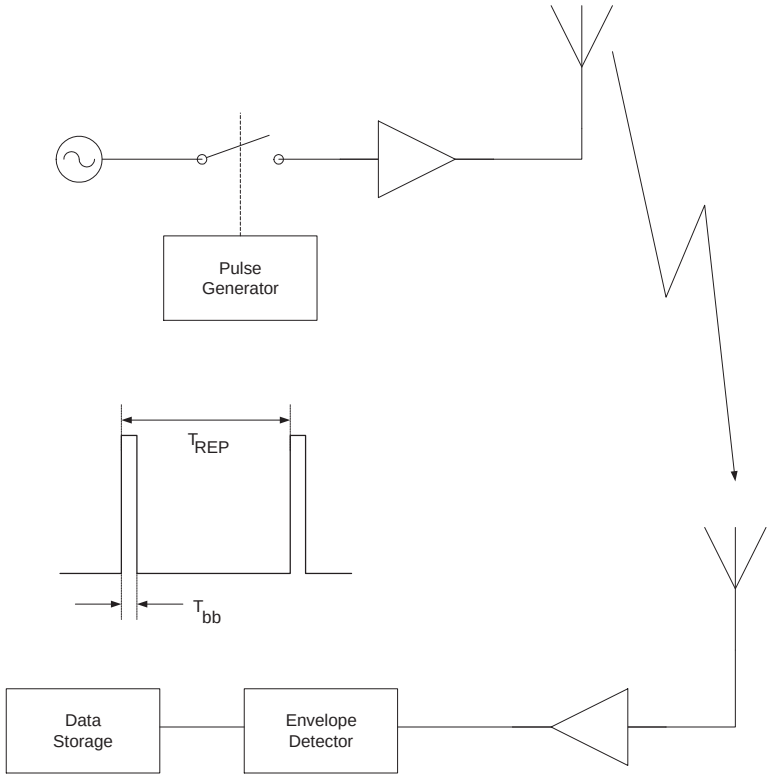

Figure 2.1: Block diagram of a simple channel sounder

multipath delay resolution; besides, the transmitted signal must have a high peak-to-mean power ratio to provide adequate detection of weak multipath components. No information about the phases of the multipath components can be obtained in this type of system due to the use of an envelope detector.

2.2 A Better Sounding Technique

A better technique for channel sounding makes use of the fact that the impulse response of a linear system can be determined by feeding white noise to it [5]. For a linear system the crosscorrelation function between input $X(t)$ and output $Y(t)$ is

defined by

$$R_{XY}(\tau) = \mathbf{E}[X(t)Y(t+\tau)] = \mathbf{E}[X(t)\int_0^\infty X(t+\tau-\lambda)h(\lambda)d\lambda] \tag{2.1}$$

Since $X(t)$ is not a function of λ it may be moved inside the integral and then the expectation may also be moved inside

$$R_{XY}(\tau) = \int_0^\infty \mathbf{E}[X(t)X(t+\tau-\lambda)]h(\lambda)d\lambda = \int_0^\infty R_X(\tau-\lambda)h(\lambda)d\lambda \tag{2.2}$$

If $X(t)$ is white noise its autocorrelation function $R_X(\tau)$ will be $\sigma_X^2\delta(\tau)$, thus (2.2) becomes

$$R_{XY}(\tau) = \int_0^\infty \sigma_X^2\delta(\tau-\lambda)h(\lambda)d\lambda = \sigma_X^2 h(\tau) \tag{2.3}$$

It is the above result that leads to an improved procedure for measuring the impulse response of a radio channel. In practice the noise signal which is being fed to the channel must be known at the receiver, and therefore experimental systems employ deterministic waveforms with noiselike characteristics. The most widely known type of such waveforms are maximal-length pseudo-random binary sequences, alternatively known as pseudo-noise (PN) m-sequences. This type of sequences were traditionally generated using shift registers together with appropriate logic [1].

A particularly important characteristic of a PN sequence is its periodic autocorrelation. The autocorrelation of a PN m-sequence has a single, very sharp peak at the zero shift point; this property allows detection of each multipath component as the received signal in a channel sounder is correlated with the transmitted PN sequence. One method of performing correlation of the received multipath signal with the originally transmitted PN sequence is to use a matched filter in the receiver, in what

[1]The period of a PN sequence produced by a linear feedback shift register with m stages cannot exceed $2^m - 1$; if the period of a particular sequence is exactly $2^m - 1$ such sequence is called a *maximal-length-sequence* or *m-sequence*.

is known as the *convolution matched-filter technique* (CMF). Consider the channel model given by (1.3)

$$h_b(\tau) = \sum_{p=0}^{P-1} a_p \exp(j\theta_p)\delta(\tau - \tau_p)$$

Let's assume now that a PN m-sequence $s(t)$ is used to sound the channel. The received signal $y(t)$ will be the superposition of several attenuated, phase shifted, and delayed copies of $s(t)$

$$\begin{aligned} y(t) = \int_{-\infty}^{\infty} s(\lambda)h(t-\lambda)d\lambda &= \int_{-\infty}^{\infty} s(\lambda) \sum_{p=0}^{P-1} a_p \exp(j\theta_p)\delta(t-\tau_p-\lambda)d\lambda \\ &= \sum_{p=0}^{P-1} a_p \exp(j\theta_p)s(t-\tau_p) \end{aligned} \tag{2.4}$$

The impulse response of the matched filter in the receiver is given by

$$h_{MF}(\tau) = s(-\tau) \tag{2.5}$$

and therefore its output $r(t)$ will be

$$\begin{aligned} r(t) = \int_{-\infty}^{\infty} y(\lambda)h_{MF}(t-\lambda)d\lambda &= \int_{-\infty}^{\infty} \sum_{p=0}^{P-1} a_p \exp(j\theta_p)s(\lambda-\tau_p)s(\lambda-t)d\lambda \\ &= \sum_{p=0}^{P-1} a_p \exp(j\theta_p) \int_{-\infty}^{\infty} s(\lambda-\tau_p)s(\lambda-t)d\lambda \\ &= \sum_{p=0}^{P-1} a_p \exp(j\theta_p) \int_{-\infty}^{\infty} s(z+t-\tau_p)s(z)dz \\ &= \sum_{p=0}^{P-1} a_p \exp(j\theta_p)R_s(t-\tau_p) \end{aligned}$$

where $R_s(\tau)$ represents the autocorrelation of the PN m-sequence $s(t)$ at a shift τ. Then the output of the matched filter will be composed of P attenuated, phase shifted and delayed copies of the autocorrelation function $R_s(\tau_p)$. With this technique the minimum resolvable delay is limited by the width of the autocorrelation peak, which

equals twice the chip period T_c for a PN sequence constructed with rectangular chips. For any other chip waveform the width of the autocorrelation peak T_w will set the limit for the achievable delay resolution.

A possible architecture for a CMF sounder is shown in Figs. 2.2 and 2.3. A PN m-sequence is generated, upconverted and amplified at the transmitter. At the receiver the received multipath signal is bandlimited, downconverted and sampled. This digital IF signal is coherently demodulated into I and Q components which are acquired and stored for posterior off-line processing. The matched filtering of the received signal as well as the detection and estimation algorithms are performed off-line, allowing for complex processing that would be hard to implement in real time.

The particular sounder architecture proposed in this thesis is based in an optimization technique for the estimation of the multipath delays τ_p [14] that does not require matched filtering of the received signal; however, the matched filter output is used as an aid in the estimation process. The smallest time delay difference that can be resolved by this technique is not limited by the width of the correlation peak of the sounding sequence as in the case of the CMF sounder.

2.3 Design Trade-offs

In a practical channel sounder there are certain design trade-offs that must be taken into account. Frequently, an improvement in the accuracy with which a certain channel parameter is determined may cause a degradation in another. We now take a closer look at these trade-offs [3].

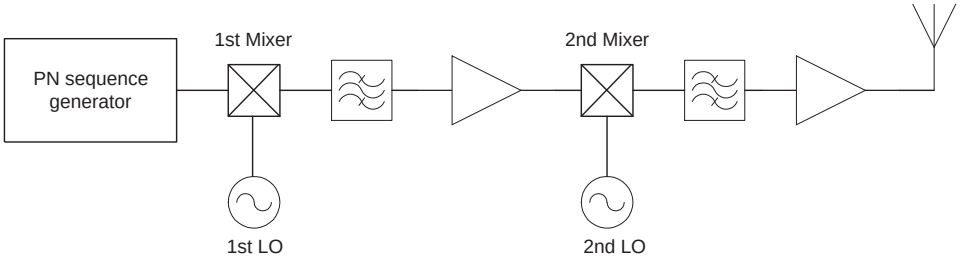

Figure 2.2: Architecture of a CMF sounder transmitter.

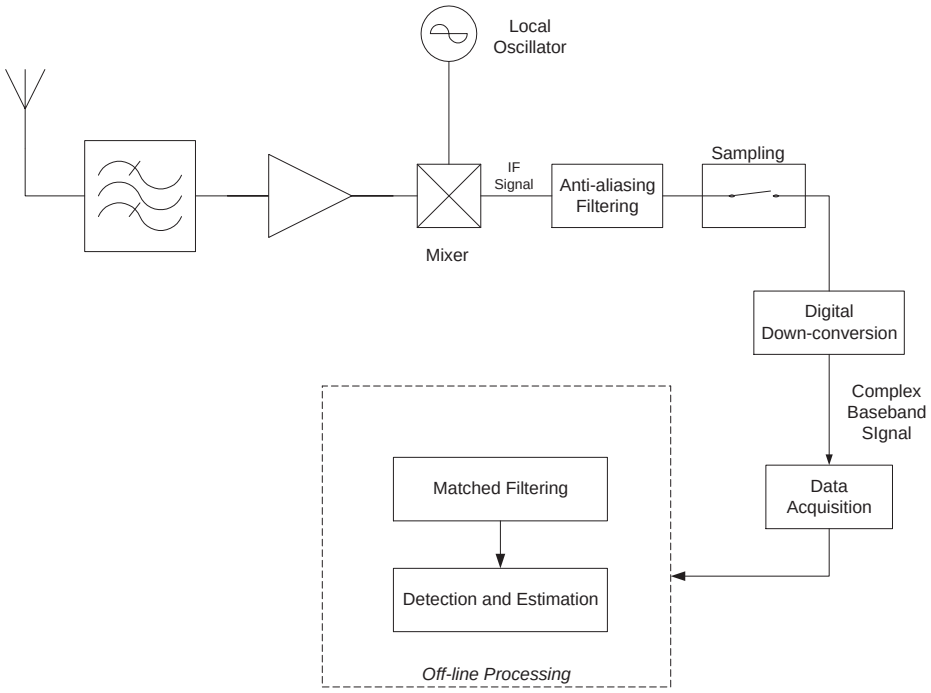

Figure 2.3: Architecture of a CMF sounder receiver.

2.3.1 Dynamic Range

The dynamic range requirements depend on the difference between the largest and smallest amplitudes of the received multipath components. For a PN sequence sounder the dynamic range is a function of the number of chips $N_c = 2^m - 1$ of the PN m-sequence, and equals $20 \log_{10}(N_c)$. For example, if a 30 db dynamic range is required, the PN sequence must be at least 31 chips long.

2.3.2 Multipath Resolution

The ability to resolve multipath components can be divided into *spatial resolution* and *maximum unambiguous path-delay resolution*. Spatial resolution is a measure of the minimum discernible path length difference between multipath components, and is a function of the minimum resolvable time delay difference, which in a CMF sounder is limited by the chip period T_c and the chip waveform. The smallest chip period that can be used is limited by the speed of the available hardware. The final choice of chip period will depend upon the desired bandwidth and the location in which measurements are to be performed, e.g. a high resolution may be required in an indoor study in which scatterers are very close together, while a much lower resolution would probably suffice for a study in a mountainous area. The maximum unambiguous path-delay resolution is a function of the period N_c of the PN m-sequence, and it must be sufficiently long to ensure that no multipath signals are detectable after this time.

2.3.3 Doppler Shift Resolution

The maximum Doppler-shift experienced by a mobile receiver moving with velocity v is

$$\nu_{max} = \frac{v f_c}{c} \tag{2.6}$$

where c is the speed of electromagnetic waves in free space and f_c is the frequency of a wave arriving at the receiver. The maximum Doppler-shift that can be measured using a CMF sounder depends on the rate at which the channel measurements are made, as determined by the period $N_c T_c$ of the sounding signal [3]:

$$\nu_{max} = \frac{1}{2N_c T_c} \tag{2.7}$$

Comparing (2.6) and (2.7) gives

$$v = \frac{c}{2N_c T_c f_c} \tag{2.8}$$

From this last equation we can see that for fixed T_c and f_c, v is inversely proportional to N_c. Thus, while doubling N_c would be advantageous in resolving long time delays and improving dynamic range, it would also mean that the mobile speed would have to be cut in half to allow for a similar Doppler-shift resolution.

2.3.4 Accuracy of Frequency Standards

In order to perform coherent demodulation it is necessary to have identical frequency standards at both transmitter and receiver. Small frequency differences between these standards will produce a slow frequency offset in the received signal that, if not corrected, will degrade amplitude and phase estimation in the proposed sounding scheme. This effect also determines the smallest Doppler-shift that can

be unambiguously resolved by the receiver. The amount of frequency offset can be estimated and compensated by post-processing of the received signal.

2.3.5 Phase Noise in Signal Sources

All practical signal sources exhibit random perturbations in amplitude and phase. The amplitude variation is usually very small and can be neglected, while the phase modulation leads to a degradation in system performance. The effect of phase noise in a CMF channel sounder is to induce random amplitude variations in the quadrature signal components. The presence of this jitter will degrade the performance of the amplitude and phase estimation; besides it will cause a slight broadening of the measured Doppler spectral components. If the phase variation is slow enough it can be estimated and compensated by appropriate post-processing of the received signal.

2.4 Bandlimited Sounding Signals

Due to legal and technical reasons, the spectrum of a sounding signal must be restricted to a certain transmission bandwidth B, which is a function of the desired delay bin resolution. The objective of a channel sounding system is to perform measurements of the impulse response of the wireless channel; and under the assumption of AWGN the optimum sounding signal should have a uniform power distribution over B. One simple approach to this problem is to generate a sounding signal by convolving the PN sequence with a pulse shape having the desired frequency response. An example of this procedure is shown in Fig. 2.4, which shows part of the the original PN sequence, a bandlimited chip waveform and the normalized spectrum of the resulting bandlimited sounding signal.

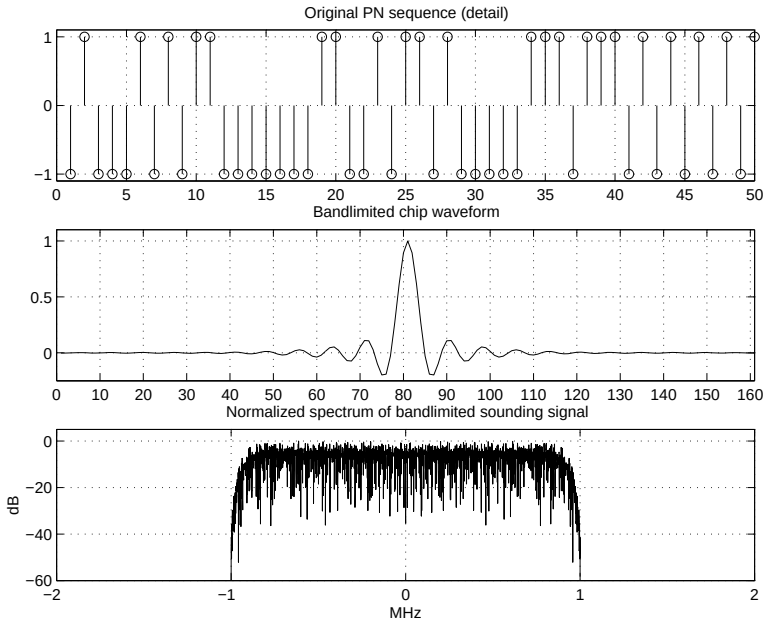

Figure 2.4: Original PN sequence, chip waveform and spectrum of bandlimited sounding signal generated from them.

If only real signals are considered the resulting sounding sequences are not optimal since they possess non-constant time-domain envelopes that may give rise to non-linear products after the final amplification stage, thus producing a signal spectrum which is not uniform within the bandwidth of interest. By using complex sounding signals and by adjusting the phases of its discrete spectral components through optimization techniques an optimal signal can be generated with an uniform envelope. Moreover, this signal can be pre-distorted to take into account the non-linearities of the final power amplifier [6] [7].

CHAPTER 3

ESTIMATION STRATEGIES FOR CHANNEL SOUNDING

We now turn our attention to the problem of extracting the channel parameters from the signal received by the channel sounder. Our objective is to obtain estimates of the amplitudes, phases, delays and number of multipath components arriving at the receiver. The received signal will be invariably contaminated by noise, and therefore some form of estimation algorithm is needed in order to extract the relevant channel parameters. We will show how amplitude and phase estimates can be readily obtained once estimates for the multipath delays are available. A delay estimation technique that overcomes the delay resolution limitations of the conventional CMF sounder is presented and evaluated.

3.1 The Problem

A PN m-sequence $\{d(i)\}_{i=1}^{L}$ and a waveform with chip duration T_c is used to generate a real sounding signal $s(t)$:

$$s(t) = \sum_{i=1}^{L} d(i)u(t - iT_c) \tag{3.1}$$

In the above expression $u(t)$ denotes the chip waveform while L represents the number of chips. The received signal will be the superposition of several attenuated, phase-shifted and delayed copies of the transmitted sounding signal, contaminated by what we will assume to be complex additive white Gaussian noise, $W(t)$, with spectral power density N_0. The complex baseband received signal is then

$$Y(t) = \sum_{p=0}^{P-1} a_p e^{j\theta_p} s(t - \tau_p) + W(t);\ \tau_p \in [\tau_{min}, \infty) \tag{3.2}$$

where a_p, θ_p and τ_p are the amplitudes, phases and delays associated with each multipath component, while P is the total number of paths considered. For the time being we will assume that P is known. Assuming $u(t)$ has an energy spectrum that is ideally bandlimited the received signal can be filtered to reduce the noise and sampled at a rate $\frac{1}{T_s}$, yielding the representation

$$Y_k = \sum_{p=0}^{P-1} a_p e^{j\theta_p} s_k(\tau_p) + N_k \tag{3.3}$$

Here we have used $s_k(\tau_p)$ to represent the sampled version of the delayed sounding signal as described by $s(kT_s - \tau_p)$; the filtered and sampled noise is in turn represented by $N(t)$ and $N_k = N(kT_s)$ respectively. The samples of this received signal are contained in a vector $\underline{Y} = \{Y_k\}_{k=1}^{M}$, where M is the number of samples considered. Assuming ideal Nyquist filters for the sampling rate $\frac{1}{T_s}$, N_k will be a complex white Gaussian noise sequence with variance $2\sigma^2 = \frac{N_o}{T_s}$. Under these conditions the joint pdf for the sample vector $\underline{Y}$ is

$$p(\underline{Y}/\underline{\Theta}) = \prod_{k=1}^{M} p_k(Y_k/\underline{\Theta}) \tag{3.4}$$

The parameter vector $\underline{\Theta} = [\underline{\tau}\ \underline{\theta}\ \underline{a}]^T$ represents the concatenation of three vectors of length P each containing the delays, phases and amplitudes associated with the P

multipath components. For each individual sample Y_k we have

$$p_k(Y_k/\underline{\Theta}) = \frac{1}{2\pi\sigma^2}\exp\left\{-\frac{1}{2\sigma^2}\left|Y_k - \sum_{p=0}^{P-1} a_p e^{j\theta_p} s_k(\tau_p)\right|^2\right\} \tag{3.5}$$

The resulting joint pdf for $\underline{Y}$ is

$$p(\underline{Y}/\underline{\Theta}) = \frac{1}{(2\pi\sigma^2)^M}\exp\left\{-\frac{1}{2\sigma^2}\sum_{k=1}^{M}\left|Y_k - \sum_{p=0}^{P-1} a_p e^{j\theta_p} s_k(\tau_p)\right|^2\right\} \tag{3.6}$$

Having no *a priori* information about the statistical structure of $\underline{\Theta}$, we will consider ML estimates. We are then interested in finding solutions to

$$\underline{\widehat{\Theta}} = \arg\min_{\underline{\Theta}}\left\{\sum_{k=1}^{M}\left|Y_k - \sum_{p=0}^{P-1} a_p e^{j\theta_p} s_k(\tau_p)\right|^2\right\} \tag{3.7}$$

This last expression can be rewritten as

$$\begin{aligned}\underline{\widehat{\Theta}} &= \arg\min_{\underline{\Theta}}\left\{\sum_{k=1}^{M}\left\{|Y_k|^2 - 2\Re\left[Y_k\sum_{p=0}^{P-1} a_p e^{-j\theta_p} s_k(\tau_p)\right] + \left|\sum_{p=0}^{P-1} a_p e^{j\theta_p} s_k(\tau_p)\right|^2\right\}\right\} \\ &= \arg\max_{\underline{\Theta}}\left\{\sum_{k=1}^{M}\left\{2\Re\left[Y_k\sum_{p=0}^{P-1} a_p e^{-j\theta_p} s_k(\tau_p)\right] - \left|\sum_{p=0}^{P-1} a_p e^{j\theta_p} s_k(\tau_p)\right|^2\right\}\right\}\end{aligned} \tag{3.8}$$

We have discarded the term containing $|Y_k|^2$ as it does not depend on the parameter vector $\underline{\Theta}$.

3.2 A General Formulation

The necessary and sufficient conditions to have a maximum in the likelihood function (3.8) are formally given by

$$\frac{d}{d\underline{\Theta}}\log p(\underline{Y}/\underline{\Theta}) = \underline{0} \tag{3.9}$$

$$\frac{d}{d\underline{\Theta}}\left(\frac{d}{d\underline{\Theta}}\log p(\underline{Y}/\underline{\Theta})\right)^T \text{ is negative definite} \tag{3.10}$$

By solving these expressions for $\underline{\Theta}$ we will find joint estimates of the delays and complex amplitudes associated to each path. Equation (3.9) represents the gradient of the likelihood function; each of its elements is given by

$$\sum_{k=1}^{M}\left\{\frac{\partial}{\partial\theta_p}\left\{2\Re\left[Y_k\sum_{q=0}^{P-1}a_q e^{-j\theta_q}s_k(\tau_q)\right]-\left|\sum_{q=0}^{P-1}a_q e^{j\theta_q}s_k(\tau_q)\right|^2\right\}\right\}=0 \tag{3.11}$$

$$\sum_{k=1}^{M}\left\{\frac{\partial}{\partial a_p}\left\{2\Re\left[Y_k\sum_{q=0}^{P-1}a_q e^{-j\theta_q}s_k(\tau_q)\right]-\left|\sum_{q=0}^{P-1}a_q e^{j\theta_q}s_k(\tau_q)\right|^2\right\}\right\}=0 \tag{3.12}$$

$$\sum_{k=1}^{M}\left\{\frac{\partial}{\partial\tau_p}\left\{2\Re\left[Y_k\sum_{q=0}^{P-1}a_q e^{-j\theta_q}s_k(\tau_q)\right]-\left|\sum_{q=0}^{P-1}a_q e^{j\theta_q}s_k(\tau_q)\right|^2\right\}\right\}=0 \tag{3.13}$$

Equation(3.10) represents a constraint on the Hessian matrix of the likelihood function. This Hessian matrix $\mathbf{H}$ is given by

$$\mathbf{H}=\begin{bmatrix} H_{\theta_{pp}} & H_{\theta_p a_q} & H_{\theta_p\tau_q} \\ H_{a_p\theta_q} & H_{a_{pp}} & H_{a_p\tau_q} \\ H_{\tau_p\theta_q} & H_{\tau_p a_q} & H_{\tau_{pp}} \end{bmatrix}$$

The elements of $\mathbf{H}$ are then

$$H_{\theta_{pp}}=\sum_{k=1}^{M}\left\{\frac{\partial^2}{\partial\theta_p^2}\left\{2\Re\left[Y_k\sum_{q=0}^{P-1}a_q e^{-j\theta_q}s_k(\tau_q)\right]-\left|\sum_{q=0}^{P-1}a_q e^{j\theta_q}s_k(\tau_q)\right|^2\right\}\right\} \tag{3.14}$$

$$H_{\theta_p a_q}=\sum_{k=1}^{M}\left\{\frac{\partial^2}{\partial\theta_p\partial a_q}\left\{2\Re\left[Y_k\sum_{q=0}^{P-1}a_q e^{-j\theta_q}s_k(\tau_q)\right]-\left|\sum_{q=0}^{P-1}a_q e^{j\theta_q}s_k(\tau_q)\right|^2\right\}\right\} \tag{3.15}$$

$$H_{\theta_p\tau_q}=\sum_{k=1}^{M}\left\{\frac{\partial^2}{\partial\theta_p\partial\tau_q}\left\{2\Re\left[Y_k\sum_{q=0}^{P-1}a_q e^{-j\theta_q}s_k(\tau_q)\right]-\left|\sum_{q=0}^{P-1}a_q e^{j\theta_q}s_k(\tau_q)\right|^2\right\}\right\} \tag{3.16}$$

$$H_{a_p\theta_q} = \sum_{k=1}^{M} \left\{ \frac{\partial^2}{\partial a_p \partial \theta_q} \left\{ 2\Re \left[Y_k \sum_{q=0}^{P-1} a_q e^{-j\theta_q} s_k(\tau_q) \right] - \left| \sum_{q=0}^{P-1} a_q e^{j\theta_q} s_k(\tau_q) \right|^2 \right\} \right\} \tag{3.17}$$

$$H_{a_{pp}} = \sum_{k=1}^{M} \left\{ \frac{\partial^2}{\partial a_p^2} \left\{ 2\Re \left[Y_k \sum_{q=0}^{P-1} a_q e^{-j\theta_q} s_k(\tau_q) \right] - \left| \sum_{q=0}^{P-1} a_q e^{j\theta_q} s_k(\tau_q) \right|^2 \right\} \right\} \tag{3.18}$$

$$H_{a_p\tau_q} = \sum_{k=1}^{M} \left\{ \frac{\partial^2}{\partial a_p \partial \tau_q} \left\{ 2\Re \left[Y_k \sum_{q=0}^{P-1} a_q e^{-j\theta_q} s_k(\tau_q) \right] - \left| \sum_{q=0}^{P-1} a_q e^{j\theta_q} s_k(\tau_q) \right|^2 \right\} \right\} \tag{3.19}$$

$$H_{\tau_p\theta_q} = \sum_{k=1}^{M} \left\{ \frac{\partial^2}{\partial \tau_p \partial \theta_q} \left\{ 2\Re \left[Y_k \sum_{q=0}^{P-1} a_q e^{-j\theta_q} s_k(\tau_q) \right] - \left| \sum_{q=0}^{P-1} a_q e^{j\theta_q} s_k(\tau_q) \right|^2 \right\} \right\} \tag{3.20}$$

$$H_{\tau_p a_q} = \sum_{k=1}^{M} \left\{ \frac{\partial^2}{\partial \tau_p \partial a_q} \left\{ 2\Re \left[Y_k \sum_{q=0}^{P-1} a_q e^{-j\theta_q} s_k(\tau_q) \right] - \left| \sum_{q=0}^{P-1} a_q e^{j\theta_q} s_k(\tau_q) \right|^2 \right\} \right\} \tag{3.21}$$

$$H_{\tau_{pp}} = \sum_{k=1}^{M} \left\{ \frac{\partial^2}{\partial \tau_p^2} \left\{ 2\Re \left[Y_k \sum_{q=0}^{P-1} a_q e^{-j\theta_q} s_k(\tau_q) \right] - \left| \sum_{q=0}^{P-1} a_q e^{j\theta_q} s_k(\tau_q) \right|^2 \right\} \right\} \tag{3.22}$$

Since verifying the definite negativeness of $\mathbf{H}$ appears to be a formidable task, we settle for a less rigorous approach: considering marginal estimates instead. In order to obtain marginal estimates the necessary and sufficient conditions to have a maximum in the likelihood function are

$$\begin{aligned} &\sum_{k=1}^{M} \left\{ \frac{\partial}{\partial \theta_p} \left\{ 2\Re \left[Y_k \sum_{q=0}^{P-1} a_q e^{-j\theta_q} s_k(\tau_q) \right] - \left| \sum_{q=0}^{P-1} a_q e^{j\theta_q} s_k(\tau_q) \right|^2 \right\} \right\} = 0 \\ &\sum_{k=1}^{M} \left\{ \frac{\partial^2}{\partial \theta_p^2} \left\{ 2\Re \left[Y_k \sum_{q=0}^{P-1} a_q e^{-j\theta_q} s_k(\tau_q) \right] - \left| \sum_{q=0}^{P-1} a_q e^{j\theta_q} s_k(\tau_q) \right|^2 \right\} \right\} < 0 \end{aligned} \tag{3.23}$$

$$\sum_{k=1}^{M}\left\{\frac{\partial}{\partial a_p}\left\{2\Re\left[Y_k\sum_{q=0}^{P-1}a_q e^{-j\theta_q}s_k(\tau_q)\right]-\left|\sum_{q=0}^{P-1}a_q e^{j\theta_q}s_k(\tau_q)\right|^2\right\}\right\}=0$$

$$\sum_{k=1}^{M}\left\{\frac{\partial^2}{\partial a_p^2}\left\{2\Re\left[Y_k\sum_{q=0}^{P-1}a_q e^{-j\theta_q}s_k(\tau_q)\right]-\left|\sum_{q=0}^{P-1}a_q e^{j\theta_q}s_k(\tau_q)\right|^2\right\}\right\}<0 \tag{3.24}$$

$$\sum_{k=1}^{M}\left\{\frac{\partial}{\partial \tau_p}\left\{2\Re\left[Y_k\sum_{q=0}^{P-1}a_q e^{-j\theta_q}s_k(\tau_q)\right]-\left|\sum_{q=0}^{P-1}a_q e^{j\theta_q}s_k(\tau_q)\right|^2\right\}\right\}=0$$

$$\sum_{k=1}^{M}\left\{\frac{\partial^2}{\partial \tau_p^2}\left\{2\Re\left[Y_k\sum_{q=0}^{P-1}a_q e^{-j\theta_q}s_k(\tau_q)\right]-\left|\sum_{q=0}^{P-1}a_q e^{j\theta_q}s_k(\tau_q)\right|^2\right\}\right\}<0 \tag{3.25}$$

We must find first and second derivatives with respect to θ_p, a_p and τ_p of (3.8). After performing algebraic operations detailed in Appendix A we arrive at the following expressions which must be satisfied by the ML estimates:

- Phase

$$\Im\left[e^{-j\theta_p}\sum_{k=1}^{M}Y_k s_k(\tau_p)\right]-\Im\left[e^{-j\theta_p}\sum_{r=0}^{P-1}a_r e^{j\theta_r}\sum_{k=1}^{M}s_k(\tau_p)s_k(\tau_r)\right]=0 \tag{3.26}$$

subject to

$$-\Re\left[e^{-j\theta_p}\sum_{k=1}^{M}Y_k s_k(\tau_p)\right]+\Re\left[e^{-j\theta_p}\sum_{r=0}^{P-1}a_r e^{j\theta_r}\sum_{k=1}^{M}s_k(\tau_p)s_k(\tau_r)\right]-a_p\sum_{k=1}^{M}s_k^2(\tau_p)<0 \tag{3.27}$$

- Amplitude

$$\Re\left[e^{-j\theta_p}\sum_{k=1}^{M}Y_k s_k(\tau_p)\right]-\Re\left[e^{-j\theta_p}\sum_{k=1}^{M}a_r e^{j\theta_r}\sum_{k=1}^{M}s_k(\tau_p)s_k(\tau_r)\right]=0 \tag{3.28}$$

subject to

$$-2a_p \sum_{k=1}^{M} S_k^2(\tau_p) < 0$$

which is always true.

- Delay

$$\Re\left[e^{-j\theta_p} \sum_{k=1}^{M} Y_k s_k'(\tau_p)\right] - \Re\left[e^{-j\theta_p} \sum_{r=0}^{P-1} a_r e^{j\theta_r} \sum_{k=1}^{M} s_k(\tau_r) s_k'(\tau_p)\right] = 0 \tag{3.29}$$

subject to

$$\Re\left[e^{-j\theta_p} \sum_{k=1}^{M} Y_k s_k''(\tau_p)\right] + \Re\left[e^{-j\theta_p} \sum_{r=0}^{P-1} a_r e^{j\theta_r} \sum_{k=1}^{M} s_k''(\tau_p) s_k(\tau_r)\right] - a_p \sum_{k=1}^{M} s_k'^2(\tau_p) < 0 \tag{3.30}$$

In the above equations we have assumed that $s(t-\tau_p)$ is differentiable with respect to τ_p so that $s_k'(\tau_k) = \frac{\partial}{\partial \tau_p} s(t-\tau_p)|_{t=kTs}$ and $s_k''(\tau_k) = \frac{\partial^2}{\partial \tau_p^2} s(t-\tau_p)|_{t=kTs}$. From these equations we observe that there is a coupling between different paths through the second terms of (3.26), (3.28) and (3.29). More precisely, different paths are coupled through the autocorrelation of the sounding signal as represented by $\sum_{k=1}^{M} s_k(\tau_p) s_k(\tau_r)$.

3.3 Least Squares Amplitude and Phase Estimates

In this section we will show that if $\underline{\tau}$ is known then the estimates for amplitude and phase greatly simplify. In the previous expressions we observe that if (3.28) is satisfied, (3.27) will be automatically satisfied too, therefore ML amplitude and phases estimates are obtained by solving (3.26) and (3.28):

$$\Re\left[e^{-j\theta_p} \sum_{k=1}^{M} Y_k s_k(\tau_p)\right] - \Re\left[\sum_{r=0}^{P-1} a_r e^{-j(\theta_p-\theta_r)} \sum_{k=1}^{M} s_k(\tau_p) s_k(\tau_r)\right] = 0$$

$$\Im\left[e^{-j\theta_p}\sum_{k=1}^{M}Y_k s_k(\tau_p)\right]-\Im\left[\sum_{r=0}^{P-1}a_r e^{-j(\theta_p-\theta_r)}\sum_{k=1}^{M}s_k(\tau_p)s_k(\tau_r)\right]=0$$

These two expressions can be merged and simplified to yield

$$\sum_{k=1}^{M}Y_k s_k(\tau_p)=\sum_{r=0}^{P-1}a_r e^{j\theta_r}\sum_{k=1}^{M}s_k(\tau_p)s_k(\tau_r) \tag{3.31}$$

As mentioned before, $\sum_{k=1}^{M}s_k(\tau_p)s_k(\tau_r)$ represents the autocorrelation of the sounding signal for a shift $\tau_{rp}=\tau_r-\tau_p$. Representing this autocorrelation as $R_s(\tau_{rp})$ we rewrite (3.31) as

$$\sum_{k=1}^{M}Y_k s_k(\tau_p)=\sum_{r=0}^{P-1}c_r R_s(\tau_{rp}) \tag{3.32}$$

where we have written c_r for $a_r e^{j\theta_r}$. Then for the P paths we will have:

$$\begin{aligned}
\sum_{k=1}^{M}Y_k s_k(\tau_0) &= \sum_{r=0}^{P-1}c_r R_s(\tau_{r0})\\
\sum_{k=1}^{M}Y_k s_k(\tau_1) &= \sum_{r=0}^{P-1}c_r R_s(\tau_{r1})\\
&\vdots\\
\sum_{k=1}^{M}Y_k s_k(\tau_P) &= \sum_{r=0}^{P-1}c_r R_s(\tau_{rP})
\end{aligned} \tag{3.33}$$

This set of equations can be written in matrix form as

$$\mathbf{S}^T(\underline{\tau})\underline{Y}=\mathbf{R}(\underline{\tau})\underline{\widehat{C}} \tag{3.34}$$

where $\mathbf{S}(\underline{\tau})$ is a $M\times P$ observation matrix whose columns are composed of delayed copies of the sounding signal $s_k(\tau_p)$, $\mathbf{R}$ is a $P\times P$ matrix whose ij^{th} element is $R_s(\tau_{ij})$, $\underline{Y}$ is the $M\times 1$ observation vector, and $\underline{\widehat{C}}$ is the $P\times 1$ attenuation vector containing estimates of the true complex amplitudes $\underline{C}=\{c_i\}_{i=0}^{P-1}$ associated with each multipath component. Assuming that $\mathbf{R}$ is invertible we can write

$$\underline{\widehat{C}}=\mathbf{R}^{-1}\mathbf{S}^T\underline{Y} \tag{3.35}$$

where for notational convenience the dependence of $\mathbf{S}$ and $\mathbf{R}$ on $\underline{\tau}$ is understood. Therefore estimates of the complex amplitudes are readily available once estimates of the delays are known. Noting that

$$\mathbf{R} = \mathbf{S}^T\mathbf{S}$$

we may rewrite (3.35) as

$$\underline{\widehat{C}} = (\mathbf{S}^T\mathbf{S})^{-1}\mathbf{S}^T\underline{Y} \tag{3.36}$$

Under this formulation the model for the received signal is then

$$\underline{Y} = \mathbf{S}\underline{C} + \underline{N} \tag{3.37}$$

where the dependence on the delay vector $\underline{\tau}$ is via the observation matrix $\mathbf{S}$.

Equation (3.36) amounts to a least squares estimator of the attenuation vector $\underline{C}$. For large enough data records, this estimator will be optimal in the sense that it will provide unbiased estimates that achieve the Cramér-Rao lower bound [8]. The estimator error variance will depend on the noise power, the length of the the sounding signal and its autocorrelation properties. This variance is minimized when

$$\mathbf{S}^T\mathbf{S} = \alpha\mathbf{I} \tag{3.38}$$

where α is a constant that depends on the length of the sounding sequence and the number of multipath components [11]. This property defines ideal autocorrelation characteristics of the sounding signal, as the diagonal elements of $\mathbf{S}^T\mathbf{S}$ are given by $R_s(\tau_{ij})$, $i \neq j$. The LS estimation error variance can then be minimized by careful design of the sounding signal.

We see how the problem of obtaining estimates of the complex amplitudes associated with each multipath component is reduced to a simple linear problem once the

number P of multipath components and their respective delays are known. Figs. 3.1 to 3.8 show plots for mean estimates and r.m.s. error vs. Cramér-Rao bounds when the estimator described by (3.36) is applied to two different signals, each composed by four equally spaced paths with amplitudes $A1 = A2 = A3 = A4 = 0.5$, and phases $P1 = 0°$, $P2 = 30°$, $P3 = 45°$, $P4 = 60°$. In the first case the time delay between paths was $\Delta = 2$ μs; while in the second case the delay between paths was $\Delta = 0.375$ μs, a delay value smaller than the sampling period of the data (500 ns). It is observed that unbiased estimates that achieve the CRB are obtained in both cases. The estimation error increases whenever Es/N_0 falls below $Es/N_0 = 20$ dB regardless of the time delay difference between paths. The amplitude and phase estimation errors at lower values of Es/N_0 are very small for $\Delta = 2$ μs, while for $\Delta = 0.375$ μs they present a slight increase; nevertheless in both cases these errors are negligible. The derivation of Cramér-Rao bounds in presented in Appendix B. CRBs were found for joint estimation of $\underline{\tau}$ and $\underline{C}$; this represents the worst possible scenario since joint estimation of multiple parameters increases the CRBs with respect to those obtained for marginal estimates [10].

3.4 Delay Estimation

Estimation of the delays associated with a multipath signal is a classical problem that has received a lot of attention. The standard approach is matched filtering [12], in which the received signal is correlated with the transmitted sounding signal $s(t)$. We have already seen how the resolution of this technique is limited by the width T_w of the main lobe of the autocorrelation of the sounding signal. In the presence of multiple paths, looking for the P highest peaks in the matched filter output is suboptimal

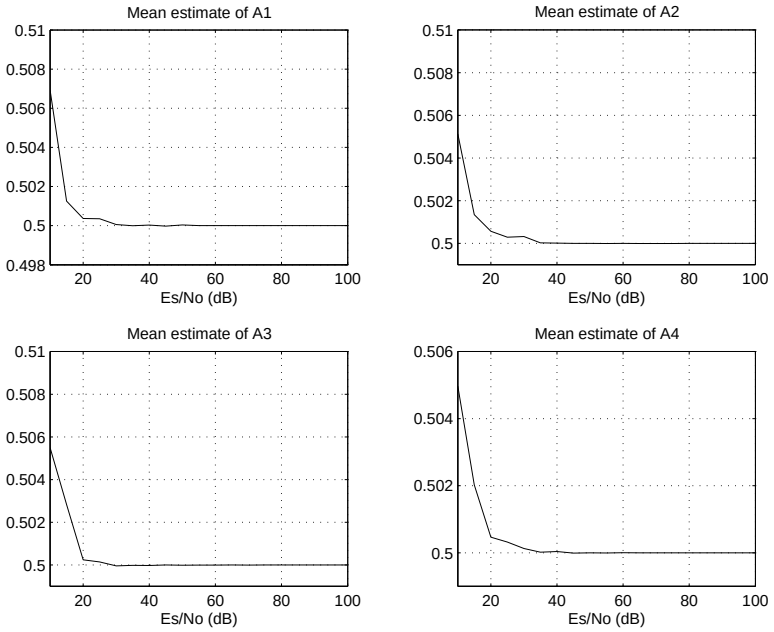

Figure 3.1: Mean amplitude estimates, $\Delta = 2$ μs, 5000 samples.

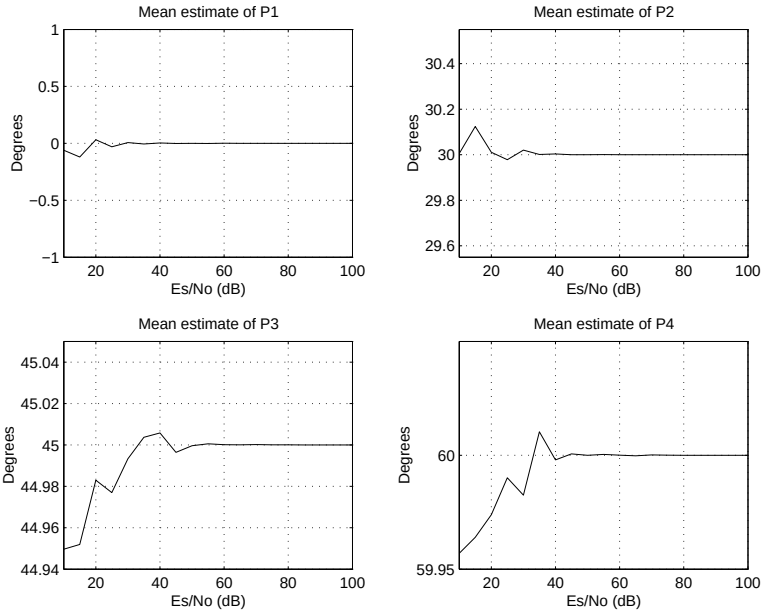

Figure 3.2: Mean phase estimates, $\Delta = 2$ μs, 5000 samples.

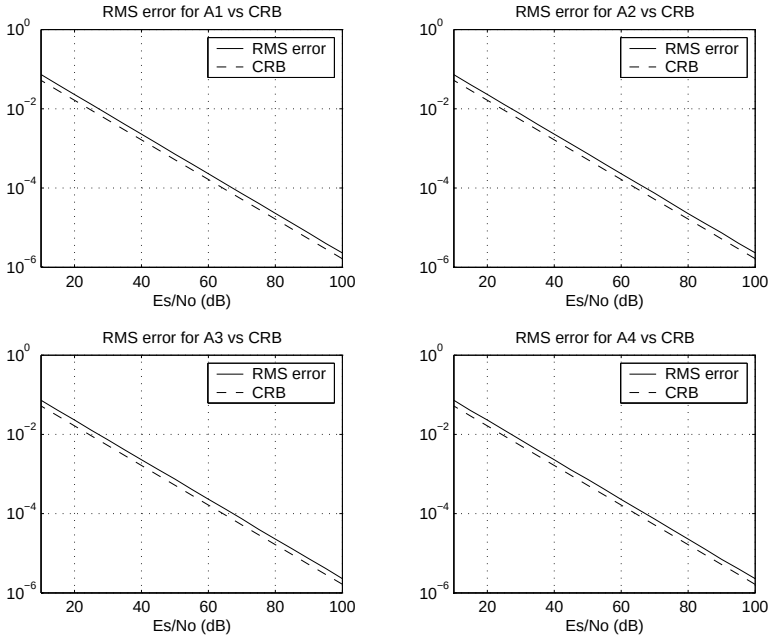

Figure 3.3: Amplitude r.m.s. error vs. CRB, $\Delta = 2$ μs, 5000 samples.

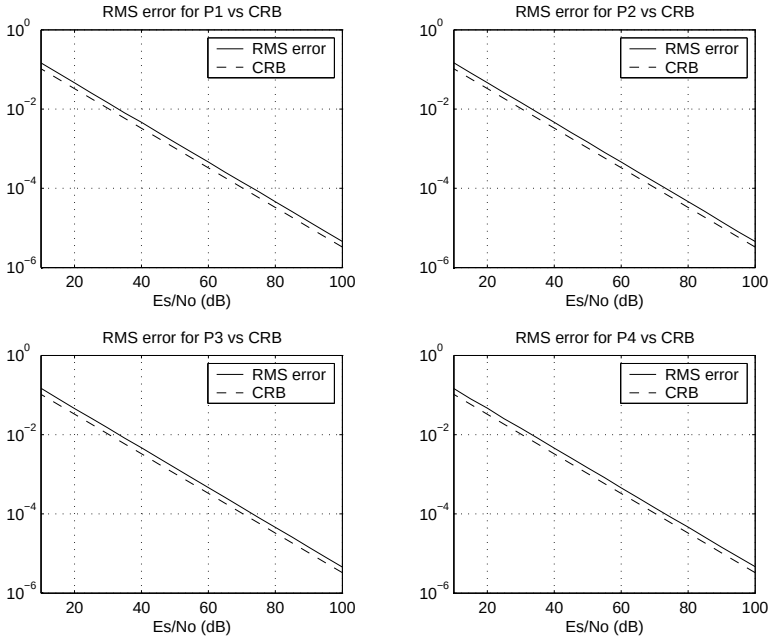

Figure 3.4: Phase r.m.s. error vs. CRB, $\Delta = 2$ μs, 5000 samples.

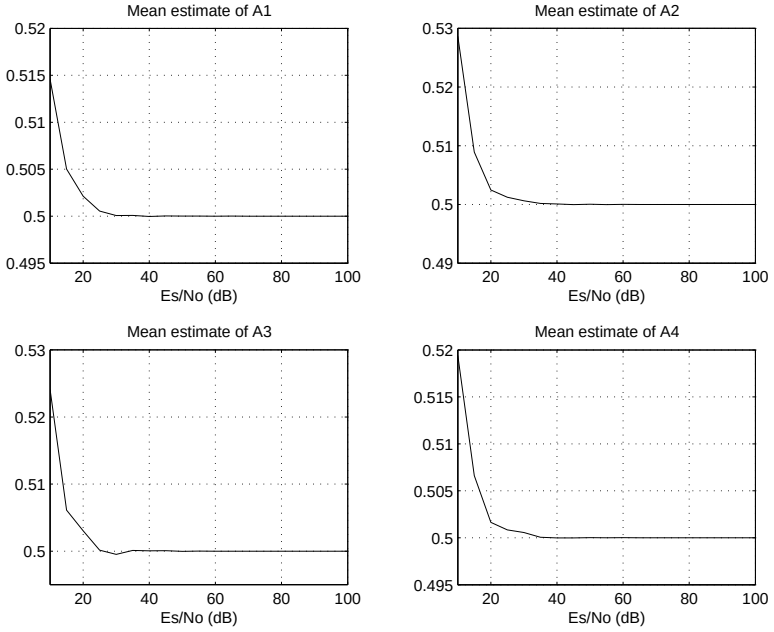

Figure 3.5: Mean amplitude estimates, $\Delta = 0.375$ μs, 5000 samples.

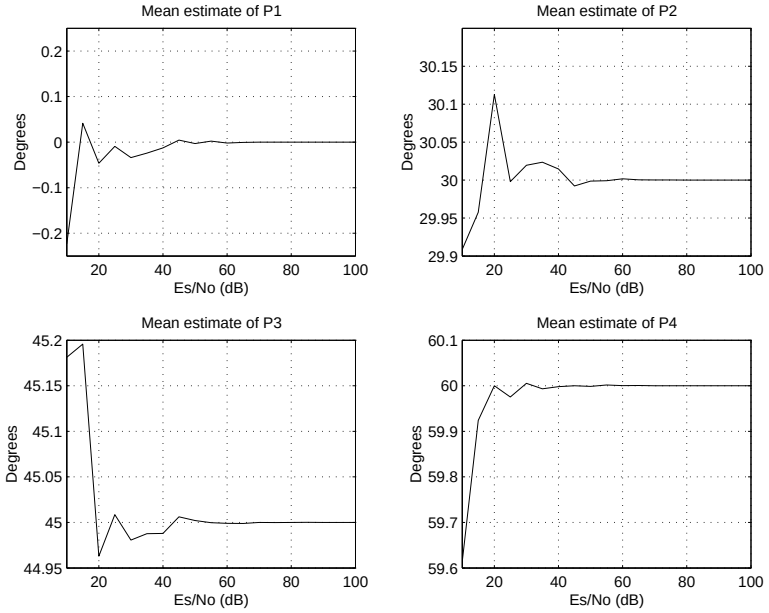

Figure 3.6: Mean phase estimates, $\Delta = 0.375$ μs, 5000 samples.

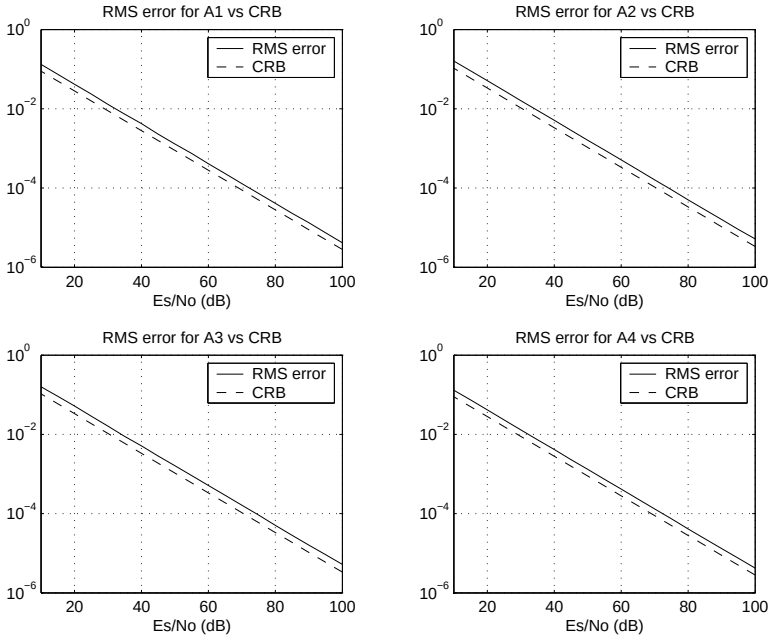

Figure 3.7: Amplitude r.m.s. error vs. CRB, $\Delta = 0.375$ μs, 5000 samples.

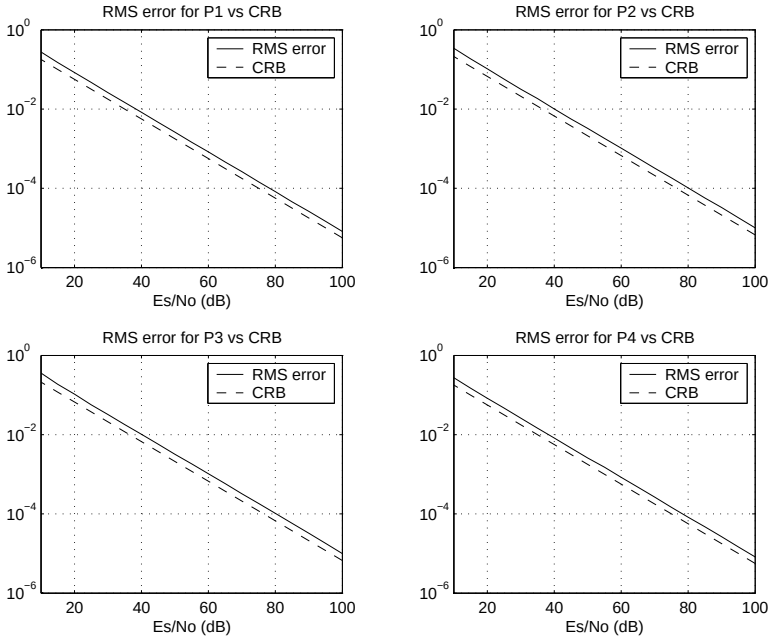

Figure 3.8: Phase r.m.s. error vs. CRB, $\Delta = 0.375$ μs, 5000 samples.

unless the time separation between multipath components is greater or equal than T_w (assuming a reasonable signal-to-noise ratio). Other approaches to this problem aim at minimizing the error between modelled and measured data according to the maximum likelihood criterion. This involves an initialization step which involves performing a multidimensional grid search over an objective function that presents numerous local minima, as Fig. 3.9 shows for a single path case; once a suitable initial estimate is located a gradient search could be performed to find the global minimum in the likelihood function. This method converges to the global minimum only if the initial grid search produces an excellent initial estimate [8]. Variations of this technique such as the expectation maximization method [13] also depend on minimization of the likelihood function using iterative methods and therefore also require a very good initial point. The required computation time can be somewhat reduced by concentrating the search on those points in the vicinity of the peaks in the output of the matched filter [18].

Another limitation of these ML-based methods is that they require a-priori knowledge of the number of multipath components P, as illustrated by (3.29) and (3.30). Maximum likelihood approaches cannot be used to estimate structure parameters such as P since the error function $\| \underline{Y} - \mathbf{S}\underline{C} \|_2^2$ can be made as small as desired by increasing the number of parameters in the channel model. Since the true number of paths P is not known the received signal model must include an additional unknown structure parameter Q:

$$Y(t) = \sum_{q=0}^{Q-1} a_q e^{j\theta_q} s(t - \tau_q) + W(t); \tag{3.39}$$

This adds complexity to our problem since now we must also find an estimate of the number of paths $\underline{P}$. To be consistent in our notation the parameter vector $\underline{\Theta}$ must

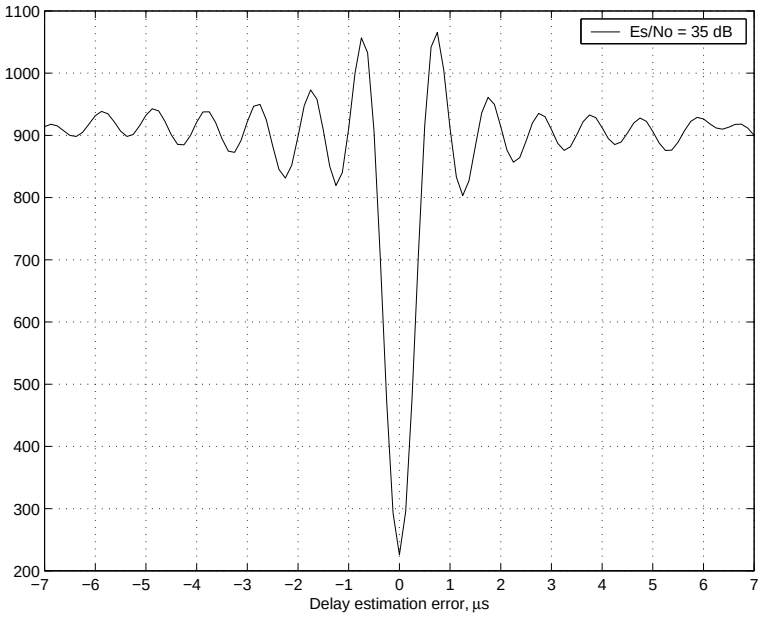

Figure 3.9: Error function for a single path.

now become

$$\underline{\Theta} = [\underline{C}\ \underline{\tau}\ Q]^T$$

The delay estimation approach that will be proposed is in essence a variation of a least squares deconvolution technique. From (3.37) the received signal can be represented as

$$\underline{Y} = \mathbf{S}\underline{C} + \underline{N}$$

In this model the $M \times P$ observation matrix $\mathbf{S}$ depends both on the number of multipath components P and their respective delays as described by the parameter vector $\underline{\tau}$. Estimates of P and $\underline{\tau}$ can then be found by performing a least squares deconvolution operation on

$$\underline{Y} = \mathbf{D}\underline{C} + \underline{N} \tag{3.40}$$

where $\mathbf{D}$ is a $M \times KM$ matrix with Hankel structure whose columns are built from delayed versions of the sounding signal. The i^{th} column of $\mathbf{D}$ is given by $s_k(i\frac{Ts}{K})$ [2], where $\frac{Ts}{K}$ is a fraction of the sampling period determined by the oversampling factor K. $\mathbf{D}$ is denoted the indicator set matrix; its columns form a non-orthogonal base that spans all possible time delay values as quantized by KM delay bins. An estimate of the attenuation vector $\underline{\widehat{C}}$ is then found by solving

$$\underline{\widehat{C}} = \arg\min_{\underline{C}} \left\{ \| \underline{Y} - \mathbf{D}\underline{C} \|_2^2 \right\} \tag{3.41}$$

$\underline{\widehat{C}}$ is now a $KM \times 1$ vector with Q non-zero components grouped into clusters. For very high signal-to-noise ratios this approach produces a vector which has P clearly identifiable non-zero lobes at those positions corresponding to the true delays; each of these lobes represents a delayed replica of the transmitted signal. The time-delay resolution of this method is limited by the sampling rate, the oversampling factor K, the bandwidth of the sounding signal and the available computing power. As an example consider a four path signal described by

$$y(t) = 0.5s(t-1.25) + 0.5e^{j30^\circ}s(t-3.25) + 0.5e^{j45^\circ}s(t-4.0) + 0.5e^{j60^\circ}s(t-5.00)$$

where all the delays have been specified in microseconds. The sounding signal $s(t)$ was a 1023-chip PN sequence bandlimited to 2 MHz . Fig. 3.10 shows the corresponding matched filter output for a signal-to-noise ratio of 25 dB. It can be appreciated that those paths with delays of 3.25 and 4 μs cannot be resolved by observing the output of the matched filter.

Fig. 3.11 show the result of the least squares deconvolution operation on $y(t)$ for signal-to-noise ratios of 100 and 25 dB. For high Es/N_0 the deconvolution operation

[2] According to previous notation this represents $s(kT_s - i\frac{T_s}{K})$

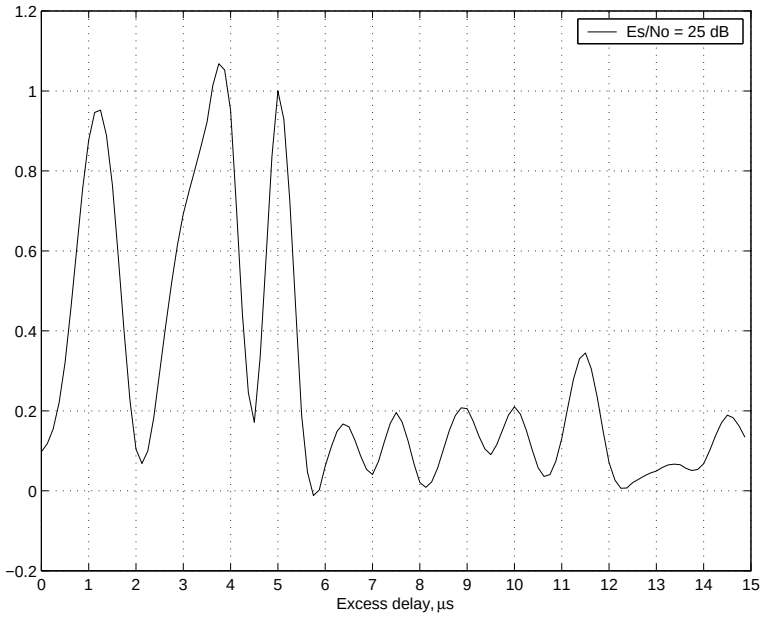

Figure 3.10: Output of matched filter.

produces 4 strongly defined lobes at those positions associated with the true multipath delays. As Es/N_0 decreases the true multipath lobes are hidden among the noise and it is difficult or impossible to find their location within $\underline{\widehat{C}}$.

The performance of the least squares deconvolution method can be substantially improved by adding a penalization term containing the ℓ_1 norm of the attenuation vector $\underline{C}$ [14]:

$$\underline{\widehat{C}} = \arg\min_{\underline{C}} \left\{ \| \underline{Y} - \mathbf{D}\underline{C} \|_2^2 + \lambda \| \underline{C} \|_1 \right\} \tag{3.42}$$

This criterion is equivalent to the following constrained optimization problem:

$$\min \| \underline{C} \|_1 \text{ subject to } \| \underline{Y} - \mathbf{D}\underline{C} \|_2^2 \leq B \tag{3.43}$$

where B represents a constraint on the least squares error and λ is the inverse of the Lagrange multiplier of (3.43). The Lagrange multiplier $\frac{1}{\lambda}$ relates the sensitivity

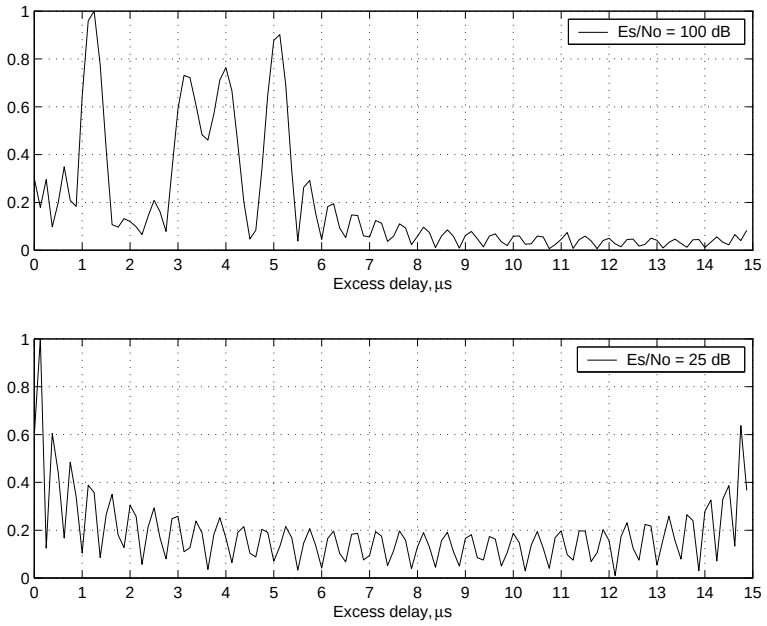

Figure 3.11: Output from least squares deconvolution method.

of the solution to variations in the constraint B [15]. Minimization of the ℓ_1 norm of the attenuation vector $\underline{C}$ leads to a fairly localized solution that can be made sparse by appropriately tuning λ. The optimization problem described by (3.42) has a unique solution that can be obtained using standard programs readily available in a number of mathematical software packages. Since we are only interested in the relative position of each path within $\widehat{\underline{C}}$ we define a new vector $\widehat{\underline{C}}_{mag}$ whose elements are given by

$$\left[\widehat{\underline{C}}_{mag}\right]_i = |C_i| \tag{3.44}$$

Fig. 3.12 shows the result of the modified deconvolution procedure when applied to $y(t)$. The resulting amplitude vector $\widehat{\underline{C}}_{mag}$ is sparse, and for high Es/N_0 the true multipath components are easily identifiable. As Es/N_0 decreases false paths start to appear around the true ones. Once $\widehat{\underline{C}}_{mag}$ is available the time delays associated

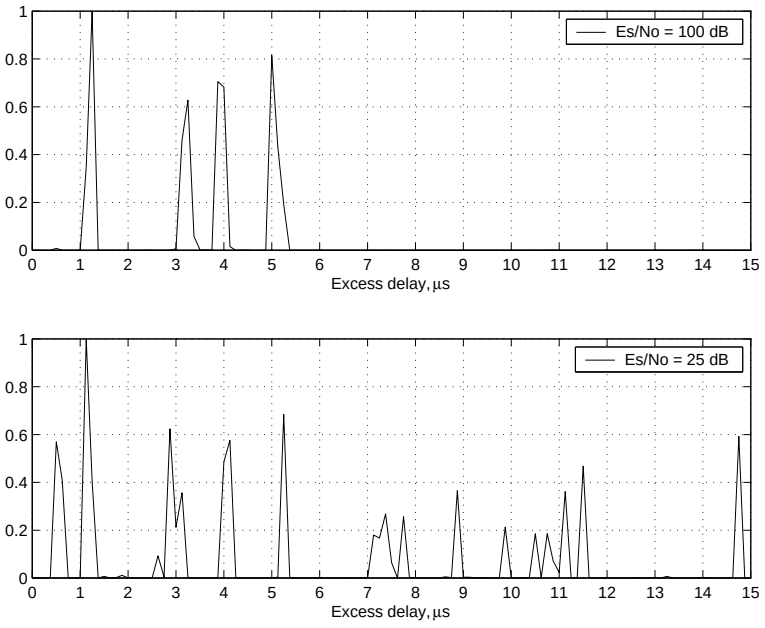

Figure 3.12: Output from modified deconvolution method.

with each path can be used to compute least squares estimates of the corresponding amplitudes and phases.

3.4.1 Tuning of λ

The inclusion of the penalization term in (3.42) produces an amplitude vector $\underline{\widehat{C}}_{mag}$ with optimum sparsity for a certain range of values of the parameter λ. If λ is too small the required sparsity will not be achieved and it will be very difficult to distinguish true paths from false ones, thus degrading the performance of the delay estimation algorithm. If on the other hand λ is too large we run the risk of missing true paths, thereby producing large errors in the subsequent LS estimation step; worse still, we may obtain an empty $\underline{\widehat{C}}_{mag}$. Fig. 3.13 illustrates the differences in $\underline{\widehat{C}}_{mag}$ produced by different values of λ. Lacking additional information about how λ is related to each

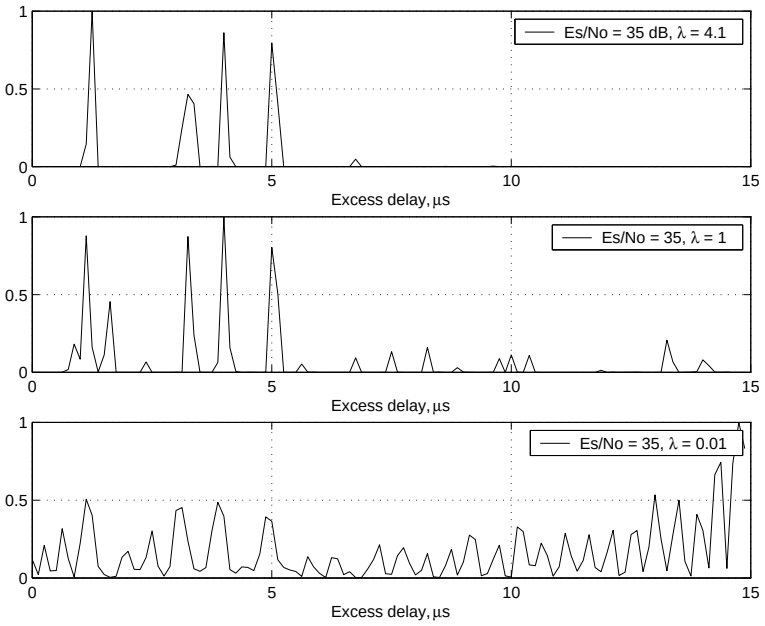

Figure 3.13: Effect of the values of λ in the output of the modified deconvolution step.

particular problem, we must follow a heuristic approach to adjust it. One possible solution is to progressively increase λ until all the elements of $\underline{\widehat{C}}_{mag}$ become zero. Let's denote this particular value λ_{max}. The algorithm is then operated at a value below λ_{max}, ensuring good performance by minimizing the number of spurious paths. Another possible approach would be to tune λ experimentally, selecting the value that produces the smallest number of false paths for a known set of channels.

3.4.2 Eliminating False Replicas

As mentioned before the outcome of the modified deconvolution procedure will be a vector $\underline{\widehat{C}}_{mag}$ that contains a number of elements associated with false paths. A first approach to the problem of discarding false replicas would be to perform thresholding on $\underline{\widehat{C}}_{mag}$.

Another solution is to take advantage of the information provided by the matched filter output about the location of the true paths, as illustrated by Fig. 3.10. Let's denote the output of the matched filter as $\underline{z}$. By interpolating $\underline{z}$ by the oversampling factor K we create a vector $\underline{Z}$ with the same length as $\underline{\widehat{C}}_{mag}$. $\underline{Z}$ can then be used to create a masking vector $\underline{M}$ that allows elimination of a number of false paths. In order to generate $\underline{M}$ the mean value of $\underline{Z}$ is computed and subtracted from $\underline{Z}$ to create another vector $\underline{Z}_{AC}$. Each time $\underline{Z}_{AC}$ goes above a predefined threshold a value of 1 is assigned to the masking vector. Fig. 3.14 illustrates this procedure, showing $\underline{Z}_{AC}$ and the masking vector M generated from it. Figs. 3.15 and 3.16 show such vector is used to suppress false paths. After the masking operation takes place we are left with Q candidate paths.

Another strategy that allows us to discard false paths is the minimum descriptor length criterion (MDL) [9] [16]:

$$\widehat{P} = \arg\min_{Q} \left\{ -\log\left\{p(\underline{Y}/\underline{\Theta}, Q)\right\} + \frac{1}{2} Q \log(M) \right\} \tag{3.45}$$

The MDL criterion enables us to obtain an estimate $\widehat{P}$ of the number of paths out of Q candidates. The MDL criterion performance is asymptotically dependent on the data vector length M [17]; nevertheless for relatively short data records a plot of the MDL values as a function of $\widehat{P}$ shows how the former reaches a plateau once the correct number of paths has been reached, as shown in Fig. 3.17 where the MDL criterion suggests $\widehat{P} = 4$ out of $Q = 5$ candidate paths. For high enough Es/N_0 (or very simple channels) there aren't any ledges in the MDL data and therefore the number of paths associated to the minimum value in the MDL criterion is chosen as an estimate of P; an example of such situation is presented in Fig. 3.18. For low Es/N_0 values extracting $\widehat{P}$ from the MDL data is not a simple task since the resulting

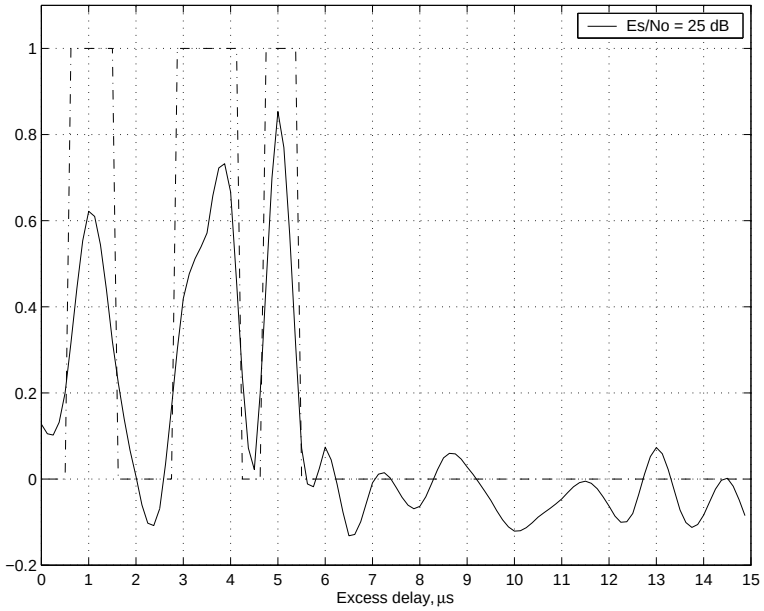

Figure 3.14: Mask generated from $\underline{Z}_{AC}$.

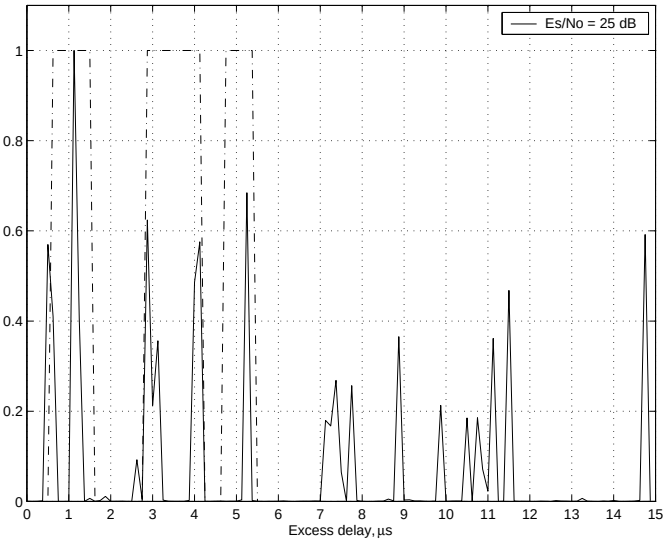

Figure 3.15: Mask on top of modified deconvolution result.

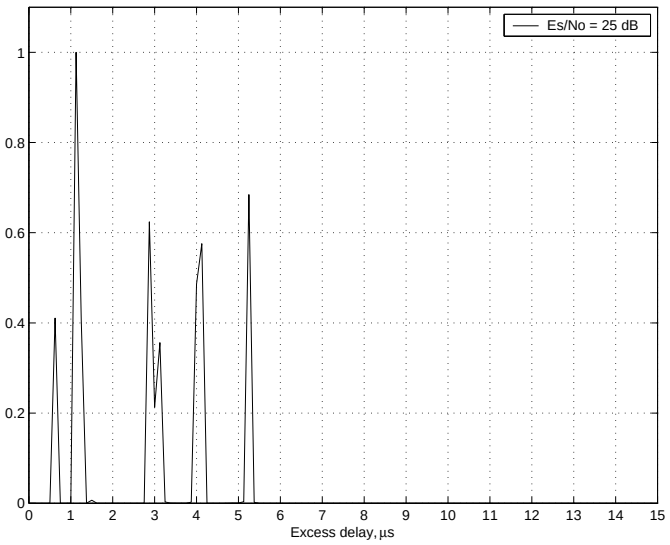

Figure 3.16: Modified deconvolution result after masking.

MDL plot may present several ledges as shown in Fig. 3.19; in such situations the strategy would be to identify that ledge that results in the smallest $\widehat{P}$ (6 paths out of 10 candidates in this particular example).

Once $\widehat{P}$ is available the delay estimation algorithm constructs different versions of the observation matrix $\mathbf{S}$ using the sets of delay estimates resulting from each possible combination of $\widehat{P}$ paths out of Q possible candidates. The error function $\| \underline{Y} - \mathbf{S}\underline{C} \|_2^2$ is computed for each combination, and that particular combination that minimizes the error function is retained as our final delay estimate.

We have already seen how LS estimates of the complex amplitudes associated with each multipath component can be obtained once estimates of their respective delays are available. The LS estimation is a necessary step since the amplitudes obtained from $\underline{\widehat{C}}_{mag}$ are biased due to the penalization term in (3.42). Whenever paths are

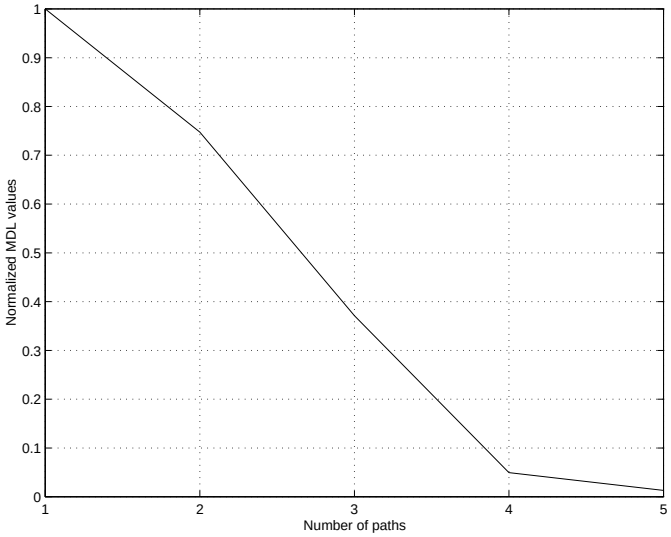

Figure 3.17: An example of an MDL plot.

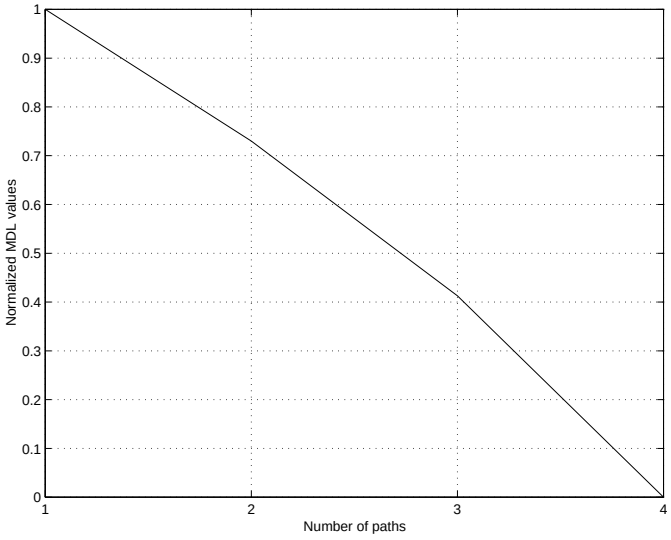

Figure 3.18: An example of an MDL plot for high Es/N_0.

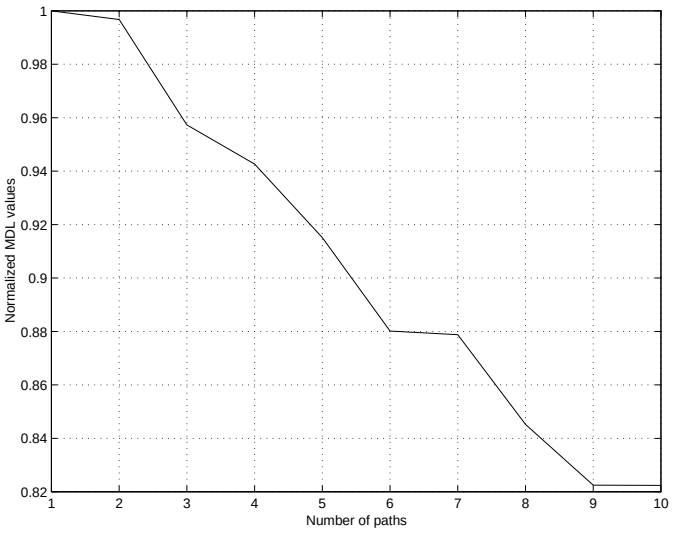

Figure 3.19: MDL plot for low Es/N_0

discarded new LS estimates must be found since the set of delay estimates used to build the observation matrix **S** will change.

The LS estimation strategy makes it difficult to discard a true path since the loss would induce large errors in the resulting estimates. However, a slightly overestimated $\widehat{P}$ is tolerable since for reasonable values of Es/N_0 the false paths will have negligible amplitudes and therefore can be safely discarded.

3.5 Algorithm Simulation

Several simulations were performed taking into account the characteristics of the available hardware and the proposed architecture of the receiver, as shown in Fig. 3.20. A RF front end converts the received signal to a 10.7 MHz IF signal which is sampled at 64 MSPS and fed to a digital receiver. The digital receiver block performs filtering and decimation functions producing a 2 MSPS complex baseband

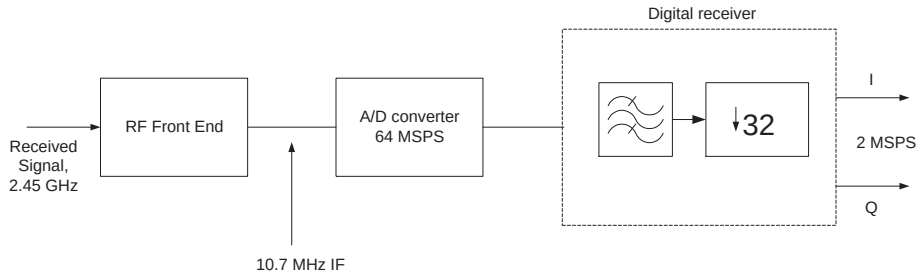

Figure 3.20: Channel sounder receiver architecture.

signal which is acquired and stored for posterior off-line estimation. Figs. 3.21 to 3.25 show a block diagram of the simulation steps; the actual estimation algorithm starts at point S using the I and Q signals from the digital receiver. The steps of the simulation and the estimation algorithm contained within it can be summarized as follows:

- **Multipath signal generation**

  A complex baseband multipath signal is built from a set of specified delays, amplitudes and phases. The amplitudes are normalized such that the sum of their squared amplitudes equals one. This multipath signal signal is generated at a rate corresponding to 64 MSPS, the maximum sampling rate allowed by the digital receiver. Complex white noise is added to the resulting signal to achieve a prescribed Es/N_0 value.

- **Generation of I and Q components**

  The received multipath signal is bandlimited to 2 MHz and decimated by 32. The result is a 2 MSPS I-Q complex baseband signal which is first matched

filtered to the chip waveform, then matched filtered to the sounding signal to generate the masking vector M.

- **Delay Estimation**
  - The modified least squares deconvolution procedure is applied to the I and Q signals. The corresponding $\underline{\widehat{C}}_{mag}$ is computed and stored in vector $C0$.
  - False and/or weak paths are suppressed by thresholding and by applying the masking vector $\underline{M}$ to $C0$.
  - A peak search is performed on $C0$; the positions of the peaks are stored in vector $pos0$. Each of these positions is associated with a time delay value.
  - An observation matrix **S1** is constructed using the delays estimates stored in $pos0$ to perform a first LS amplitude estimation; the complex amplitudes resulting from this step are stored in vector $C1$.
  - A peak search is performed on $C1$; the positions of the peaks are stored in vector $pos1$.
  - The union of the sets in $pos0$ and $pos1$ is stored in $pos2$; that is $pos2 = pos0 \cup pos1$. This is a necessary step since for low Es/N_0 there are peaks in $C0$ that do not appear in $C1$ and vice versa. The contents of $pos2$ represents a set of Q candidate delay estimates.
  - Another observation matrix **S2** is constructed using the delay estimates in $pos2$ to perform a second LS amplitude estimation; the resulting estimates are stored in vector $C2$.
  - The Q amplitude estimates in $C2$ are sorted in descending order. Their corresponding positions are stored in vector $pos3$.

- The MDL criterion is computed using the time delays values associated with the Q candidate paths stored in $pos3$. An estimate $\widehat{P}$ of the true number of paths is obtained by finding ledges in the MDL data.
- All possible combinations of $\widehat{P}$ path delays out of the Q candidates in $pos2$ are used to construct observation matrices $\mathbf{S_i}$; the squared error function $\| \underline{Y} - \mathbf{S_i}\underline{C} \|_2^2$ associated with each of these matrices is computed and the particular combination with produces the smallest squared error is retained as the final set of path delays.

- LS **Estimation of Amplitudes and Phases**

  A final LS estimation of amplitudes and phases is performed using the delay estimates obtained in the previous step.

3.5.1 Algorithm Performance

Simulations were run to assess the performance of our channel estimation algorithm. In a first simulation a 4-path channel with amplitudes $A1 = A2 = A3 = A4 = 0.5$ and phases $P1 = 0°$, $P2 = 30°$, $P3 = 45°$ and $P4 = 60°$ was used. The time delay between paths was $\Delta = 2$ μs. The algorithm used a 600-samples segment of the received signal; this length was chosen in order to have a reasonable execution time of about 20 minutes per run. The length of the channel estimate was set to 8 μs; while an oversampling factor of $K = 4$ produced a time delay resolution of 125 ns.

Figs. 3.26 to 3.31 show the mean delay, amplitude and phase estimates together with their corresponding RMS error vs. CRB plots. Notice that the delay RMS error vs. CRB plots are presented in linear scale due to the quantization imposed by the

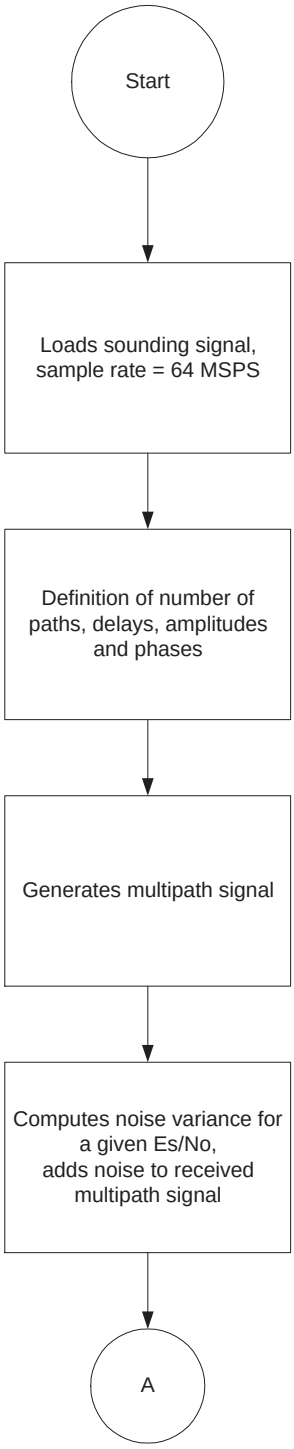

Figure 3.21: Block diagram of simulation.

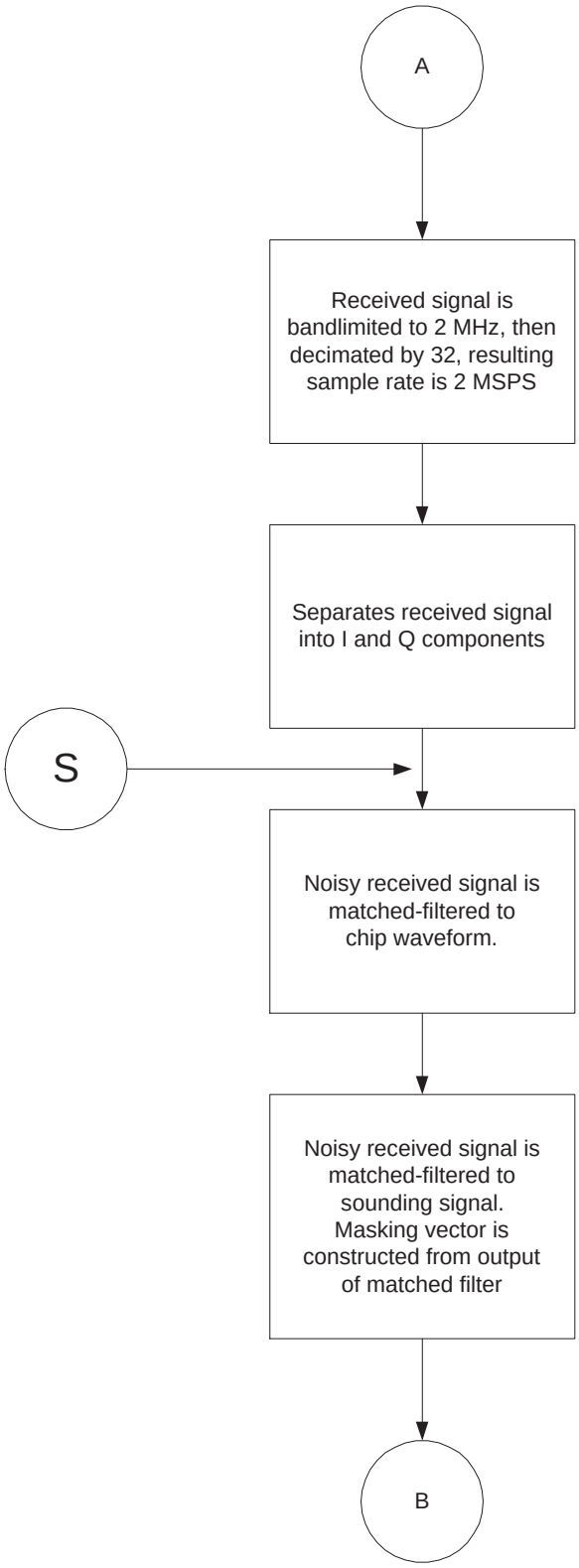

Figure 3.22: Block diagram of simulation (continued).

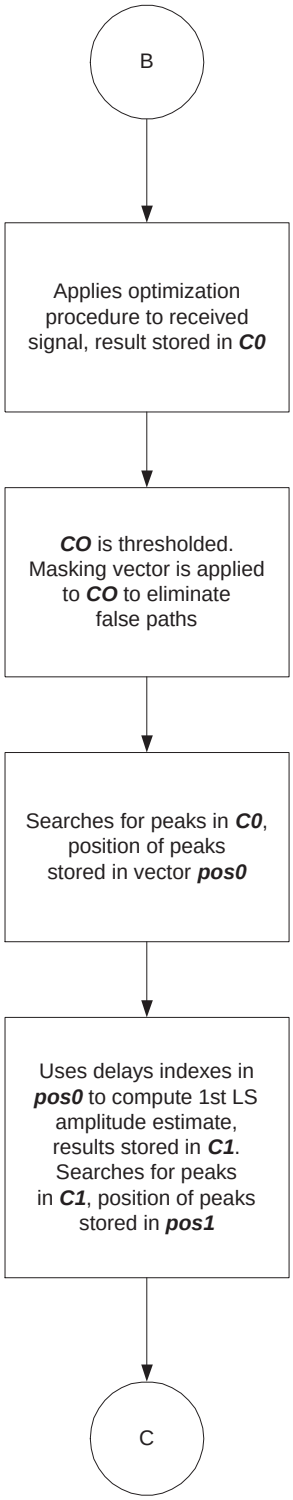

Figure 3.23: Block diagram of simulation (continued).

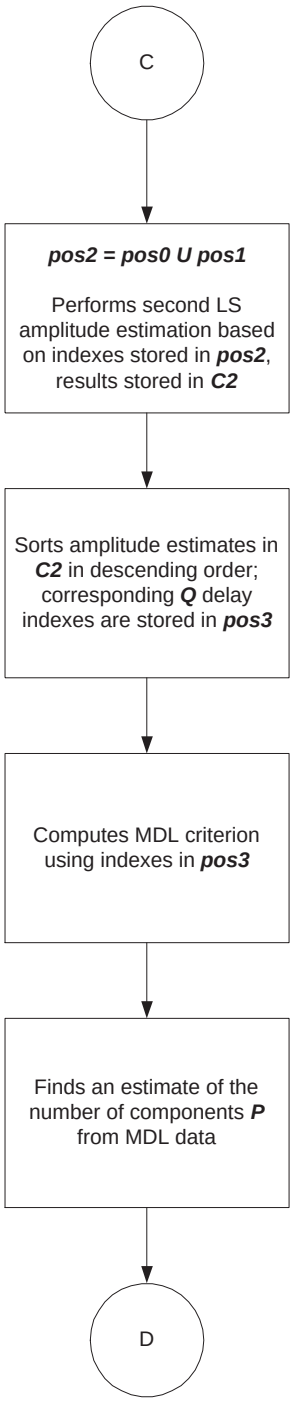

Figure 3.24: Block diagram of simulation (continued).

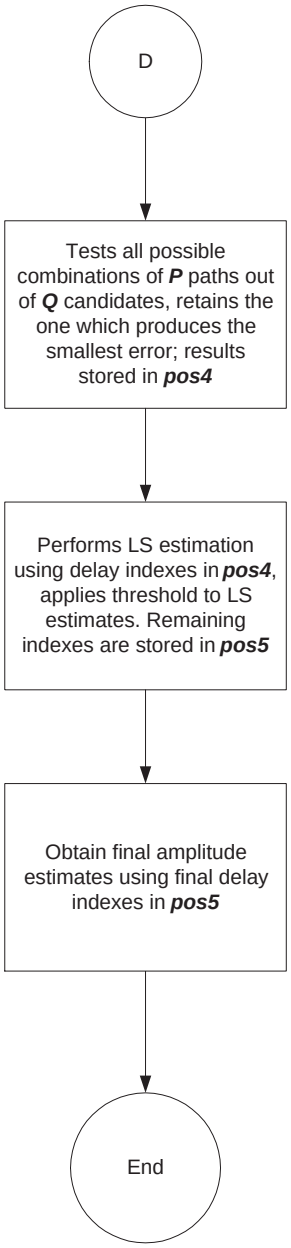

Figure 3.25: Block diagram of simulation (continued).

width of the delay bin; the RMS error falls below the CRB once the former becomes smaller that the width of the delay bin. It is observed that the algorithm produces unbiased estimates that approach the CRB and that the estimation error becomes important below 20 dB Es/N_0.

In order to assess the performance of the algorithm for varying path separations a simple channel containing two paths with equal amplitude and different relative delays was simulated and estimated for several values of Es/N_0. The first of these paths had a delay of 0.25 μs, while the delay of the second path was changed from 0.375 μs to 0.75 μs in steps of 0.125 μs (the width of the delay bins). The Es/N_0 values used in this simulation were 20, 30, 40 and 50 dB. Plots of the resulting channel taps are presented in Figs. 3.32 to 3.35. These plots show how paths separated by one single delay bin cannot be consistently resolved by the algorithm even for relatively high Es/N_0 values. As the path separation is increased reliable results are obtained for Es/N_0 above or equal 40 dB. This value was taken as the minimum signal-to-noise value necessary for reliable channel estimation.

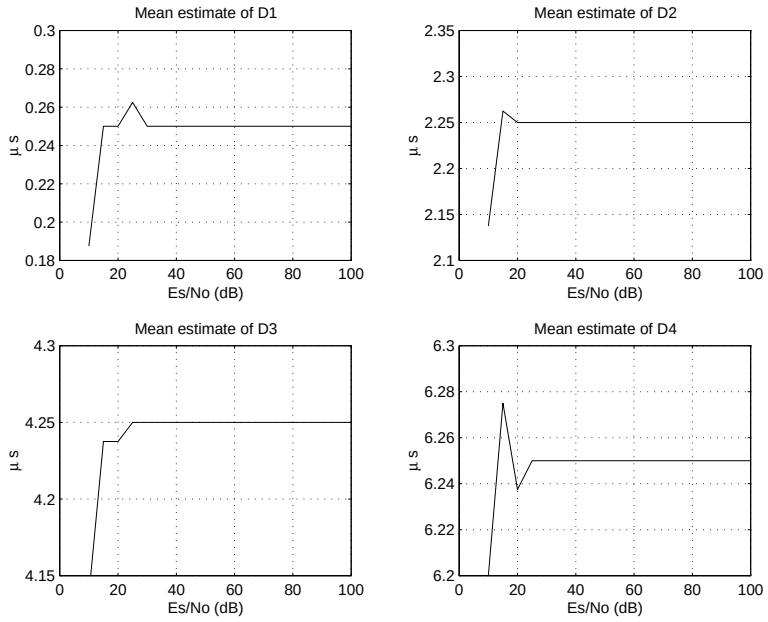

Figure 3.26: Mean delay estimates, $\Delta = 2$ μs, 10 samples.

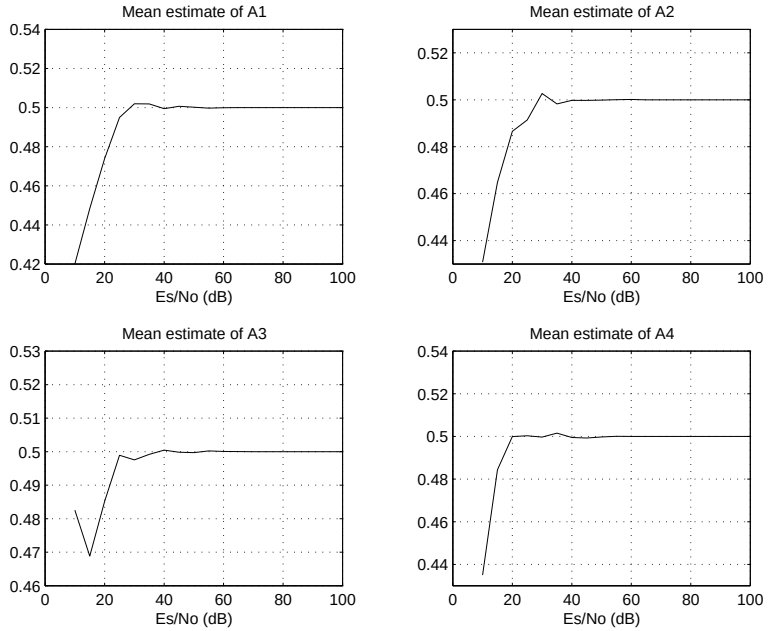

Figure 3.27: Mean amplitude estimates, $\Delta = 2$ μs, 10 samples.

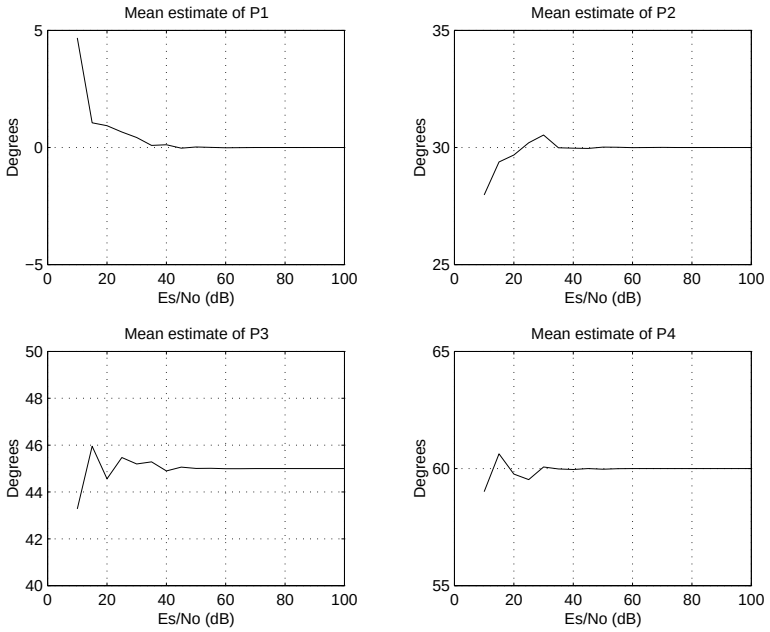

Figure 3.28: Mean phase estimates, $\Delta = 2$ μs, 10 samples.

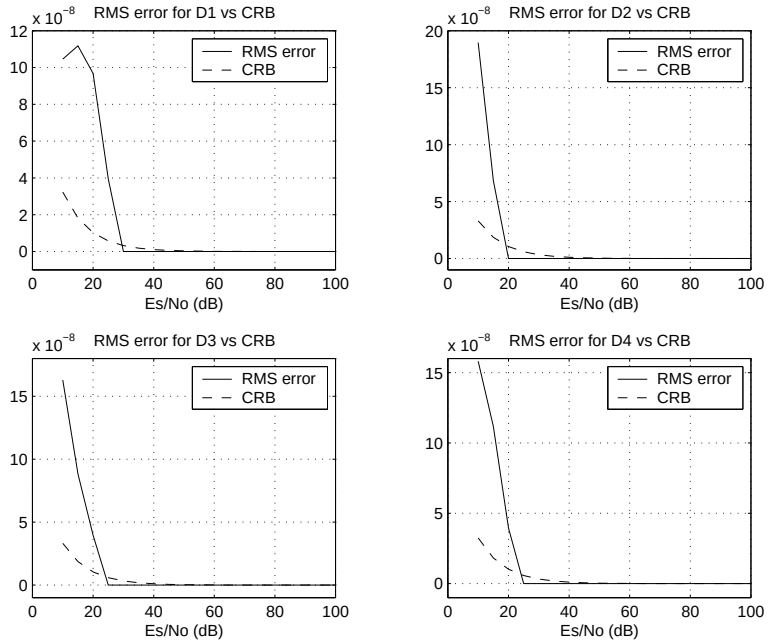

Figure 3.29: Delay R.M.S. error vs. CRB, $\Delta = 2$ μs, 10 samples.

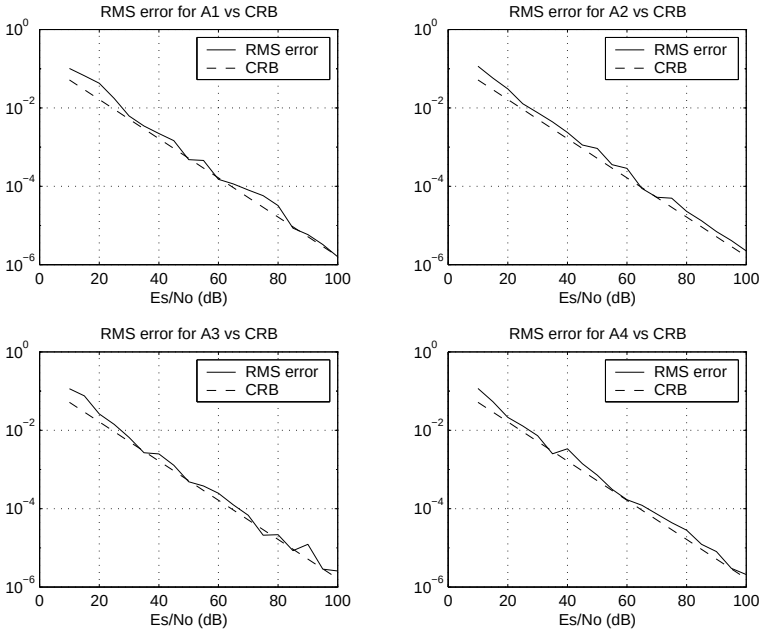

Figure 3.30: Amplitude R.M.S. error vs. CRB, $\Delta = 2$ μs, 10 samples.

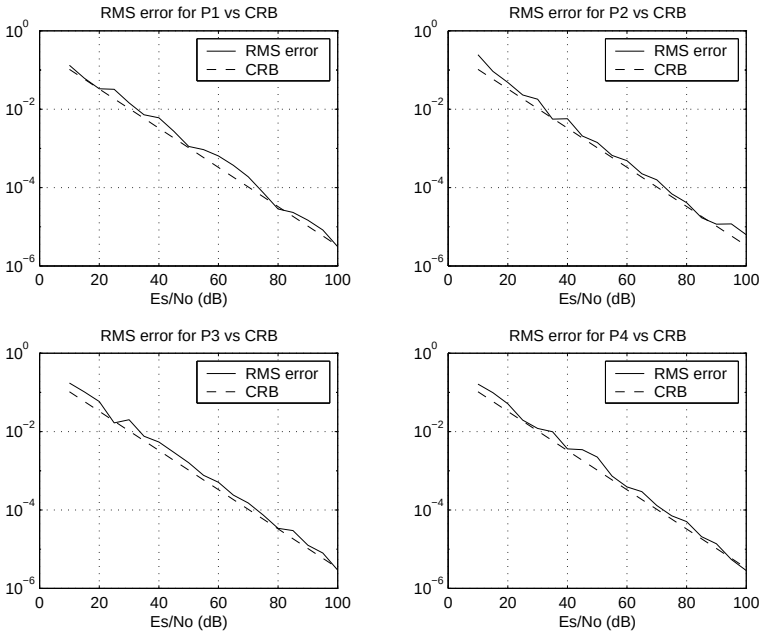

Figure 3.31: Phase R.M.S. error vs. CRB, $\Delta = 2$ μs, 10 samples.

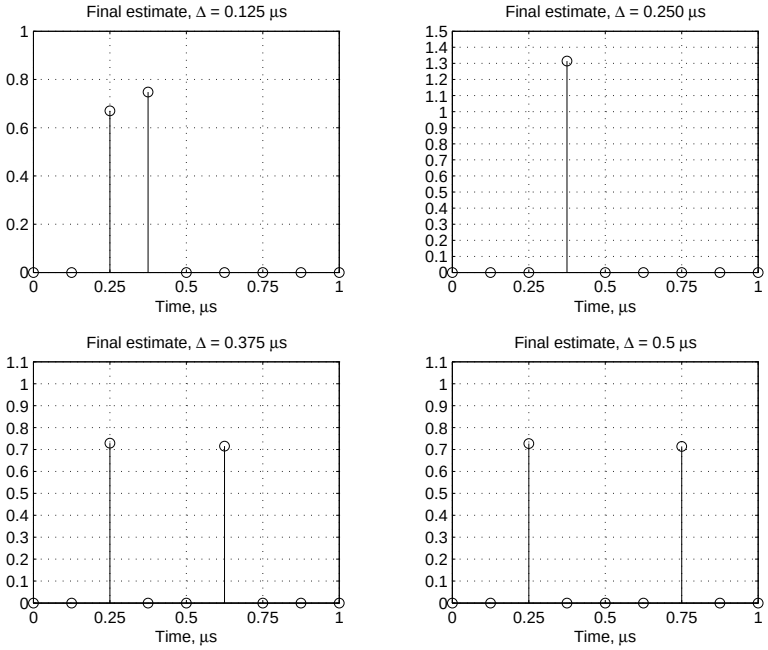

Figure 3.32: Channel tap estimates, $Es/N_0 = 20$ dB.

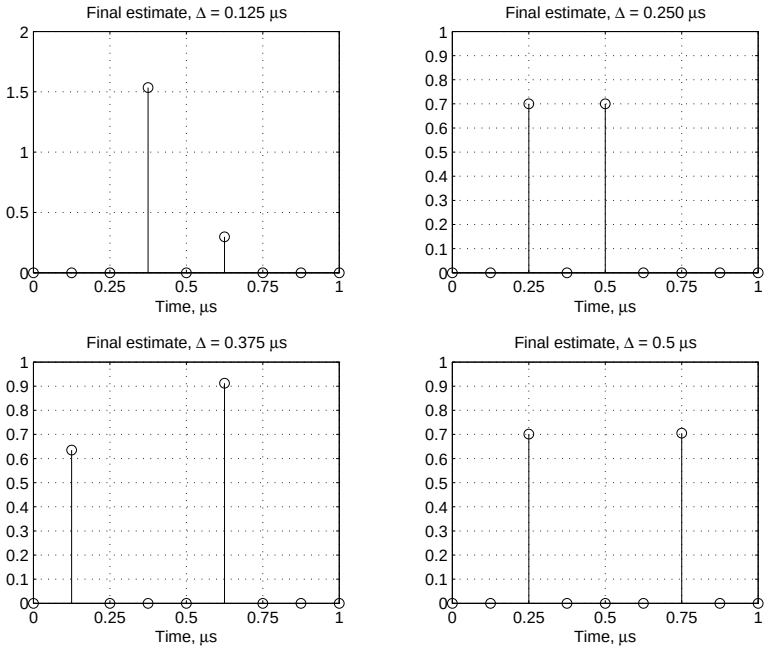

Figure 3.33: Channel tap estimates, $Es/N_0 = 30$ dB.

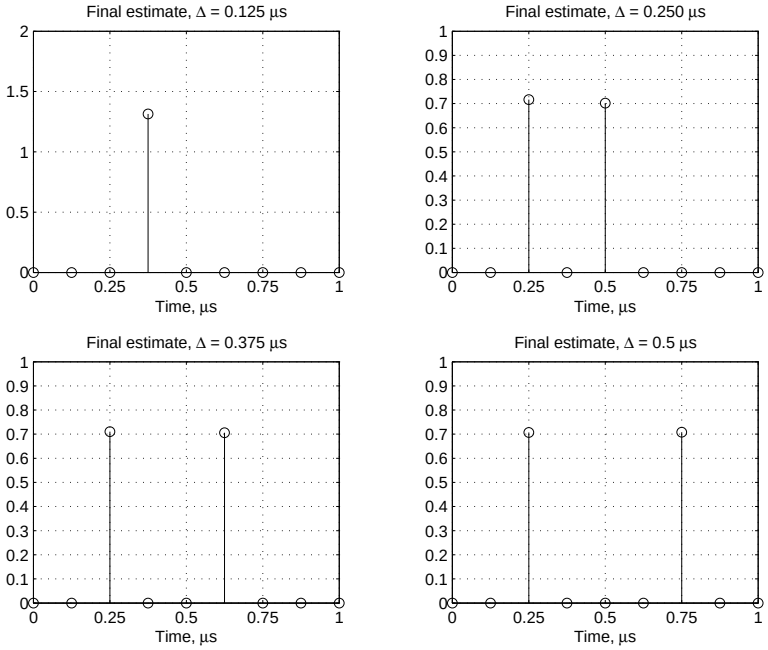

Figure 3.34: Channel tap estimates, $Es/N_0 = 40$ dB.

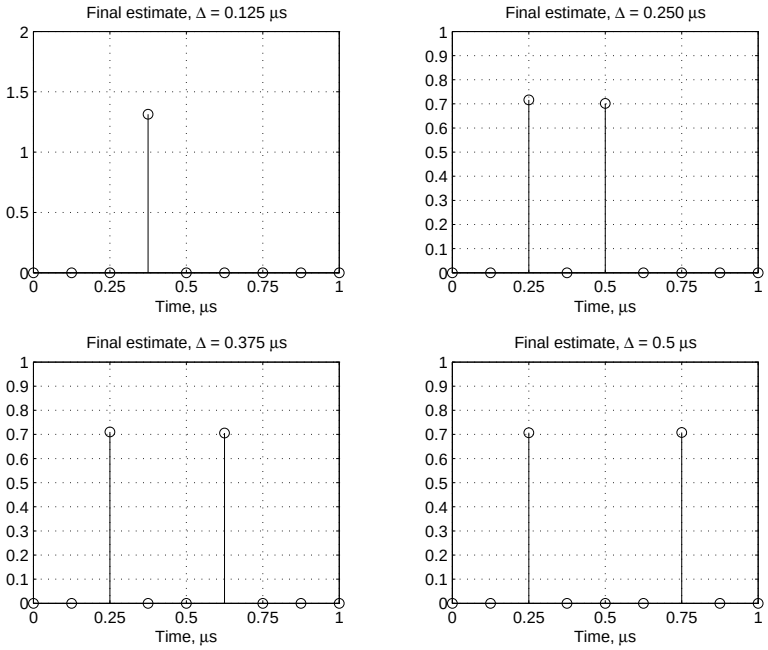

Figure 3.35: Channel tap estimates, $Es/N_0 = 50$ dB.

CHAPTER 4

THE PROPOSED CHANNEL SOUNDER

In this Chapter we examine the hardware implementation of the proposed channel sounder and the design considerations taken into account. Results of laboratory tests and channel soundings performed on OSU's central campus are presented and discussed.

4.1 System Specifications

There were two main design constraints that influenced the sounder design: frequency of operation and transmission bandwidth. The sounder was intended to operate in the Industrial, Scientific and Medical (ISM) band at a center frequency of 2.45 GHz with a maximum transmitted power of 20 dBm. The maximum transmission bandwidth allowed by the digital receiver is 2 MHz; however, the actual transmission bandwidth was set to 1.5625 MHz due to hardware limitations. This bandwidth value determined the design of the sounding signal and the structure of the estimation algorithm.

4.1.1 Sounding Signal Design

As mentioned above, the transmission bandwidth of the sounding signal was limited to 1.5625 MHz. The approach used to generate this sounding signal was to

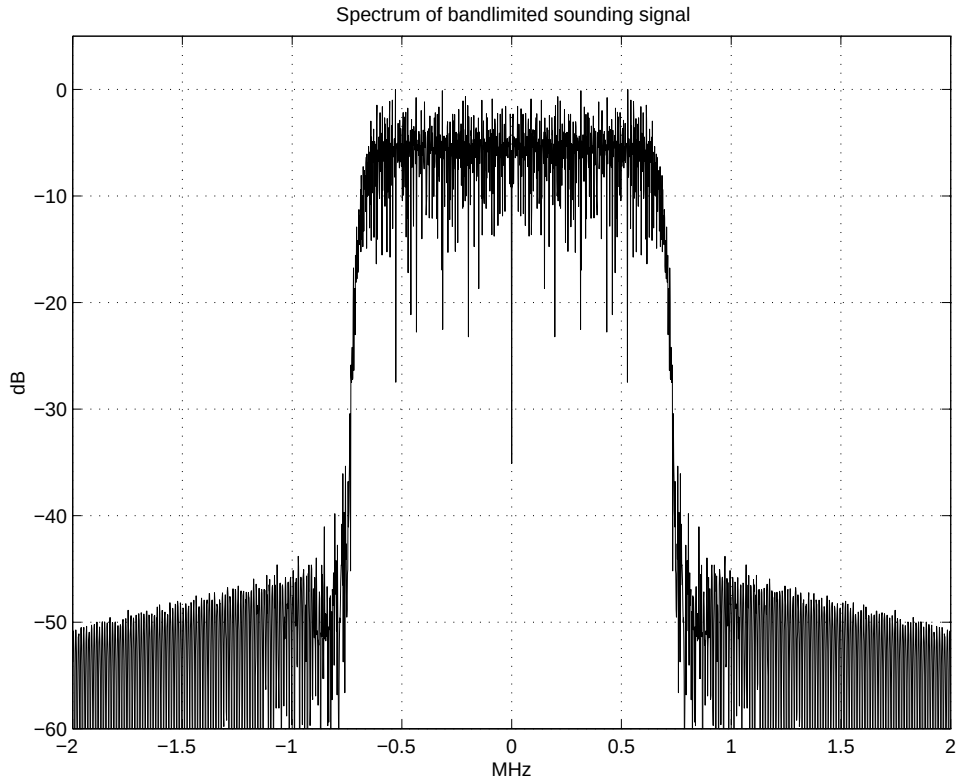

Figure 4.1: Normalized spectrum of bandlimited sounding signal.

convolve a PN m-sequence with a pulse shape having the desired spectral characteristics. A PN sequence 1023 chips long was generated using a characteristic polynomial given in [19]; this sequence was convolved with a root raised cosine pulse with an excess bandwidth factor of 0.11. Fig. 4.1 shows the signal spectrum after acquisition at the receiver. The sounding signal thus generated provides a dynamic range of 60 dB. The sounding signal is stored in the transmitter as a 4092 samples sequence which is read at a rate of 7.1591 MSPS; therefore the resulting signal has a period of 571.78 μs.

The sounder is intended to make measurements in an urban environment similar to the one found at OSU campus. In this setting the maximum path length difference to be expected is around 1.5 Km, which corresponds to a maximum unambiguous path delay resolution of 5 μs; therefore the period of our sounding signal is long enough to allow observation of the entire channel response. Assuming a 2.45 GHz carrier, a bandwidth of 1.5625 MHz and a relative speed of 90 Km/h (25 m/s) between transmitter and receiver, the maximum Doppler shift will be 204.3 Hz. To this Doppler shift corresponds a minimum period of 4.9 ms, which is 8.6 times bigger than the period of our sounding signal. For this reason the observed Doppler shift will be negligible in the proposed channel sounding system . This maximum Doppler shift value of 204.3 Hz also justifies the use of the channel model given in (1.2).

4.1.2 Construction of the Indicator Set Matrix

The construction of the indicator set matrix **D** determines the way in which the range of expected excess delays is discretized into delay bins. The size and structure of **D** are functions of the sampling rate and the available computing power. Choosing $K = 4$ and remembering that our final sample rate is 1.5625 MSPS our delay bins will be 160 ns wide; this is equivalent to a minimum spatial resolution of 48 m.

4.2 Receiver System

We now describe the hardware implementation of the channel sounder receiver and its resulting specifications.

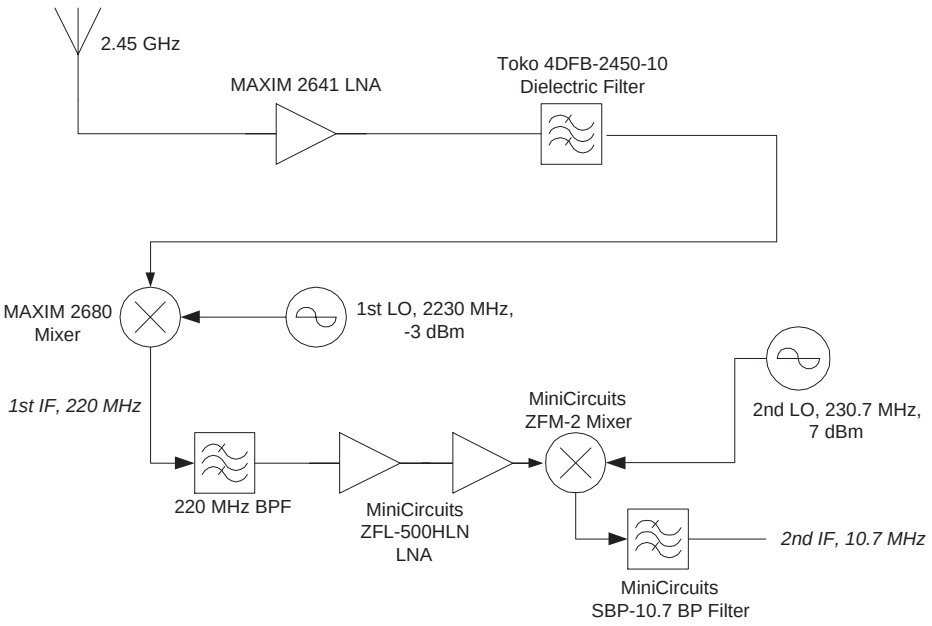

Figure 4.2: RF front end.

4.2.1 RF Front End

The RF front end shown on Fig 4.2 downconverts a received signal with a center frequency of 2.45 GHz to a 10.7 MHz IF signal. It has a first IF stage tuned at 220 MHz and a second IF stage tuned at 10.7 MHz, with a net power gain of 48 dB and a net noise figure of 3.1 dB . The IF stages require local oscillators operating at 2230 MHz, -3 dBm and 230.7 MHz, 7 dBm respectively. The receiving antenna was a air-loaded patch antenna with 9 dBi gain and a azimuthal half-power beamwidth of 60°.

4.2.2 A/D Converter and Digital Receiver

The downconversion of the IF signal provided by the RF front end is performed by a Coryell & Wiprud EV4014 Quad Receiver Board. The main components on this

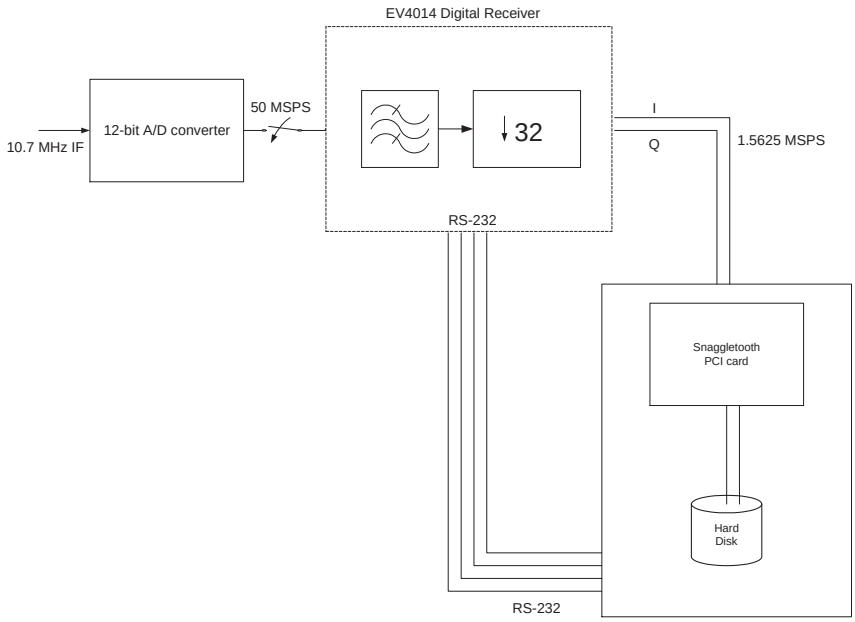

Figure 4.3: Downconversion and data acquisition stages.

board are two 50 MSPS, 12-bit A/D converters and a Graychip GC4014 four-channel digital receiver with a maximum per-channel bandwidth of 2 MHz. The receiver has four 14-bits digital inputs each with a top speed of 64 MSPS and a top output rate of 2 MSPS per channel; each output sample consists of two 16-bit words containing I and Q data respectively. The output can be configured as an ADSP-2106x SHARC DSP link port, allowing for a direct interface with this family of devices. Fig. 4.3 shows the implemented architecture using the EV4014 board.

The EV4014 must be programmed by loading a simple script through the board's RS-232 port each time the sounder is powered on. Among the most important parameters that are set in this script are gain, channel configuration, decimation rate and local oscillator frequency. A complete guide to the architecture and programming of the EV-4014 is found in [20].

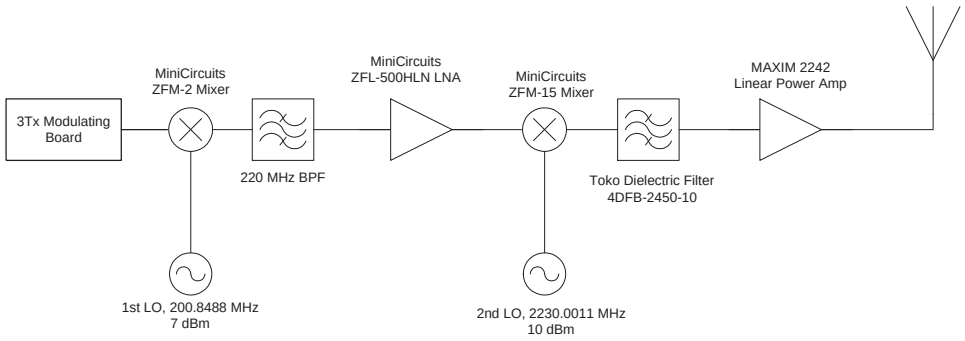

Figure 4.4: Channel sounder transmitter.

4.2.3 Data Acquisition

A Bittware's Snaggletooth PCI card was used to acquire data from the EV4014 receiver. This PCI card contains 2 ADSP-21062 SHARC DSP processors, each of them with 2 Mbits of internal memory. The acquisition process is started by running a small script from a utility provided by the card's manufacturer; this script sets the parameters for a DMA transfer from one of the ADSP-21062 link ports to the chip's internal memory. Each acquisition contains 8192 complex samples from the EV4014 output (about 5.24 ms worth of sounding data); and each I-Q sample of the acquired signal is stored in the eight most significant bytes of a 12-bytes, 2's complement ASCII word. A small MATLAB code was written to separate I and Q data and to convert them to decimal format.

4.3 Transmitter System

A block diagram of the transmitter is shown on Fig. 4.4. Its functional blocks are described in the following subsections. An estimate of the coverage of the sounder is also inluded.

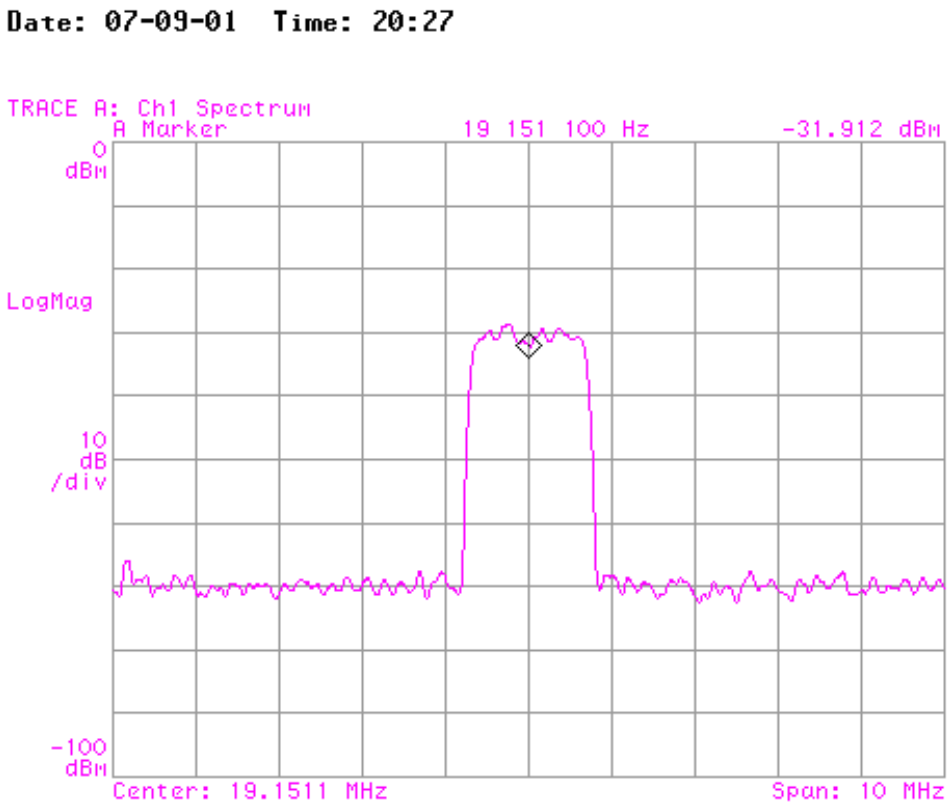

Figure 4.5: Spectrum of sounding signal at the output if the 3-Tx board.

4.3.1 The 3-Tx Modulating Board

The sounding signal is generated using a custom-built 3-Tx modulating board. The 3-Tx board loads a sampled version of the sounding signal either from a ROM or from a RS-232 port and modulates it onto a 19.1511 MHz carrier. It contains 3 AD-9856 upconverters controlled by an on-board ADSP-2181 DSP chip and uses a 14.31818 MHz reference clock signal which should be precise enough to avoid frequency and phase drift during channel measurement. Fig 4.5 shows the measured output spectrum of the IF signal produced by the board.

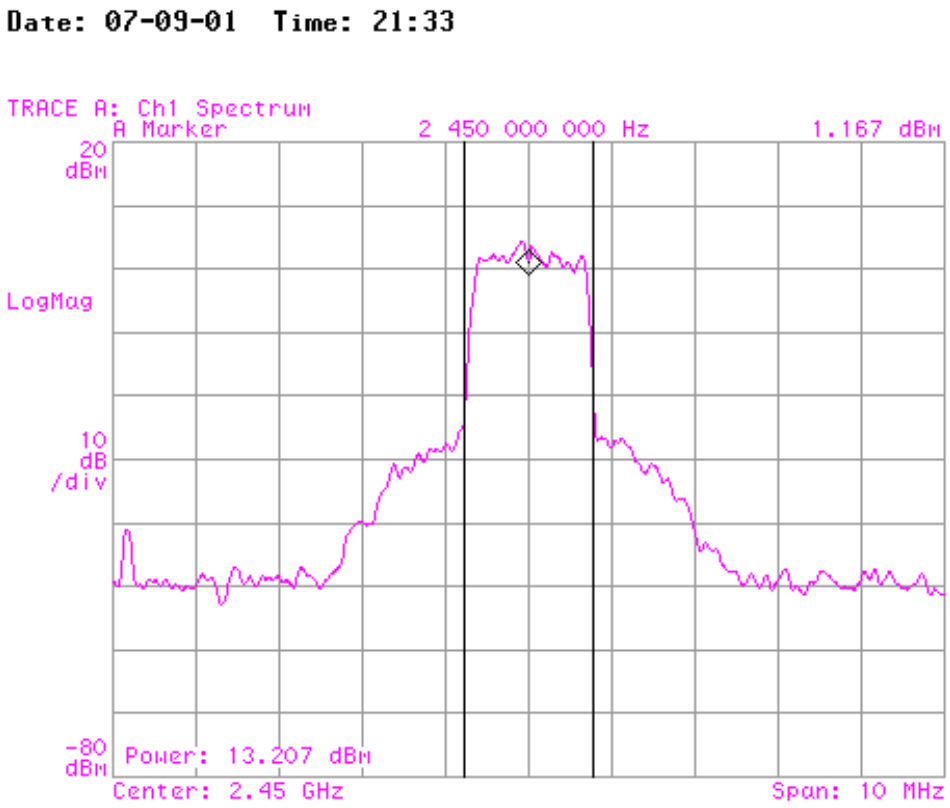

Figure 4.6: Spectrum of transmitted signal and transmitted power.

4.3.2 Upconversion Stage

This section of the transmitter upconverts the 19.1511 MHz IF signal provided by the 3-Tx board to a carrier frequency of 2.45 GHz. The input signal is fed to an IF stage tuned to 220 MHz; after a second upconversion to 2.45 GHz there is a linear power amplifier with a maximum rated output power of 22.5 dBm at 2.45 GHz. The transmitted power achieved by this configuration was approximately 13 dBm, as seen in Fig. 4.6. The transmitter antenna was an air-loaded patch antenna with 11.5 dBi gain and an azimuthal half-power beamwidth of 75°.

4.3.3 Coverage Calculations

From the simulations performed in Chapter 3 we know that a minimum Es/N_0 of about 40 dB is required to ensure proper performance from the channel estimation algorithm. Taking this into account we can make the following approximation

$$\frac{E_s}{N_0} = \frac{S_p T_s}{N_0} = 40\ dB \tag{4.1}$$

S_p represents the total power in the multipath signal and T_s represents the period of the sounding signal. The above can be rewritten as

$$S_p(dBm) = 40 - 10\log(T_s) + N_0 \tag{4.2}$$

Assuming $N_0 = 174$ dBm/Hz the minimum received power to ensure reliable channel estimates should be -101.57 dBm. This value was used to compute the sounder coverage using the PCS Extension to the Hata propagation model [21]. The transmitter antenna has a gain of 9.5 dBi and was placed at about 30 meters above street level; the receiver antenna has a gain of 11.5 dBi. With these values the coverage predicted by the PCS model was 0.61 Km., enough to cover part of OSU's central campus.

4.4 Laboratory Testing

Several laboratory tests were performed in order to verify the performance of the channel sounding system by using a TAS4500 channel emulator. This device provides a convenient mean for testing communications systems since it emulates the delay, fading, and path loss characteristics of a wireless mobile channel. The experimental setup used for these tests is shown in Fig. 4.7.

In a first series of tests the TAS4500 was programmed to emulate four channels, each with four equally spaced paths with relatives amplitudes $A1 = 1$, $A2 = A3 =$

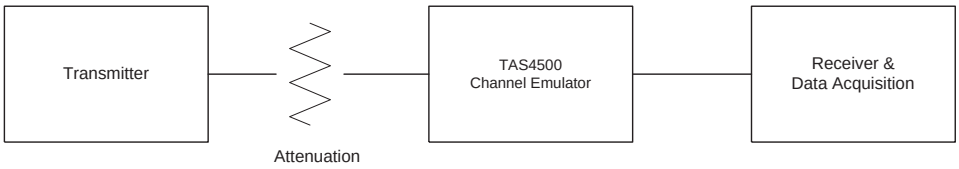

Figure 4.7: Laboratory test setup.

0.71 and $A4 = 0.5$. For each of these channels the delay between paths was set to $\Delta = 2$ μs, $\Delta = 1.5$ μs, $\Delta = 1$ μs and $\Delta = 0.5$ μs. In order to obtain an estimate of the noise variance required by the minimum descriptor length algorithm, measurements of the noise floor at the receiver were performed by acquiring the received signal with the receiver front end terminated by a matched load. The TAS4500 does not provide control over the phase of each path, and thus it was not possible to evaluate the phase estimates produced by our algorithm.

Figs 4.8 to 4.11 present final estimates for each channel. It is seen how the algorithm resolves the emulated paths down to 0.5 μs, a value which is already smaller than the sampling period of the data (0.64 μs). Small errors of the order of one delay bin in the delay estimation can be appreciated in the channel tap plots .

In order to evaluate the dynamic range of the algorithm a channel with five paths and amplitudes $A1 = 1, A2 = 0.7, A3 = 0.5, A4 = 0.3$ and $A5 = 0.1$ was emulated. A value of $\Delta = 1$ μs was employed. Fig. 4.12 shows the resulting channel estimate. In spite of small errors in the delay estimates the algorithm produced reliable results.

4.4.1 Frequency Offset Correction

A small amount of frequency offset Ω_{off} and phase offset θ_{off} in the received signal is unavoidable since practical oscillators cannot provide perfect precision and/or

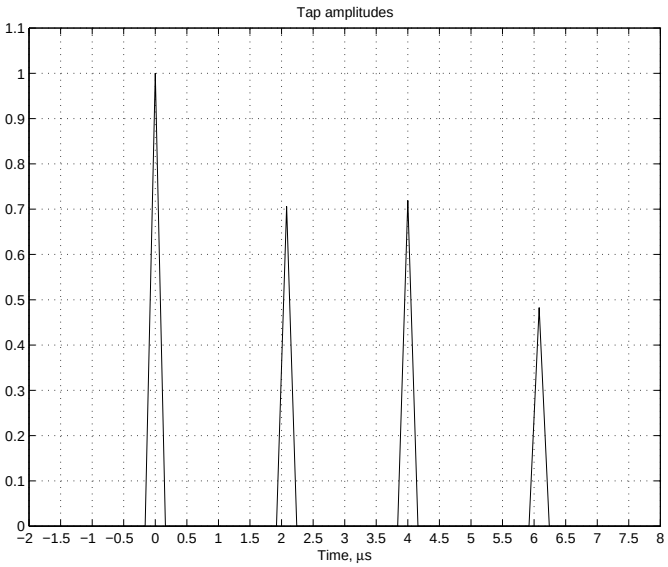

Figure 4.8: Final channel estimates, $\Delta = 2\mu$s.

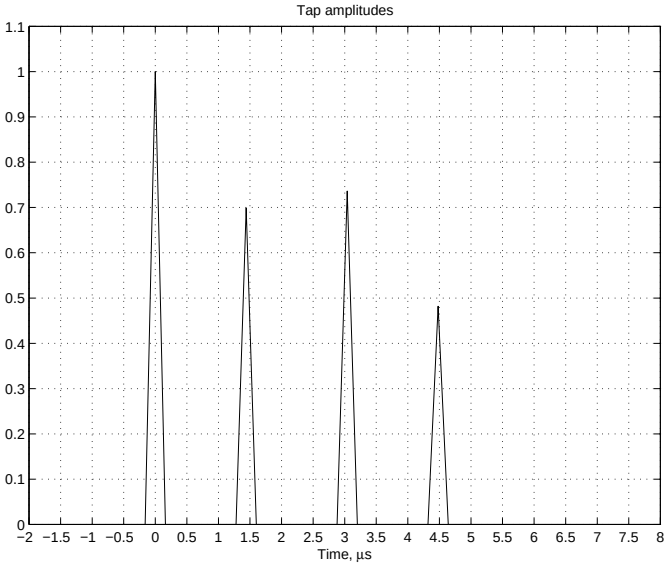

Figure 4.9: Final channel estimates, $\Delta = 1.5\mu$s.

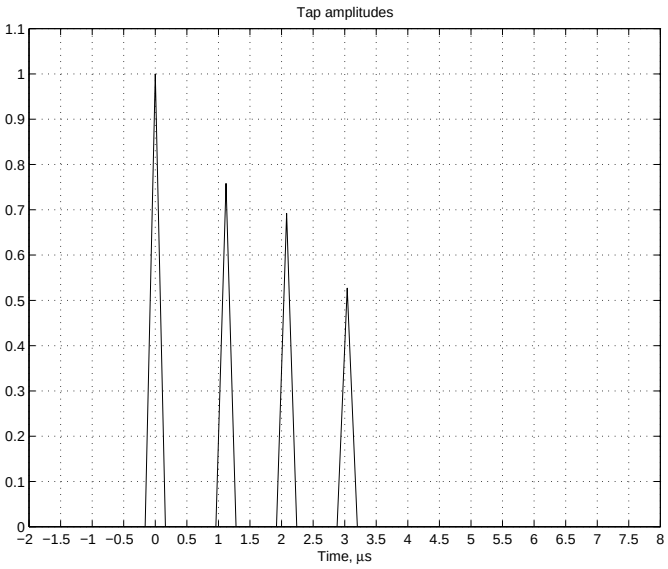

Figure 4.10: Final channel estimates, $\Delta = 1\mu$s.

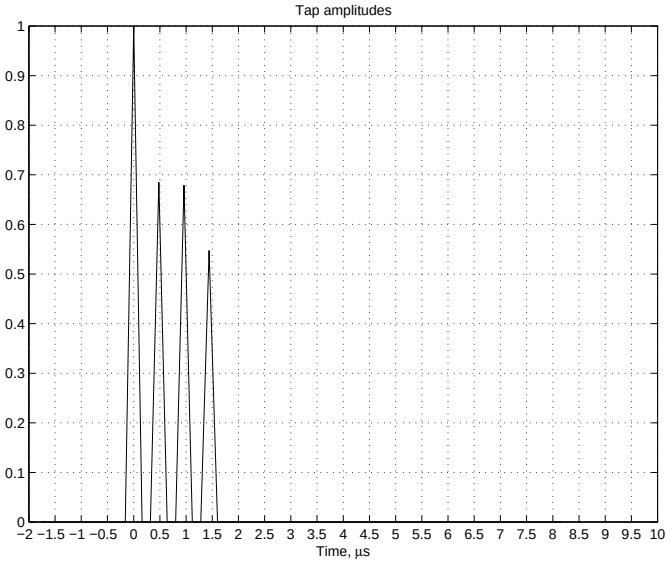

Figure 4.11: Final channel estimates, $\Delta = 0.5\mu$s.

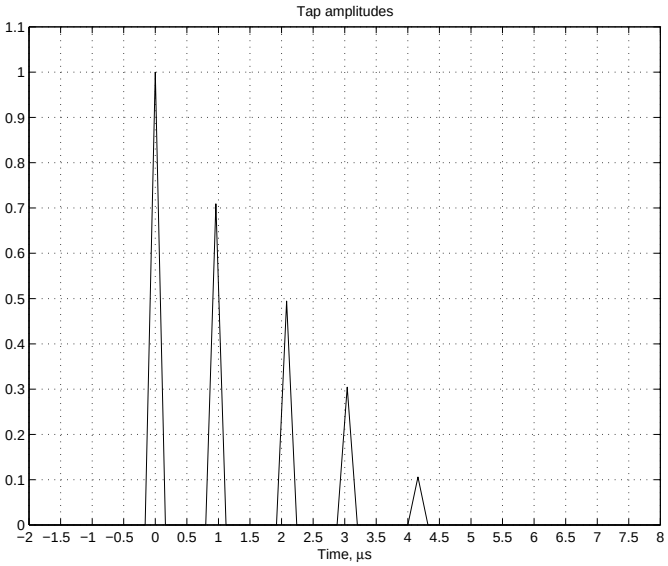

Figure 4.12: Final channel estimates; $\Delta = 1\mu$s.

stability. For this reason a frequency and phase offset estimation algorithm was used to compensate these effects. The algorithm finds joint ML estimates of the frequency and phase offset first by performing a grid search and then a gradient search in Ω_{off} and θ_{off} to minimize

$$\sum_{k=1}^{M} \left| Y_k - e^{j(k\Omega_{off}+\theta_{off})} s_k(\tau_p) \right|^2 \tag{4.3}$$

This minimization is done by using the same optimization routine used in the modified deconvolution algorithm. In the above expression $s_k(\tau_p)$ is a filtered copy of the sounding signal which is synchronized to the received signal by using the peaks of the crosscorrelation between the received signal and the original sounding signal. Figs. 4.13 and 4.14 show the I and Q components of the received signal before and after offset compensation.

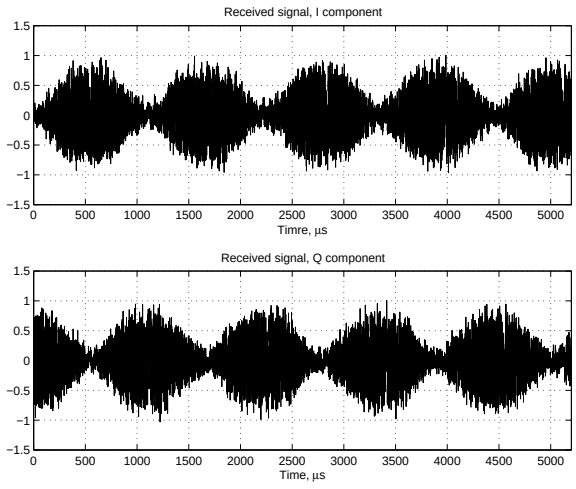

Figure 4.13: Received signal before offset compensation.

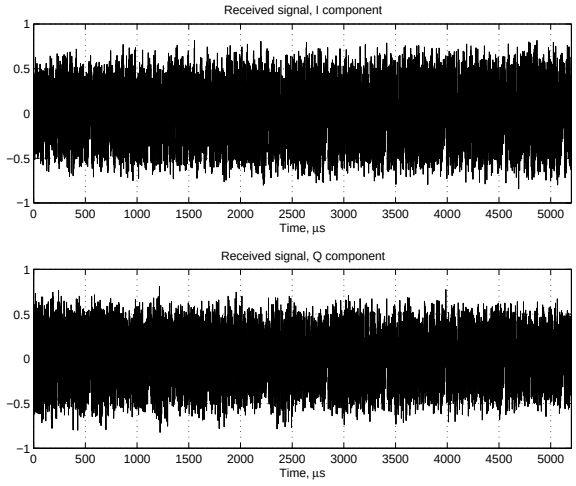

Figure 4.14: Received signal after offset compensation.

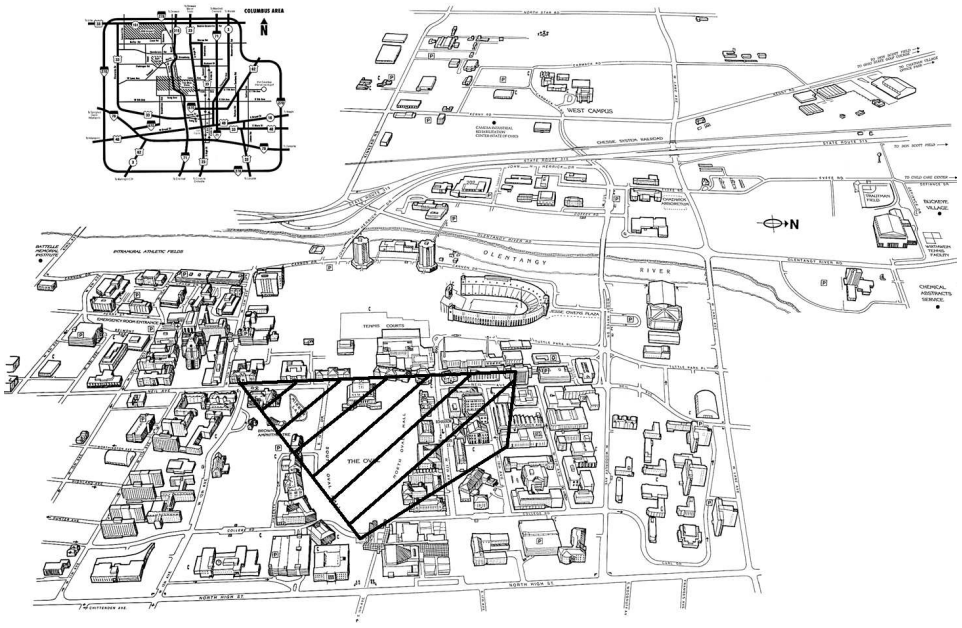

Figure 4.15: Campus map and area covered by channel soundings.

4.5 Field Measurement Results

A set of 33 channel soundings were acquired on OSU's central campus at 12 different locations; in some of these locations the soundings were repeated for different antenna orientations. In each case the variance σ_r^2 of the received signal was recorded as an estimate of the incoming signal power. A number of measurements of ambient noise were also performed in order to obtain estimates of the noise variance, a value needed by the estimation algorithm. Fig. 4.15 shows the area in which the measurements took place. The transmitting antenna was aimed southwards through one of the windows in the fifth floor of the Electrical Engineering Building, which is located in the upper right hand corner of the polygon that represents the area covered by our measurements. All the measurements were done with a stationary receiver. Although

the amount of information presented here is far from being statistically conclusive, it nevertheless shows some interesting characteristics in the measured channels.

A 600-samples long segment from each sounding was processed using the channel estimation algorithm described in Chapter 3; the received signal was reconstructed using the channel estimates produced by the algorithm, and the mean square error between normalized versions of the reconstructed signal and the originally received signal was computed. Figs. 4.16 to 4.29 show examples of the channel estimates produced by the algorithm, as well as plots of the received and reconstructed signals.

4.5.1 Received Power vs. Mean Square Error

A scatter plot of $20\log_{10}\sigma_r$ vs. the mean squared error between received and reconstructed signal is shown in Fig. 4.30. An inspection of this plot shows how the MSE decreases as the variance of the received signal (and thus its power) increases. There are however five outliers that appear for $20\log_{10}\sigma_r$ between 50 and 90 dB; in these cases there is not a reduction in MSE with increasing signal power. This may be due to closely spaced paths which are not resolved by the algorithm, since the corresponding locations were close to the transmitter and since there is nevertheless a good match between received and reconstructed signals for these locations. This argument is supported by Fig. 4.31, which shows another scatter plot of MSE against the maximum tap amplitude from each channel estimate: it is seen that the same 5 outliers are present again. Non-linear effects in the receiver (due to the relatively high signal levels) do not explain these outliers since two of them occur for values of $20\log_{10}\sigma_r$ between 50 and 60 dB, a range within which the MSE for other soundings is lower. Further measurements are required to test this hypothesis.

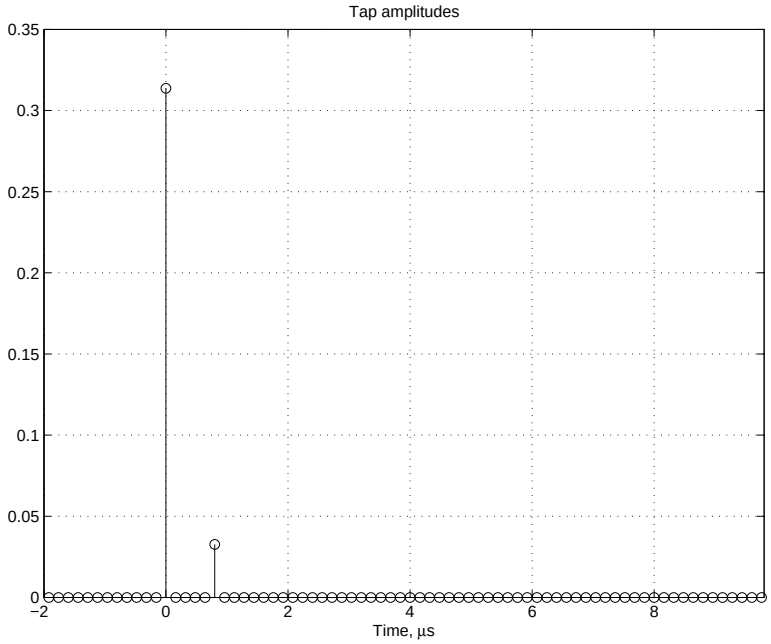

Figure 4.16: Channel estimate; July 1st, sounding # 1.

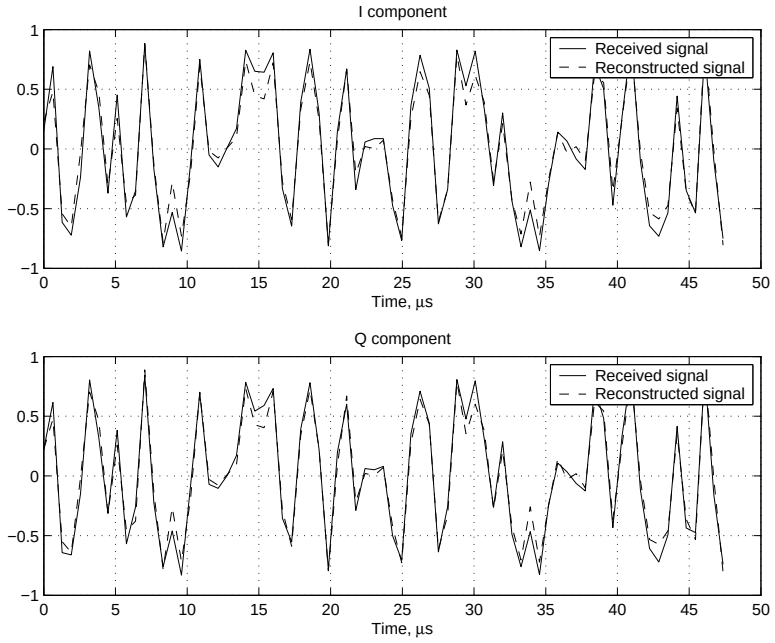

Figure 4.17: Normalized received signal vs. reconstructed signal, July 1st, sounding # 1.

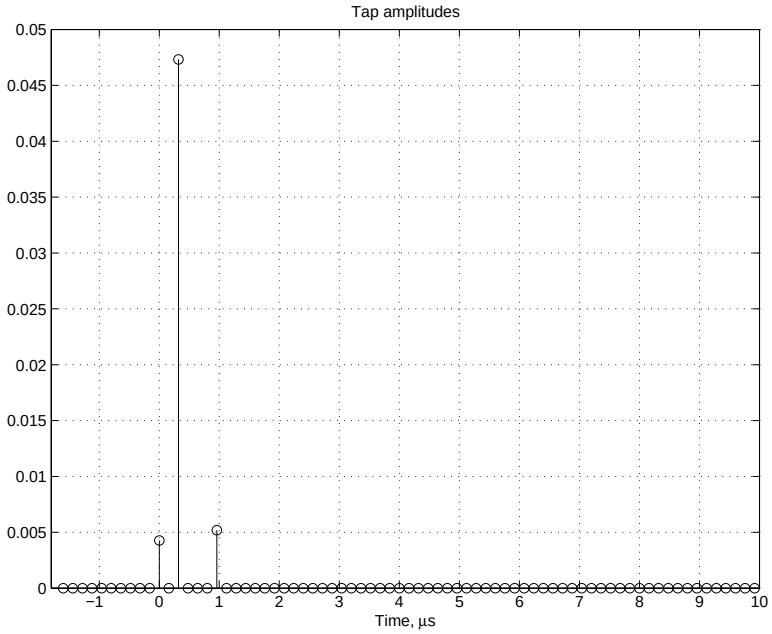

Figure 4.18: Channel estimate; July 1st, sounding # 9.

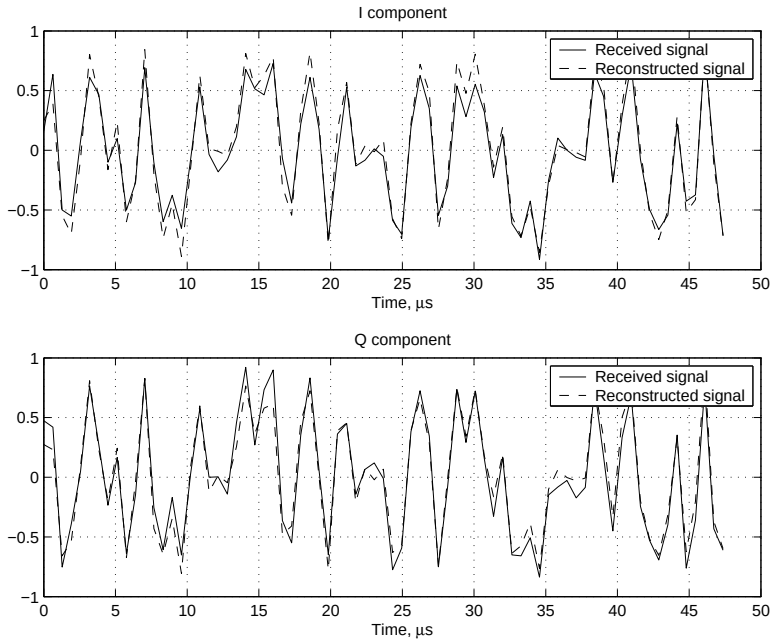

Figure 4.19: Normalized received signal vs. reconstructed signal, July 1st, sounding # 9.

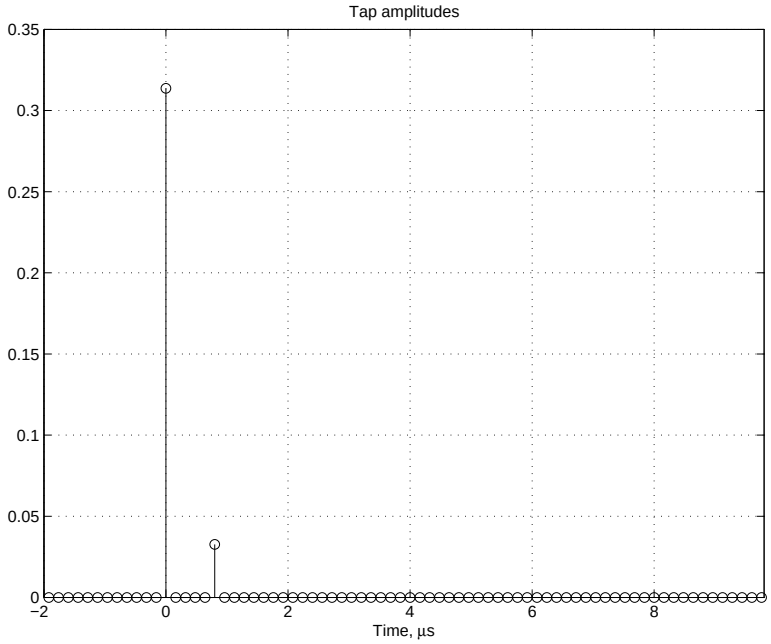

Figure 4.20: Channel estimate; July 14th, sounding # 2.

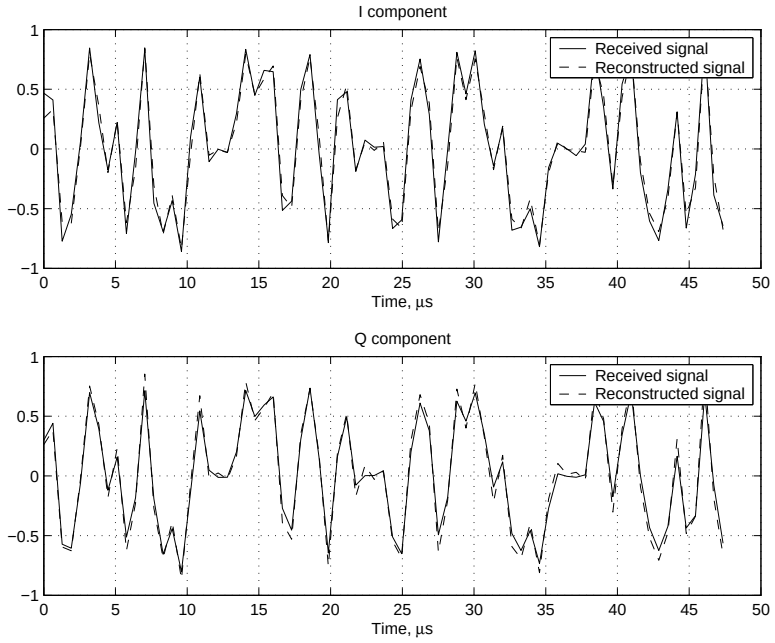

Figure 4.21: Normalized received signal vs. reconstructed signal, July 14th, sounding # 2.

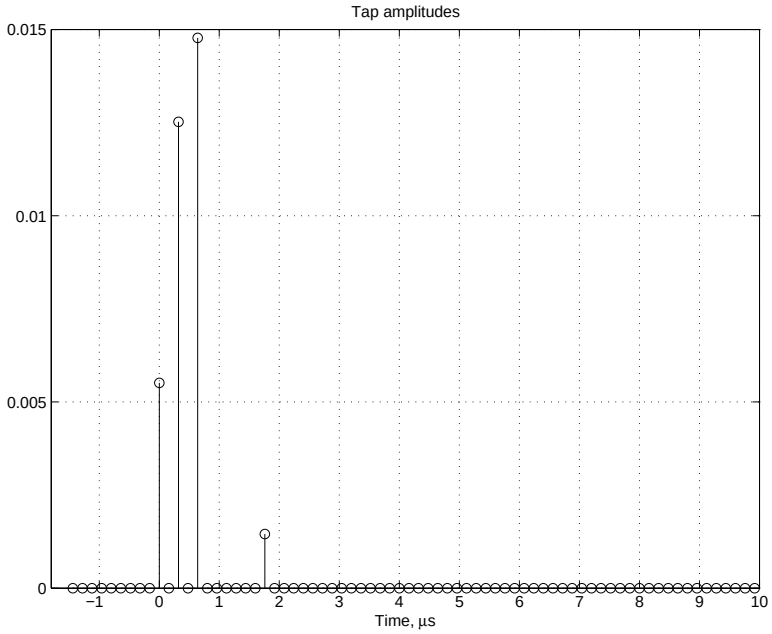

Figure 4.22: Channel estimate; July 26th, sounding # 5.

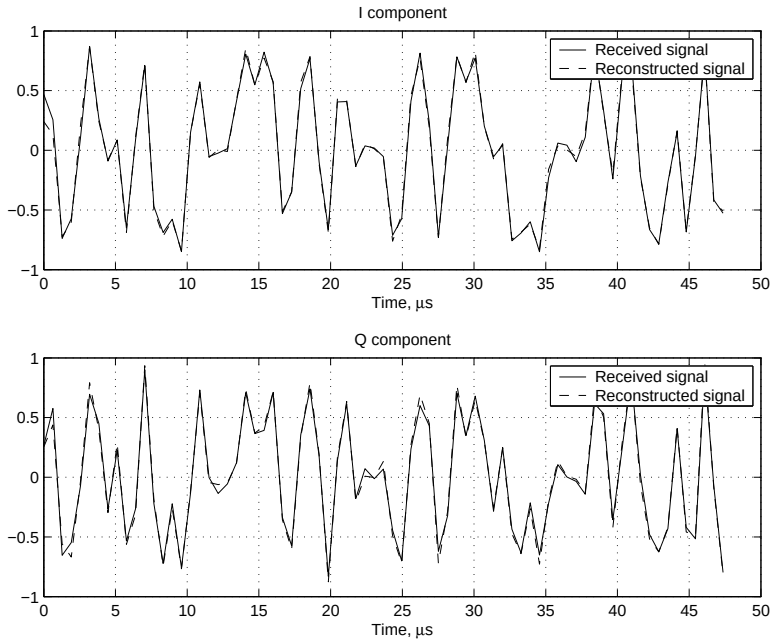

Figure 4.23: Normalized received signal vs. reconstructed signal, July 26th, sounding # 5.

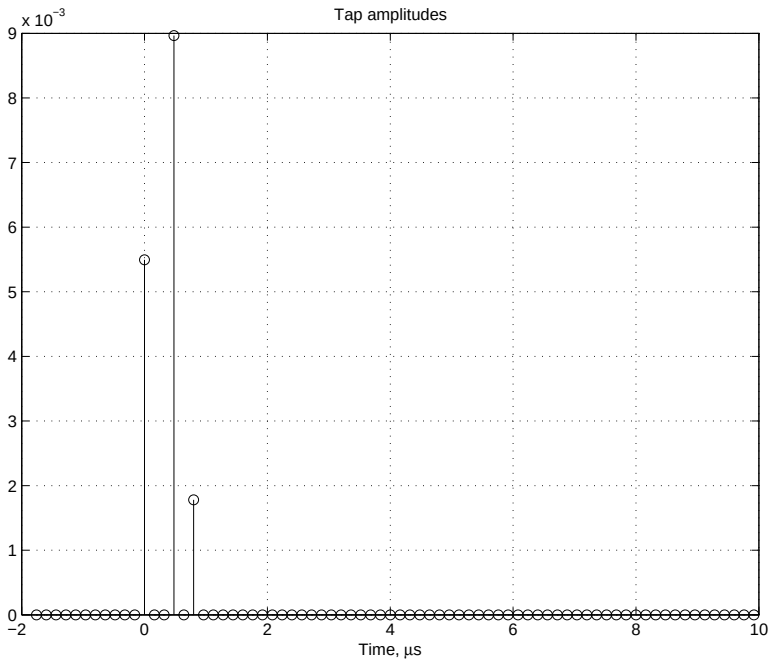

Figure 4.24: Channel estimate; July 26th, sounding # 7.

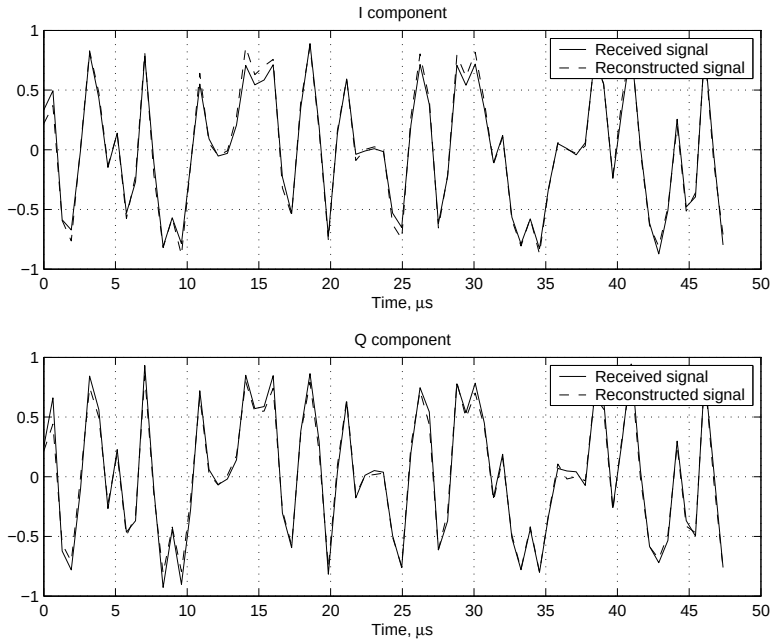

Figure 4.25: Normalized received signal vs. reconstructed signal, July 26th, sounding # 7.

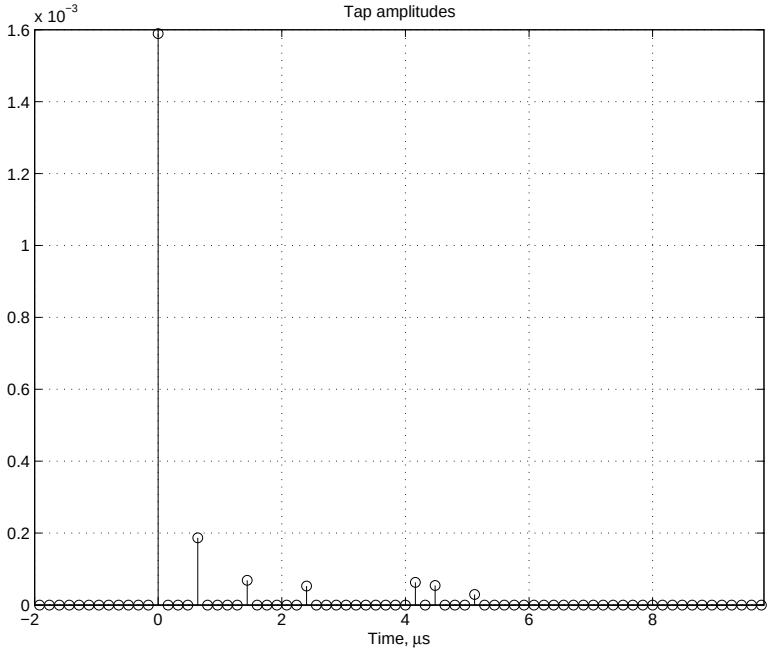

Figure 4.26: Channel estimate; July 26th, sounding # 11.

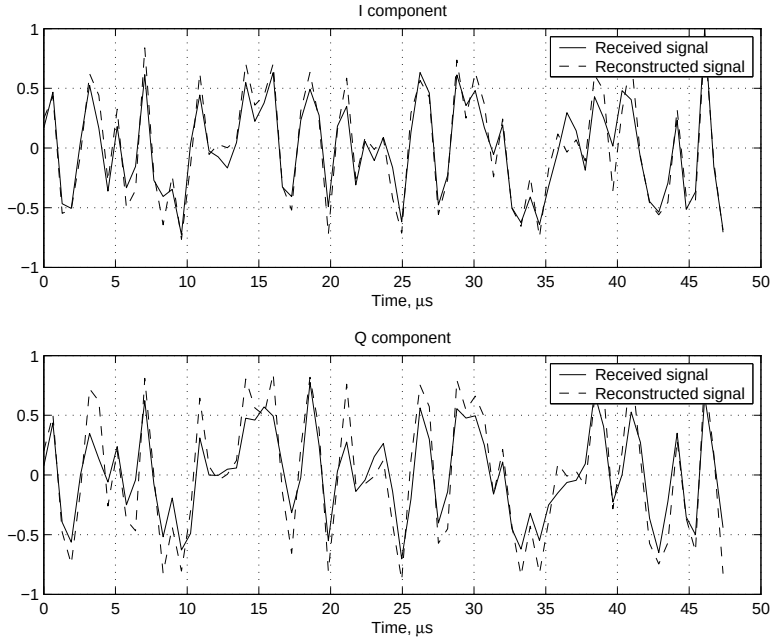

Figure 4.27: Normalized received signal vs. reconstructed signal, July 26th, sounding # 11.

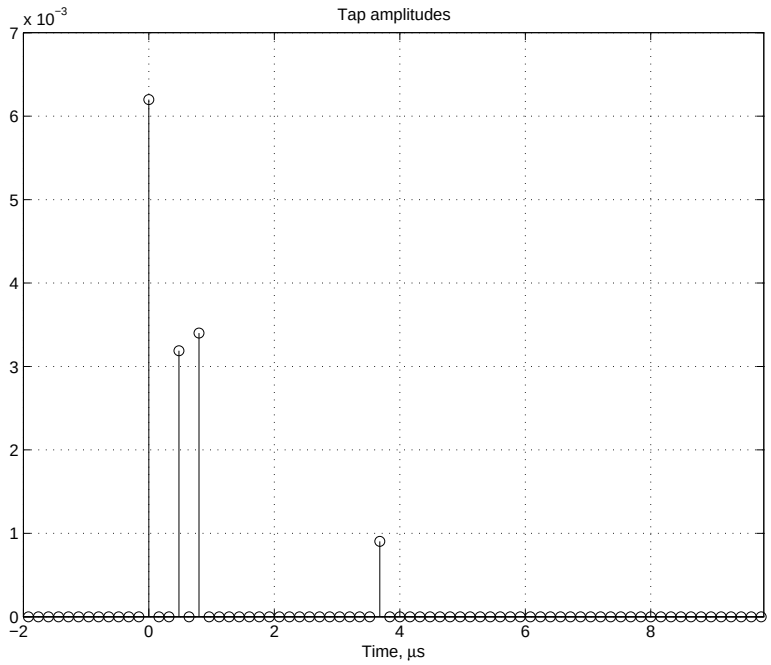

Figure 4.28: Channel estimate; July 26th, sounding # 14.

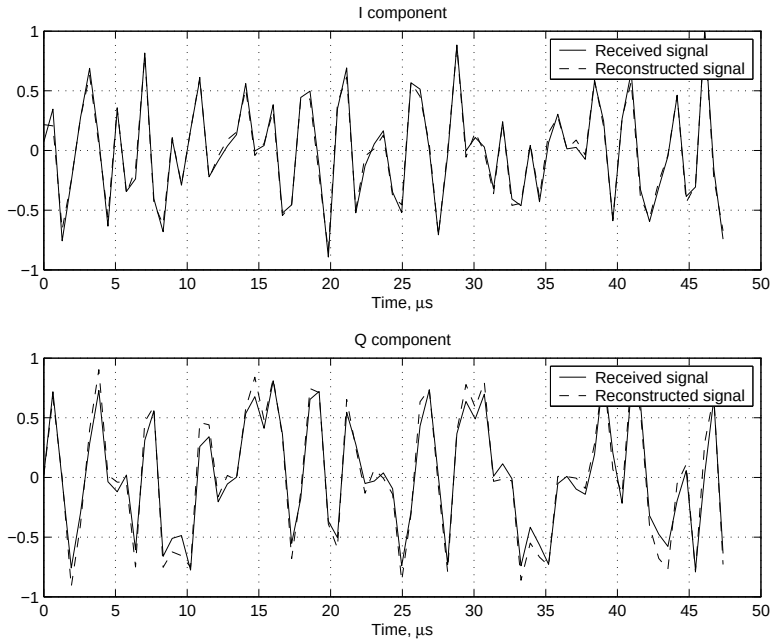

Figure 4.29: Normalized received signal vs. reconstructed signal, July 26th, sounding # 14.

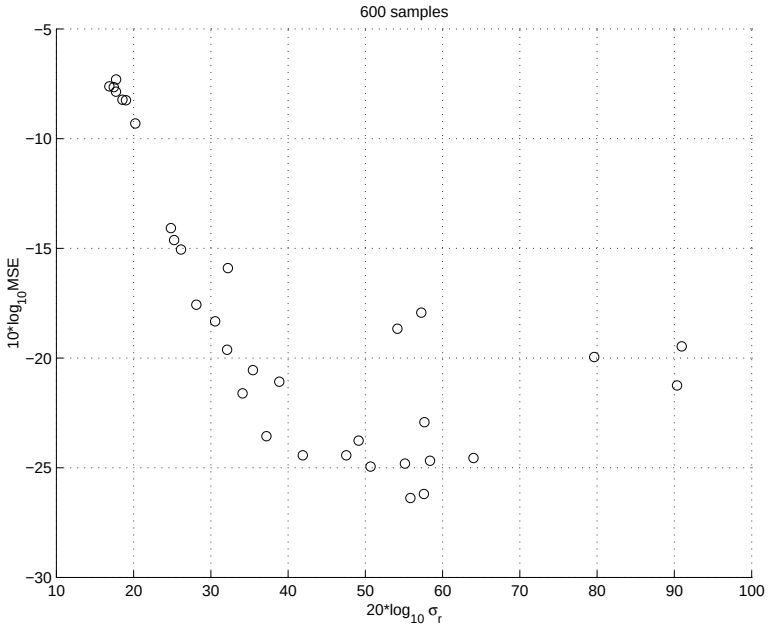

Figure 4.30: Received power estimate vs MSE.

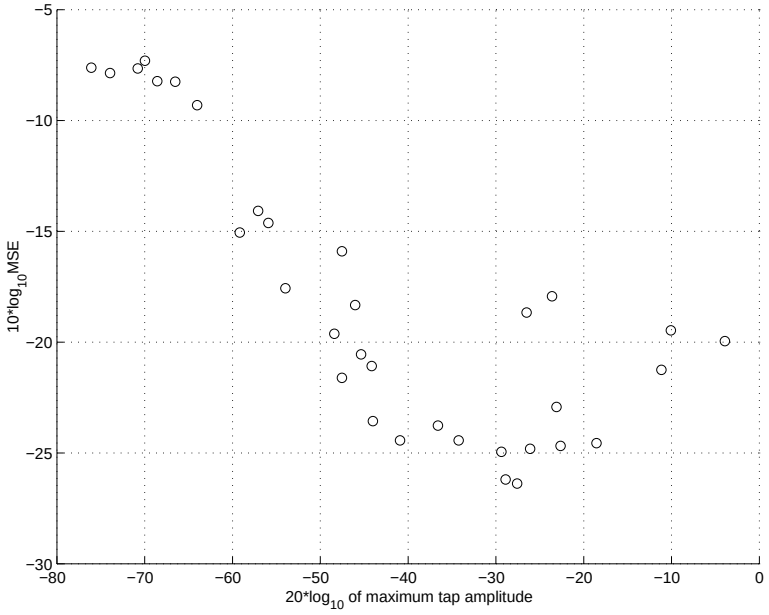

Figure 4.31: Maximum tap amplitude vs MSE.

4.5.2 Delay Spread, Number of Paths, Power in Main Tap

Figs. 4.32 and 4.33 show histograms for the delay spread and the number of paths in the measured channels. From this histograms it can be inferred that in most cases the channel structure is relatively simple: few paths (3 or less) and small delay spread (smaller than 1.5 μs). The mean values of the delay spread and the number of paths were 2.20 μs and 3.48, with standard deviations of 2.85 μs and 1.92 respectively.

Fig. 4.34 shows a histogram for the fraction of the signal power associated with the biggest channel tap. This histogram shows how in most cases the signal power is concentrated in the strongest channel path: the mean value for this power fraction was 0.8265 with a standard deviation of 0.17.

Fig. 4.35 shows a scatter plots for the number of paths vs. $20\log_{10}\sigma_r$, while Fig. 4.36 shows a scatter plot of MSE vs. number of paths. Both plot suggest that a large number of paths is associated with large estimation errors and low received power levels. These findings show how most channels have a simple structure for low MSE values.

4.5.3 LOS vs Non-LOS paths

We have already mentioned that some of the measurements were taken at short distances from the transmitter. Fig. 4.37 presents a scatter plot of the received power vs. the power fraction contained in the strongest channel tap. There aren't any paths with a small fraction of the received power concentrated in the strongest path for low received power levels (lower right hand corner of plot). This is an intuitively expected result since non-line-of-sight paths associated with smaller power levels must have a more complicated structure with power diluted among the different arriving paths.

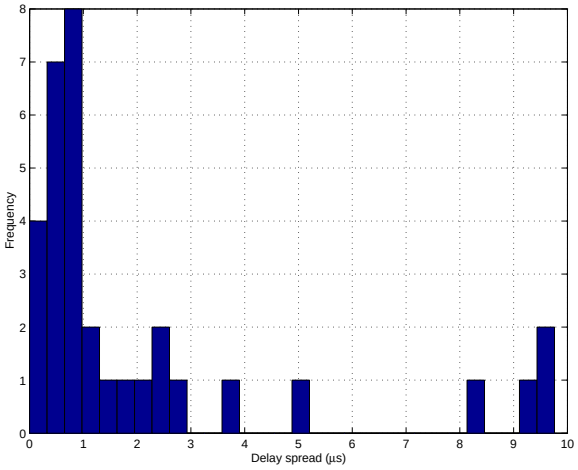

Figure 4.32: Histogram for delay spread.

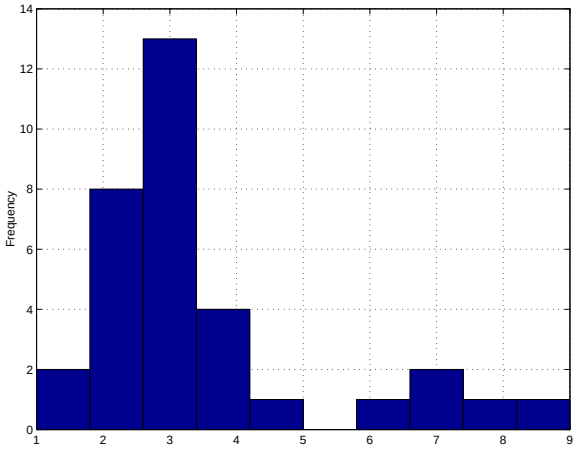

Figure 4.33: Histogram for number of paths.

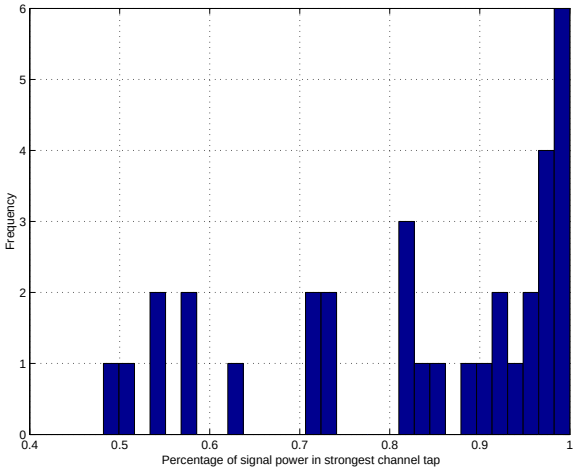

Figure 4.34: Histogram for power fraction in strongest channel tap.

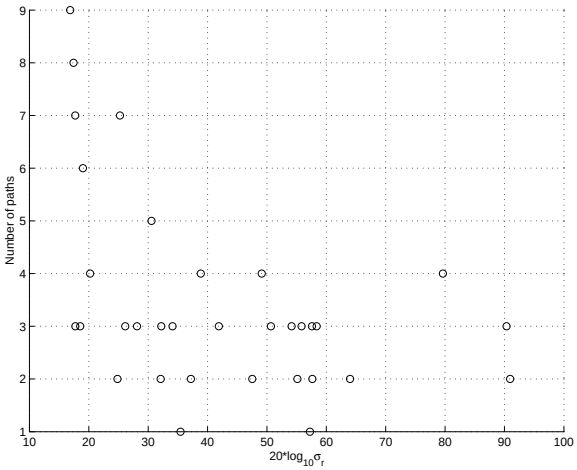

Figure 4.35: Number of paths vs. received power.

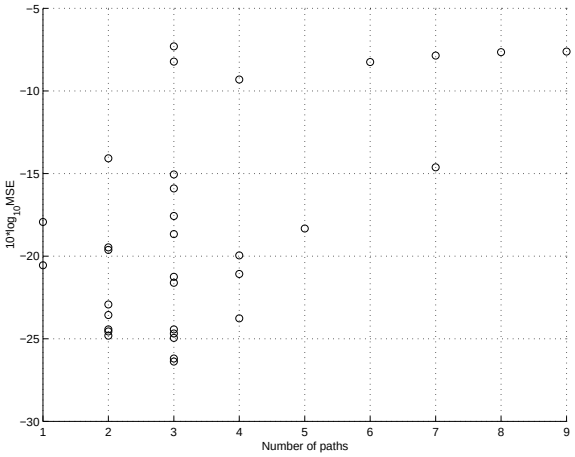

Figure 4.36: MSE vs. number of paths.

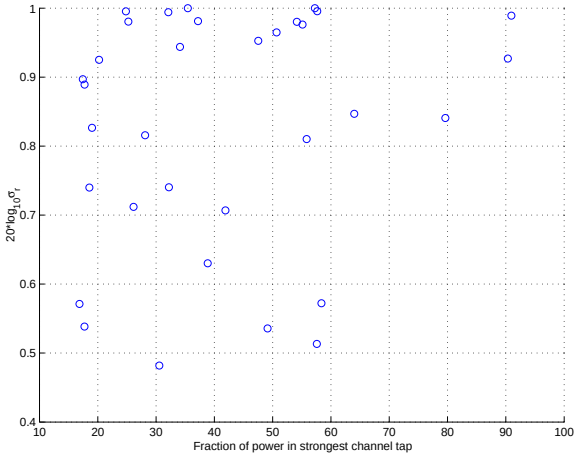

Figure 4.37: Power fraction in strongest channel tap vs. received power.

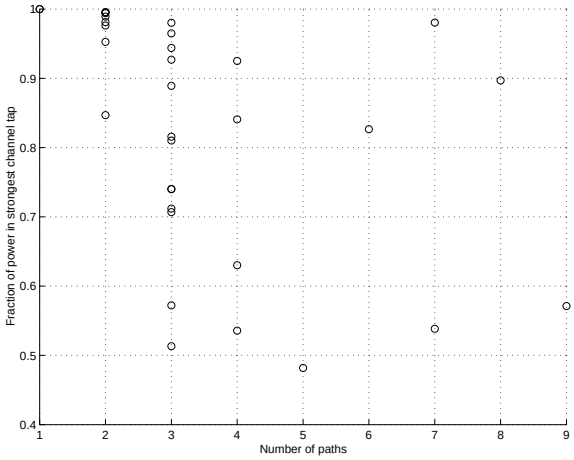

Figure 4.38: Number of paths vs. power fraction in strongest channel tap.

Fig. 4.38 presents another scatter plot for the power fraction in the strongest tap vs. the number of paths: it is seen how most of the channels with the highest power fraction associated with the main tap correspond to channels with three or less paths.

CHAPTER 5

CONCLUSIONS AND FUTURE WORK

A prototype of a wideband channel sounder was built, tested and used to perform channel measurements on OSU's central campus. A channel estimation algorithm that improves the resolution capabilities of the sounder was also developed to extract channel parameters from the soundings. During the course of this thesis several issues arised that deserve further exploration; there are also several improvements that can be made in the estimation algorithm and the sounding system.

5.1 MAP estimates

The development of the channel estimation algorithm was based on the premise that the channels to be estimated are composed of a small number of multiple arrivals, though no detailed *a priori* knowledge about the channel parameter statistics was assumed. Supposing that we have prior statistics on channel parameters, the MAP estimate would be given by

$$\underline{\widehat{\Theta}}_{MAP} = \arg\max_{\underline{\Theta}} p\left(\underline{\Theta}/\underline{Y}\right) \tag{5.1}$$

By using Bayes rule $p\left(\underline{\Theta}/\underline{Y}\right)$ can be written as

$$p\left(\underline{\Theta}/\underline{Y}\right) = \frac{p\left(\underline{Y}/\underline{\Theta}\right) p(\underline{\Theta})}{p(\underline{Y})} \tag{5.2}$$

Since the denominator in (5.2) does not depend on the channel parameter vector $\underline{\Theta}$ the form of the MAP estimates becomes

$$\underline{\widehat{\Theta}}_{MAP} = \arg\max_{\underline{\Theta}} \{p\left(\underline{Y}/\underline{\Theta}\right) p(\underline{\Theta})\} \tag{5.3}$$

which can be conveniently written as

$$\underline{\widehat{\Theta}}_{MAP} = \arg\max_{\underline{\Theta}} \{\log p\left(\underline{Y}/\underline{\Theta}\right) + \log(p(\underline{\Theta})\} \tag{5.4}$$

For the time being we will ignore the delay component of the parameter vector $\underline{\Theta} = [\underline{\tau}\ \underline{\theta}\ \underline{a}]^T$, and therefore $\underline{\Theta} = [\underline{\theta}\ \underline{a}]^T = \underline{C}$. We are then interested in finding a particular $p(\underline{C})$ such that under the AWGN assumption the MAP estimate takes the form of (3.42), that is

$$\underline{\widehat{C}} = \arg\min_{\underline{C}} \left\{ \| \underline{Y} - \mathbf{D}\underline{C} \|_2^2 + \lambda \| \underline{C} \|_1 \right\}$$

By using the indicator set matrix $\mathbf{D}$ we assume that $\underline{C}$ is a sparse vector in which the positions of the taps obey a distribution which is yet to be determined. A suitable pdf for $\underline{C}$ would be given by assuming independent and identically distributed taps described by an exponential pdf:

$$p(\underline{C}) = \prod_{k=1}^{M} p_k(C_k) = \prod_{k=1}^{M} \lambda \exp(-\lambda C_k) \tag{5.5}$$

That is

$$p(\underline{C}) = \lambda^M \exp(-\lambda \sum_{k=1}^{M} C_k) \tag{5.6}$$

Recall now that $p\left(\underline{Y}/\underline{\Theta}\right)$ is given by

$$p(\underline{Y}/\underline{\Theta}) = \frac{1}{(2\pi\sigma^2)^M} \exp\left\{ -\frac{1}{2\sigma^2} \sum_{k=1}^{M} \left| Y_k - \sum_{p=0}^{P-1} c_p s_k(\tau_p) \right|^2 \right\}$$

The above expression can be conveniently rewritten as

$$p(\underline{Y}/\underline{\Theta}) = \frac{1}{(2\pi\sigma^2)^M} \exp\left\{-\frac{1}{2\sigma^2}\sum_{k=1}^{M} \parallel \underline{Y} - \mathbf{D}\underline{C} \parallel^2\right\} \tag{5.7}$$

Remarkably, when (5.7) and (5.6) are substituted into (5.4) an estimator with the form of (3.42) is obtained! However, a precise formulation of this estimator should take into account a pdf for the delay. Therefore a formal formulation of the MAP estimator could be

$$\underline{\widehat{\Theta}}_{MAP} = \arg\max_{\underline{\Theta}} \{\log p\left(\underline{Y}/[\underline{C}, \underline{\tau}]\right) + \log(p([\underline{C}, \underline{\tau}])\} \tag{5.8}$$

Further simplification could be possible since a common assumption about the tap phases is to model them by an uniform pdf. It is very interesting that by assuming an exponential pdf we obtain a MAP estimate with the same form as the modified least square algorithm used for our delay estimation. This is an issue that deserves further attention.

5.2 New Delay Estimation Methods

It was found that once delay estimates of the multipath components are available it is quite easy to obtain estimates of their complex amplitudes. The use of the modified deconvolution method to find delay estimates is convenient since it produces a sparse representation of the channel taps, however it is computationally expensive. It would be worthwhile to explore other less computationally demanding techniques. Delay estimation methods is an extense subject on its own right that offers plenty of research opportunities.

Another related issue in the estimation process is the length of the signals that were fed to the estimation algorithm. Due to the computation time this length was

limited to 600 samples. It would be highly desirable to increase the length of this signal segment as much as possible since the estimation error will be reduced by 3 dB each time the segment length is doubled. It would also be interesting to have an idea of the growth in computation time as a function of the data segment length.

5.3 Improvement on Estimation of $\widehat{P}$

As explained in Chapter 3, an estimate of the true number of paths $\widehat{P}$ is obtained by finding ledges in the outcome of the minimum descriptor length algorithm. For reasonable signal to noise ratios it is fairly easy to identify those ledges; however as the signal to noise ratio decreases it becomes increasingly difficult to automate its location. In the actual implementation of the algorithm the 1st and 2nd derivatives of the MDL data are used to find $\widehat{P}$; this approach works well as long as the signal to noise ratio is reasonable. The algorithm's performance would be enhanced if a reliable method for finding those ledges regardless of the value of Es/N_0 could be implemented. Since this is basically a pattern identification problem approaches such as the use of neural networks could be considered.

5.4 Increase in Bandwidth and Transmitted Power

Both the bandwidth and the transmitted power were limited due to hardware issues. In the case of the bandwidth this limitation was owed to the available A/D converters. The maximum transmitted power could be as high as 20 dBm, a value that was not achieved because of the available signal levels before the final amplification stage. The use of other A/D converter able to perform cleanly at 64 MSPS and the use of another final amplification stage in the transmitter would improve both

the resolution and the coverage of the sounder. For instance, according to the PCS extension propagation model, by increasing the transmitted power to 30 dBm the sounder coverage would be increased to 1.92 Km, enough to cover most of OSU's campus. On the other hand, increasing the conversion rate to 64 MSPS while keeping the same oversampling factor of $K = 4$ would increase the time delay resolution of the algorithm to 125 ns with a corresponding minimum spatial resolution of 37.5 m.

5.5 Use of Omnidirectional Antennas

As mentioned in Chapter 4 directional antennas were used both at the transmitter and the receiver; according to some reports such antennas could impose structure on the received multipath signal. The use of omnidirectional antennas would remove such structure.

5.6 An Extensive Sounding Campaign

We mentioned that the size of the channel measurements database collected during this Thesis is insufficient to extract statistically significant conclusions. Therefore an extensicve measurement effort is needed in order to achieve reliable channel characterization.

APPENDIX A

DERIVATION OF ML ESTIMATES OF THE CHANNEL PARAMETERS

We will derive expressions that must be satisfied in order to find ML estimates of $\underline{\Theta} = [\underline{\theta}\ \underline{a}\ \underline{\tau}]^T$.

A.1 ML Phase Estimates

We want to find expressions for

$$\sum_{k=1}^{M} \left\{ \frac{\partial}{\partial \theta_p} \left\{ 2\Re \left[Y_k \sum_{q=0}^{P-1} a_q e^{-j\theta_q} s_k(\tau_q) \right] - \left| \sum_{q=0}^{P-1} a_q e^{j\theta_q} s_k(\tau_q) \right|^2 \right\} \right\} = 0 \tag{A.1}$$

subject to

$$\sum_{k=1}^{M} \left\{ \frac{\partial^2}{\partial \theta_p^2} \left\{ 2\Re \left[Y_k \sum_{q=0}^{P-1} a_q e^{-j\theta_q} s_k(\tau_q) \right] - \left| \sum_{q=0}^{P-1} a_q e^{j\theta_q} s_k(\tau_q) \right|^2 \right\} \right\} < 0 \tag{A.2}$$

We first notice that

$$\begin{aligned}
\frac{\partial}{\partial \theta_p} \left| \sum_{q=0}^{P-1} a_q e^{j\theta_q} s_k(\tau_q) \right|^2 &= \frac{\partial}{\partial \theta_p} \left\{ \left[\sum_{q=0}^{P-1} a_q e^{j\theta_q} s_k(\tau_q) \right] \left[\sum_{r=0}^{P-1} a_r e^{-j\theta_r} s_k(\tau_r) \right] \right\} \\
&= j a_p e^{j\theta_p} s_k(\tau_p) \sum_{r=0}^{P-1} a_r e^{-j\theta_r} s_k(\tau_r) - \\
&\qquad j a_p e^{-j\theta_p} s_k(\tau_p) \sum_{q=0}^{P-1} a_q e^{j\theta_q} s_k(\tau_q) \\
&= j a_p s_k(\tau_p) \left[e^{j\theta_p} \sum_{r=0}^{P-1} a_r e^{-j\theta_r} s_k(\tau_r) - e^{-j\theta_p} \sum_{r=0}^{P-1} a_r e^{j\theta_r} s_k(\tau_r) \right]
\end{aligned}$$

$$= \quad 2a_p s_k(\tau_p)\Im\left[e^{-j\theta_p}\sum_{r=0}^{P-1} a_r e^{j\theta_r} s_k(\tau_r)\right]$$

For the second derivative of $\left|\sum_{q=0}^{P-1} a_q e^{j\theta_q} s_k(\tau_q)\right|^2$ we have

$$\begin{aligned}
\frac{\partial^2}{\partial\theta_p^2}\left|\sum_{q=0}^{P-1} a_q e^{j\theta_q} s_k(\tau_q)\right|^2 &= \frac{\partial}{\partial\theta_p}\left[2a_p s_k(\tau_p)\Im\left[e^{-j\theta_p}\sum_{r=0}^{P-1} a_r e^{j\theta_r} s_k(\tau_r)\right]\right] \\
&= 2a_p s_k(\tau_p)\Im\left[-je^{-j\theta_p}\sum_{r=0}^{P-1} a_r e^{j\theta_r} s_k(\tau_r) + je^{-j\theta_p} a_p e^{j\theta_p} s_k(\tau_p)\right] \\
&= 2a_p s_k(\tau_p)\left\{\Im\left[-je^{-j\theta_p}\sum_{r=0}^{P-1} a_r e^{j\theta_r} s_k(\tau_r)\right] + a_p s_k(\tau_p)\right\} \\
&= -2a_p s_k(\tau_p)\Re\left[e^{-j\theta_p}\sum_{r=0}^{P-1} a_r e^{j\theta_r} s_k(\tau_r)\right] + 2a_p^2 s_k^2(\tau_p)
\end{aligned}$$

In a similar fashion we obtain

$$\frac{\partial}{\partial\theta_p}\left[2\Re\left[Y_k\sum_{q=0}^{P-1} a_q e^{-j\theta_q} s_k(\tau_q)\right]\right] = 2\Re\left[-jY_k a_p e^{-j\theta_p} s_k(\tau_p)\right] = 2a_p s_k(\tau_p)\Im\left[Y_k e^{-j\theta_p}\right]$$

and

$$\begin{aligned}
\frac{\partial^2}{\partial\theta_p^2}\left[2\Re\left[Y_k\sum_{q=0}^{P-1} a_q e^{-j\theta_q} s_k(\tau_q)\right]\right] &= \frac{\partial}{\partial\theta_p}\left[2a_p s_k(\tau_p)\Im\left[Y_k e^{-j\theta_p}\right]\right] \\
&= -2a_p s_k(\tau_p)\Re\left[Y_k e^{-j\theta_p}\right]
\end{aligned}$$

Substitution of these derivatives into (A.1) and (A.2) yields

$$\sum_{k=1}^{M}\left\{2a_p s_k(\tau_p)\Im\left[Y_k e^{-j\theta_p}\right] - 2a_p s_k(\tau_p)\Im\left[e^{-j\theta_p}\sum_{r=0}^{P-1} a_r e^{j\theta_r} s_k(\tau_r)\right]\right\} = 0 \qquad \text{(A.3)}$$

$$\sum_{k=1}^{M}\left\{-2a_p s_k(\tau_p)\Re\left[Y_k e^{-j\theta_p}\right] + 2a_p s_k(\tau_p)\Re\left[e^{-j\theta_p}\sum_{r=0}^{P-1} a_r e^{j\theta_r} s_k(\tau_r)\right] - 2a_p^2 s_k^2(\tau_p)\right\} < 0 \qquad \text{(A.4)}$$

Switching the order in which the summations are performed and symplifying we obtain

$$\Im\left[e^{-j\theta_p}\sum_{k=1}^{M} Y_k s_k(\tau_p)\right] - \Im\left[e^{-j\theta_p}\sum_{r=0}^{P-1} a_r e^{j\theta_r}\sum_{k=1}^{M} s_k(\tau_p) s_k(\tau_r)\right] = 0 \qquad \text{(A.5)}$$

subject to

$$-\Re\left[e^{-j\theta_p}\sum_{k=1}^{M}Y_k s_k(\tau_p)\right]+\Re\left[e^{-j\theta_p}\sum_{r=0}^{P-1}a_r e^{j\theta_r}\sum_{k=1}^{M}s_k(\tau_p)s_k(\tau_r)\right]-a_p\sum_{k=1}^{M}s_k^2(\tau_p)<0 \quad \text{(A.6)}$$

A.2 ML Amplitude Estimates

We want to find

$$\sum_{k=1}^{M}\left\{\frac{\partial}{\partial a_p}\left\{2\Re\left[Y_k\sum_{q=0}^{P-1}a_q e^{-j\theta_q}s_k(\tau_q)\right]-\left|\sum_{q=0}^{P-1}a_q e^{j\theta_q}s_k(\tau_q)\right|^2\right\}\right\}=0 \quad \text{(A.7)}$$

subject to

$$\sum_{k=1}^{M}\left\{\frac{\partial^2}{\partial a_p^2}\left\{2\Re\left[Y_k\sum_{q=0}^{P-1}a_q e^{-j\theta_q}s_k(\tau_q)\right]-\left|\sum_{q=0}^{P-1}a_q e^{j\theta_q}s_k(\tau_q)\right|^2\right\}\right\}<0 \quad \text{(A.8)}$$

Following the operations performed before for the ML phase estimate we have:

$$\begin{aligned}
\frac{\partial}{\partial a_p}\left|\sum_{q=0}^{P-1}a_q e^{j\theta_q}s_k(\tau_q)\right|^2 &= \frac{\partial}{\partial a_p}\left\{\left[\sum_{q=0}^{P-1}a_q e^{j\theta_q}s_k(\tau_q)\right]\left[\sum_{r=0}^{P-1}a_r e^{-j\theta_r}s_k(\tau_r)\right]\right\}\\
&= e^{j\theta_p}s_k(\tau_p)\sum_{r=0}^{P-1}a_r e^{-j\theta_r}s_k(\tau_r)+\\
&\qquad e^{-j\theta_p}s_k(\tau_p)\sum_{q=0}^{P-1}a_q e^{j\theta_q}s_k(\tau_q)\\
&= s_k(\tau_p)\left[e^{j\theta_p}\sum_{r=0}^{P-1}a_r e^{-j\theta_r}s_k(\tau_r)+e^{-j\theta_p}\sum_{r=0}^{P-1}a_r e^{j\theta_r}s_k(\tau_r)\right]\\
&= 2s_k(\tau_p)\Re\left[e^{-j\theta_p}\sum_{r=0}^{P-1}a_r e^{j\theta_r}s_k(\tau_r)\right]
\end{aligned}$$

$$\begin{aligned}
\frac{\partial^2}{\partial a_p^2}\left|\sum_{q=0}^{P-1}a_q e^{j\theta_q}s_k(\tau_q)\right|^2 &= \frac{\partial}{\partial a_p}\left[2s_k(\tau_p)\Re\left[e^{-j\theta_p}\sum_{r=0}^{P-1}a_r e^{j\theta_r}s_k(\tau_r)\right]\right]\\
&= 2s_k(\tau_p)\Re\left[a_p s_k(\tau_p)\right]\\
&= 2a_p s_k^2(\tau_p)
\end{aligned}$$

$$\frac{\partial}{\partial a_p}\left[2\Re\left[Y_k\sum_{q=0}^{P-1}a_q e^{-j\theta_q}s_k(\tau_q)\right]\right]=2\Re\left[Y_k e^{-j\theta_p}s_k(\tau_p)\right]=2s_k(\tau_p)\Re\left[e^{-j\theta_p}Y_k\right]$$

$$\frac{\partial^2}{\partial a_p^2}\left[2\Re\left[Y_k\sum_{q=0}^{P-1}a_q e^{-j\theta_q}s_k(\tau_q)\right]\right]=\frac{\partial}{\partial a_p}\left[2s_k(\tau_p)\Re\left[e^{-j\theta_p}Y_k\right]\right]=0$$

Substitution of these derivatives into (A.7) and (A.8) yields

$$\sum_{k=1}^{M}\left\{2s_k(\tau_p)\Re\left[Y_k e^{-j\theta_p}\right]-2s_k(\tau_p)\Re\left[e^{-j\theta_p}\sum_{r=0}^{P-1}a_r e^{j\theta_r}s_k(\tau_r)\right]\right\}=0 \tag{A.9}$$

subject to

$$-2a_p\sum_{k=1}^{M}S_k^2(\tau_p)<0$$

which is always true. Rearranging and simplifying (A.9) we arrive at

$$\Re\left[e^{-j\theta_p}\sum_{k=1}^{M}Y_k s_k(\tau_p)\right]-\Re\left[e^{-j\theta_p}\sum_{r=0}^{P-1}a_r e^{j\theta_r}\sum_{k=1}^{M}s_k(\tau_p)s_k(\tau_r)\right]=0 \tag{A.10}$$

A.3 ML Delay Estimates

This time we must find expressions for

$$\sum_{k=1}^{M}\left\{\frac{\partial}{\partial\tau_p}\left\{2\Re\left[Y_k\sum_{q=0}^{P-1}a_q e^{-j\theta_q}s_k(\tau_q)\right]-\left|\sum_{q=0}^{P-1}a_q e^{j\theta_q}s_k(\tau_q)\right|^2\right\}\right\}=0 \tag{A.11}$$

subject to

$$\sum_{k=1}^{M}\left\{\frac{\partial^2}{\partial\tau_p^2}\left\{2\Re\left[Y_k\sum_{q=0}^{P-1}a_q e^{-j\theta_q}s_k(\tau_q)\right]-\left|\sum_{q=0}^{P-1}a_q e^{j\theta_q}s_k(\tau_q)\right|^2\right\}\right\}<0 \tag{A.12}$$

Proceeding as in the previous cases we have

$$\begin{aligned}
\frac{\partial}{\partial\tau_p}\left|\sum_{q=0}^{P-1}a_q e^{j\theta_q}s_k(\tau_q)\right|^2 &= \frac{\partial}{\partial\tau_p}\left\{\left[\sum_{q=0}^{P-1}a_q e^{j\theta_q}s_k(\tau_q)\right]\left[\sum_{r=0}^{P-1}a_r e^{-j\theta_r}s_k(\tau_r)\right]\right\}\\
&= a_p e^{j\theta_p}s_k'(\tau_p)\sum_{r=0}^{P-1}a_r e^{-j\theta_r}s_k(\tau_r)+\\
&\qquad a_p e^{-j\theta_p}s_k'(\tau_p)\sum_{q=0}^{P-1}a_q e^{j\theta_q}s_k(\tau_q)\\
&= a_p s_k'(\tau_p)\left[e^{j\theta_p}\sum_{r=0}^{P-1}a_r e^{-j\theta_r}s_k(\tau_r)+e^{-j\theta_p}\sum_{r=0}^{P-1}a_r e^{j\theta_r}s_k(\tau_r)\right]\\
&= 2a_p s_k'(\tau_p)\Re\left[e^{-j\theta_p}\sum_{r=0}^{P-1}a_r e^{j\theta_r}s_k(\tau_r)\right]
\end{aligned}$$

$$\frac{\partial^2}{\partial\tau_p^2}\left|\sum_{q=0}^{P-1}a_q e^{j\theta_q}s_k(\tau_q)\right|^2 = \frac{\partial}{\partial\tau_p}\left[2a_p s_k'(\tau_p)\Re\left[e^{-j\theta_p}\sum_{r=0}^{P-1}a_r e^{j\theta_r}s_k(\tau_r)\right]\right]$$
$$= 2a_p s_k''(\tau_p)\Re\left[e^{-j\theta_p}\sum_{r=0}^{P-1}a_r e^{j\theta_r}s_k(\tau_r)\right] + 2a_p^2 s_k'^2(\tau_p)$$

$$\frac{\partial}{\partial\tau_p}\left[2\Re\left[Y_k\sum_{q=0}^{P-1}a_q e^{-j\theta_q}s_k(\tau_q)\right]\right] = 2\Re\left[Y_k a_p e^{-j\theta_p}s_k'(\tau_p)\right] = 2a_p s_k'(\tau_p)\Re\left[e^{-j\theta_p}Y_k\right]$$

$$\frac{\partial^2}{\partial\tau_p^2}\left[2\Re\left[Y_k\sum_{q=0}^{P-1}a_q e^{-j\theta_q}s_k(\tau_q)\right]\right] = \frac{\partial}{\partial\tau_p}\left[2a_p s_k'(\tau_p)\Re\left[e^{-j\theta_p}Y_k\right]\right] = 2a_p s_k''(\tau_p)\Re\left[e^{-j\theta_p}Y_k\right]$$

where we have assumed that $s(t-\tau)$ is differentiable with respect to τ so $s_k'(\tau_k) = \frac{d}{dt}s(t-\tau_p)|_{t=kTs}$ and $s_k''(\tau_k) = \frac{d^2}{dt^2}s(t-\tau_p)|_{t=kTs}$. Substitution of these derivatives into (A.11) and (A.12) yields

$$\sum_{k=1}^{M}\left\{2a_p s_k'(\tau_p)\Re\left[e^{-j\theta_p}Y_k\right] - 2a_p s_k'(\tau_p)\Re\left[e^{-j\theta_p}\sum_{r=0}^{P-1}a_r e^{j\theta_r}s_k(\tau_r)\right]\right\} = 0 \qquad \text{(A.13)}$$

$$\sum_{k=1}^{M}\left\{2a_p s_k''(\tau_p)\Re\left[e^{-j\theta_p}Y_k\right] - 2a_p s_k''(\tau_p)\Re\left[e^{-j\theta_p}\sum_{r=0}^{P-1}a_r e^{j\theta_r}s_k(\tau_r)\right] - 2a_p^2 s_k'^2(\tau_p)\right\} < 0 \qquad \text{(A.14)}$$

Rearranging and simplifying the above expressions we arrive at

$$\Re\left[e^{-j\theta_p}\sum_{k=1}^{M}Y_k s_k'(\tau_p)\right] - \Re\left[e^{-j\theta_p}\sum_{r=0}^{P-1}a_r e^{j\theta_r}\sum_{k=1}^{M}s_k(\tau_r)s_k'(\tau_p)\right] = 0 \qquad \text{(A.15)}$$

subject to

$$\Re\left[e^{-j\theta_p}\sum_{k=1}^{M}Y_k s_k''(\tau_p)\right] - \Re\left[e^{j\theta_p}\sum_{r=0}^{P-1}a_r e^{-j\theta_r}\sum_{k=1}^{M}s_k''(\tau_p)s_k(\tau_r)\right] - a_p\sum_{k=1}^{M}s_k'^2(\tau_p) < 0 \qquad \text{(A.16)}$$

APPENDIX B

DERIVATION OF CRAMÉR-RAO LOWER BOUNDS

We will derive the Cramér-Rao Lower Bound (CRLB) for joint estimates of the parameter vector $\underline{\Theta} = [\underline{\theta}\ \underline{a}\ \underline{\tau}]^T$. The CRLB is a benchmark against which the performance of any unbiased estimator of $\underline{\Theta}$ can be compared.

From (3.6) the likelihood equation is

$$L(\underline{\Theta}, \underline{Y}) = -\frac{1}{2\sigma^2} \sum_{k=1}^{M} \left\{ 2\Re \left[Y_k \sum_{p=0}^{P-1} a_p e^{-j\theta_p} s_k(\tau_p) \right] - \left| \sum_{p=0}^{P-1} a_p e^{j\theta_p} s_k(\tau_p) \right|^2 \right\} \tag{B.1}$$

The observation sequence Y_k is of the form

$$Y_k = \sum_{r=0}^{P-1} a_r e^{j\theta_r} s_k(\tau_r) + N_k$$

where N_k is zero-mean complex white Gaussian noise with variance $2\sigma^2$.

The elements of the Fisher Information Matrix are given by

$$J_{pq} = \mathbf{E} \left\{ \frac{\partial}{\partial \Theta_p} L(\underline{\Theta}, \underline{Y}) \frac{\partial}{\partial \Theta_q} L(\underline{\Theta}, \underline{Y}) \right\} = -\mathbf{E} \left\{ \frac{\partial^2}{\partial \Theta_p \partial \Theta_q} L(\underline{\Theta}, \underline{Y}) \right\}$$

The elements of the Fisher Information Matrix that must be computed in this case are $J_{\theta_p\theta_q}$, $J_{a_pa_q}$, $J_{\tau_p\tau_q}$, $J_{\theta_pa_q}$, $J_{a_p\theta_q}$, $J_{\theta_p\tau_q}$, $J_{\tau_p\theta_q}$, $J_{a_p\tau_q}$, and $J_{\tau_pa_q}$. We will assume that $s(t-\tau)$ is differentiable with respect to τ so $s'_k(\tau_k) = \frac{d}{dt} s(t-\tau_p)|_{t=kTs}$ and $s''_k(\tau_k) = \frac{d^2}{dt^2} s(t-\tau_p)|_{t=kTs}$.

- $J_{\theta_p\theta_q}$: A first derivative of the likelihood equation with respect to θ_q was already computed in (A.3):

$$\frac{\partial}{\partial\theta_q}L(\underline{\Theta},\underline{Y}) = \frac{1}{2\sigma^2}\sum_{k=1}^{M}\left\{2a_q s_k(\tau_q)\Im\left[Y_k e^{-j\theta_q}\right] - 2a_q s_k(\tau_q)\Im\left[e^{-j\theta_q}\sum_{r=0}^{P-1}a_r e^{j\theta_r}s_k(\tau_r)\right]\right\}$$

Differentiating with respect to θ_p we obtain

$$\begin{aligned}\frac{\partial^2}{\partial\theta_p\partial\theta_q}L(\underline{\Theta},\underline{Y}) &= \frac{1}{2\sigma^2}\sum_{k=1}^{M}\left\{-2a_q s_k(\tau_q)\Im\left[e^{-j\theta_q}ja_p e^{j\theta_p}s_k(\tau_p)\right]\right\} \\ &= -\frac{1}{\sigma^2}a_p a_q\Re\left[e^{j(\theta_p-\theta_q)}\right]\sum_{k=1}^{M}s_k(\tau_p)s_k(\tau_q) \qquad \text{(B.2)}\end{aligned}$$

This expression does not depend on Y_k, therefore

$$J_{\theta_p\theta_q} = -\mathbf{E}\left\{\frac{\partial^2}{\partial\theta_p\partial\theta_q}L(\underline{\Theta},\underline{Y})\right\} = \frac{1}{\sigma^2}a_p a_q\Re\left[e^{j(\theta_p-\theta_q)}\right]\sum_{k=1}^{M}s_k(\tau_p)s_k(\tau_q) \qquad \text{(B.3)}$$

For $\theta_p = \theta_q$ we obtain

$$J_{\theta_p\theta_p} = \frac{1}{\sigma^2}a_p^2\sum_{k=1}^{M}s_k^2(\tau_p) \qquad \text{(B.4)}$$

- $J_{a_pa_q}$: Again we take advantage of the fact that a first derivative of the likelihood equation with respect to a_q has already been computed in (A.9):

$$\frac{\partial}{\partial a_q}L(\underline{\Theta},\underline{Y}) = \frac{1}{2\sigma^2}\sum_{k=1}^{M}\left\{2s_k(\tau_q)\Re\left[Y_k e^{-j\theta_q}\right] - 2s_k(\tau_q)\Re\left[e^{-j\theta_q}\sum_{r=0}^{P-1}a_r e^{j\theta_r}s_k(\tau_r)\right]\right\}$$

Differentiating with respect to a_p:

$$\begin{aligned}\frac{\partial^2}{\partial a_p\partial a_q}L(\underline{\Theta},\underline{Y}) &= \frac{1}{2\sigma^2}\sum_{k=1}^{M}\left\{-2s_k(\tau_q)\Re\left[e^{-j\theta_q}e^{j\theta_p}s_k(\tau_p)\right]\right\} \\ &= -\frac{1}{\sigma^2}\Re\left[e^{j(\theta_p-\theta_q)}\right]\sum_{k=1}^{M}s_k(\tau_p)s_k(\tau_q) \qquad \text{(B.5)}\end{aligned}$$

Once again we have an expression that does not depend on Y_k, thus

$$J_{a_pa_q} = -\mathbf{E}\left\{\frac{\partial^2}{\partial a_p\partial a_q}L(\underline{\Theta},\underline{Y})\right\} = \frac{1}{\sigma^2}\Re\left[e^{j(\theta_p-\theta_q)}\right]\sum_{k=1}^{M}s_k(\tau_p)s_k(\tau_q) \qquad \text{(B.6)}$$

For $a_p = a_q$ (B.6) reduces to

$$J_{a_p a_p} = \frac{1}{\sigma^2} \sum_{k=1}^{M} s_k^2(\tau_p) \tag{B.7}$$

- $J_{\tau_p \tau_q}$: We already have computed a derivative of the likelihood equation with respect to τ_q in (A.13):

$$\frac{\partial}{\partial \tau_q} L(\underline{\Theta}, \underline{Y}) = \frac{1}{2\sigma^2} \sum_{k=1}^{M} \left\{ 2a_q s_k'(\tau_q) \Re\left[e^{-j\theta_q} Y_k\right] - 2a_q s_k'(\tau_q) \Re\left[e^{-j\theta_q} \sum_{r=0}^{P-1} a_r e^{j\theta_r} s_k(\tau_r)\right] \right\}$$

Differentiating with respecto to τ_p:

$$\begin{aligned} \frac{\partial^2}{\partial \tau_p \partial \tau_q} L(\underline{\Theta}, \underline{Y}) &= \frac{1}{2\sigma^2} \sum_{k=1}^{M} \left\{ -2a_q s_k'(\tau_q) \Re\left[e^{-j\theta_q} a_p e^{j\theta_p} s_k'(\tau_p)\right] \right\} \\ &= -\frac{1}{\sigma^2} a_p a_q \Re\left[e^{j(\theta_p - \theta_q)}\right] \sum_{k=1}^{M} s_k'(\tau_p) s_k'(\tau_q) \end{aligned} \tag{B.8}$$

Therefore

$$J_{\tau_p \tau_q} = -\mathbf{E}\left\{ \frac{\partial^2}{\partial \tau_p \partial \tau_q} L(\underline{\Theta}, \underline{Y}) \right\} = \frac{1}{\sigma^2} a_p a_q \Re\left[e^{j(\theta_p - \theta_q)}\right] \sum_{k=1}^{M} s_k'(\tau_p) s_k'(\tau_q) \tag{B.9}$$

For $\tau_p = \tau_q$ (B.9) reduces to

$$J_{\tau_p \tau_p} = \frac{1}{\sigma^2} a_p^2 \sum_{k=1}^{M} s_k'^2(\tau_p) \tag{B.10}$$

- $J_{\theta_p a_q}$: We have

$$\frac{\partial}{\partial a_q} L(\underline{\Theta}, \underline{Y}) = \frac{1}{2\sigma^2} \sum_{k=1}^{M} \left\{ 2s_k(\tau_q) \Re\left[Y_k e^{-j\theta_q}\right] - 2s_k(\tau_q) \Re\left[e^{-j\theta_q} \sum_{r=0}^{P-1} a_r e^{j\theta_r} s_k(\tau_r)\right] \right\}$$

Differentiating with respect to θ_p:

$$\begin{aligned} \frac{\partial^2}{\partial \theta_p \partial a_q} L(\underline{\Theta}, \underline{Y}) &= \frac{1}{2\sigma^2} \sum_{k=1}^{M} \left\{ -2s_k(\tau_q) \Re\left[e^{-j\theta_q} j a_p e^{j\theta_p} s_k(\tau_p)\right] \right\} \\ &= \frac{1}{\sigma^2} \Im\left[e^{j(\theta_p - \theta_q)}\right] \sum_{k=1}^{M} s_k(\tau_p) s_k(\tau_q) \end{aligned} \tag{B.11}$$

Therefore

$$J_{\theta_p a_q} == -\mathbf{E}\left\{\frac{\partial^2}{\partial\theta_p \partial a_q} L(\underline{\Theta}, \underline{Y})\right\} = -\frac{1}{\sigma^2}\Im\left[e^{j(\theta_p-\theta_q)}\right]\sum_{k=1}^{M} s_k(\tau_p)s_k(\tau_q) \quad \text{(B.12)}$$

- $J_{a_p\theta_q}$: We have

$$\frac{\partial}{\partial\theta_q} L(\underline{\Theta}, \underline{Y}) = \frac{1}{2\sigma^2}\sum_{k=1}^{M}\left\{2a_q s_k(\tau_q)\Im\left[Y_k e^{-j\theta_q}\right] - 2a_q s_k(\tau_q)\Im\left[e^{-j\theta_q}\sum_{r=0}^{P-1} a_r e^{j\theta_r} s_k(\tau_r)\right]\right\}$$

Differentiating with respect to a_p

$$\begin{aligned}\frac{\partial^2}{\partial a_p \partial\theta_q} L(\underline{\Theta}, \underline{Y}) &= \frac{1}{2\sigma^2}\sum_{k=1}^{M}\left\{-2a_q s_k(\tau_q)\Im\left[e^{-j\theta_q}e^{j\theta_p}s_k(\tau_p)\right]\right\} \\ &= -\frac{1}{\sigma^2}a_q\Im\left[e^{j(\theta_p-\theta_q)}\right]\sum_{k=1}^{M} s_k(\tau_p)s_k(\tau_q) \quad \text{(B.13)}\end{aligned}$$

Therefore

$$J_{a_p\theta_q} = -\mathbf{E}\left\{\frac{\partial^2}{\partial a_p \partial\theta_q} L(\underline{\Theta}, \underline{Y})\right\} = \frac{1}{\sigma^2}a_q\Im\left[e^{j(\theta_p-\theta_q)}\right]\sum_{k=1}^{M} s_k(\tau_p)s_k(\tau_q) \quad \text{(B.14)}$$

- $J_{\theta_p\tau_q}$: We have

$$\frac{\partial}{\partial\tau_q} L(\underline{\Theta}, \underline{Y}) = \frac{1}{2\sigma^2}\sum_{k=1}^{M}\left\{2a_q s_k'(\tau_q)\Re\left[e^{-j\theta_q}Y_k\right] - 2a_q s_k'(\tau_q)\Re\left[e^{-j\theta_q}\sum_{r=0}^{P-1} a_r e^{j\theta_r} s_k(\tau_r)\right]\right\}$$

Differentiating with respect to θ_p:

$$\begin{aligned}\frac{\partial^2}{\partial\theta_p \partial\tau_q} L(\underline{\Theta}, \underline{Y}) &= \frac{1}{2\sigma^2}\sum_{k=1}^{M}\left\{-2a_q s_k'(\tau_q)\Re\left[e^{-j\theta_q}ja_p e^{j\theta_p}s_k(\tau_p)\right]\right\} \\ &= \frac{1}{\sigma^2}a_p a_q\Im\left[e^{j(\theta_p-\theta_q)}\right]\sum_{k=1}^{M} s_k(\tau_p)s_k'(\tau_q) \quad \text{(B.15)}\end{aligned}$$

Therefore

$$J_{\theta_p\tau_q} = -\mathbf{E}\left\{\frac{\partial^2}{\partial\theta_p \partial\tau_q} L(\underline{\Theta}, \underline{Y})\right\} = -\frac{1}{\sigma^2}a_p a_q\Im\left[e^{j(\theta_p-\theta_q)}\right]\sum_{k=1}^{M} s_k(\tau_p)s_k'(\tau_q) \quad \text{(B.16)}$$

- $J_{\tau_p\theta_q}$: We have

$$\frac{\partial}{\partial\theta_q}L(\underline{\Theta},\underline{Y}) = \frac{1}{2\sigma^2}\sum_{k=1}^{M}\left\{2a_q s_k(\tau_q)\Im\left[Y_k e^{-j\theta_q}\right] - 2a_q s_k(\tau_q)\Im\left[e^{-j\theta_q}\sum_{r=0}^{P-1}a_r e^{j\theta_r}s_k(\tau_r)\right]\right\}$$

Differentiating with respect to τ_p:

$$\begin{aligned}\frac{\partial^2}{\partial\tau_p\partial\theta_q}L(\underline{\Theta},\underline{Y}) &= \frac{1}{2\sigma^2}\sum_{k=1}^{M}\left\{-2a_q s_k(\tau_q)\Im\left[e^{-j\theta_q}a_p e^{j\theta_p}s_k'(\tau_p)\right]\right\} \\ &= -\frac{1}{\sigma^2}a_p a_q\Im\left[e^{j(\theta_p-\theta_q)}\right]\sum_{k=1}^{M}s_k'(\tau_p)s_k(\tau_q) \qquad \text{(B.17)}\end{aligned}$$

Therefore

$$J_{\tau_p\theta_q} = -\mathbf{E}\left\{\frac{\partial^2}{\partial\tau_p\partial\theta_q}L(\underline{\Theta},\underline{Y})\right\} = \frac{1}{\sigma^2}a_p a_q\Im\left[e^{j(\theta_p-\theta_q)}\right]\sum_{k=1}^{M}s_k'(\tau_p)s_k(\tau_q) \qquad \text{(B.18)}$$

- $J_{a_p\tau_q}$: We have

$$\frac{\partial}{\partial\tau_q}L(\underline{\Theta},\underline{Y}) = \frac{1}{2\sigma^2}\sum_{k=1}^{M}\left\{2a_q s_k'(\tau_q)\Re\left[e^{-j\theta_q}Y_k\right] - 2a_q s_k'(\tau_q)\Re\left[e^{-j\theta_q}\sum_{r=0}^{P-1}a_r e^{j\theta_r}s_k(\tau_r)\right]\right\}$$

differentiating with respect to a_p:

$$\begin{aligned}\frac{\partial^2}{\partial a_p\partial\tau_q}L(\underline{\Theta},\underline{Y}) &= \frac{1}{2\sigma^2}\sum_{k=1}^{M}\left\{-2a_q s_k'(\tau_q)\Re\left[e^{-j\theta_q}e^{j\theta_p}s_k(\tau_p)\right]\right\} \\ &= -\frac{1}{\sigma^2}a_q\Re\left[e^{j(\theta_p-\theta_q)}\right]\sum_{k=1}^{M}s_k(\tau_p)s_k'(\tau_q) \qquad \text{(B.19)}\end{aligned}$$

Therefore

$$J_{a_p\tau_q} = -\mathbf{E}\left\{\frac{\partial^2}{\partial a_p\partial\tau_q}L(\underline{\Theta},\underline{Y})\right\} = \frac{1}{\sigma^2}a_q\Re\left[e^{j(\theta_p-\theta_q)}\right]\sum_{k=1}^{M}s_k(\tau_p)s_k'(\tau_q) \qquad \text{(B.20)}$$

- $J_{\tau_p a_q}$: Using derivatives already invoked before we have

$$\frac{\partial}{\partial a_q}L(\underline{\Theta},\underline{Y}) = \frac{1}{2\sigma^2}\sum_{k=1}^{M}\left\{2s_k(\tau_q)\Re\left[Y_k e^{-j\theta_q}\right] - 2s_k(\tau_q)\Re\left[e^{-j\theta_q}\sum_{r=0}^{P-1}a_r e^{j\theta_r}s_k(\tau_r)\right]\right\}$$

Differentiating with respect to τ_p

$$\begin{aligned}\frac{\partial^2}{\partial\tau_p\partial a_q}L(\underline{\Theta},\underline{Y}) &= \frac{1}{2\sigma^2}\sum_{k=1}^{M}\left\{-2s_k(\tau_q)\Re\left[e^{-j\theta_q}a_p e^{j\theta_p}s_k'(\tau_p)\right]\right\} \\ &= -\frac{1}{\sigma^2}a_p\Re\left[e^{j(\theta_p-\theta_q)}\right]\sum_{k=1}^{M}s_k'(\tau_p)s_k(\tau_q) \qquad \text{(B.21)}\end{aligned}$$

Therefore

$$J_{\tau_p a_q} = -\mathbf{E}\left\{\frac{\partial^2}{\partial\tau_p\partial a_q}L(\underline{\Theta},\underline{Y})\right\} = \frac{1}{\sigma^2}a_p\Re\left[e^{j(\theta_p-\theta_q)}\right]\sum_{k=1}^{M}s_k'(\tau_p)s_k(\tau_q) \qquad \text{(B.22)}$$

BIBLIOGRAPHY

[1] Macario R.C. *Modern Personal Radio Systems.* , IEE Press, London 1996.

[2] Rappaport T. *Wireless Communications Systems.* , Addison-Wesley, Reading, 1990.

[3] Parsons J., Demery D., Turkmani A. Sounding Techniques for Wideband Mobile Radio Channels: a review. *IEE Proceedings*, 138(5):437–446, October 1991.

[4] Braun W., Dersch U. A Physical Mobile Radio Channel Model. *IEEE Transactions on Mobile Technology*, Vol. 40, No. 2, May 1991.

[5] Cooper R., McGillem C. *Probabilistic Methods of Signal and Systems Analysis.* Holt, Rhinehart and Winston, 1971.

[6] Felhauer T., Baier P., König W., Mohr W. Optimum Spread Spectrum Signals for Wideband Channel Sounding. *Electronic Letters*, Vol. 29, No. 6, March 1993.

[7] Molina A., Fannin P., Timoney J. Generation of Optimum Excitation Waveforms for Mobile Radio Channel Sounding. *IEEE Transactions on Vehicular Technology*, Vol. 44, No. 2, May 1995.

[8] Kay, Steven M. *Fundamentals os Statistical Signal Processing. Volume 1: Estimation Theory.* Prentice-Hall Signal Processing Series, New Jersey, 1993.

[9] Kay, Steven M. *Fundamentals os Statistical Signal Processing. Volume 2: Detection Theory.* Prentice-Hall Signal Processing Series, New Jersey, 1993.

[10] Scharf, L. *Statistical Signal Processing.* Addison-Wesley, Reading, 1991.

[11] Arslan H., Bottomley G. Channel Estimation in Narrowband Wireless Communications Sytems. *Wireless Communications and Mobile Computing*, 1:201-219, 2001.

[12] Van Trees, H.L. *Detection, Estimation and Modulation Theory.* John Wiley & Sons, New York, 1968.

[13] Feder M., Weinstein, E. Parameter estimation of superimposed signal using the EM algorithm. *IEEE Trans. on Acoustics, Speech and Signal Processing*, Vol. 36 No. 4, April 1988.

[14] Fuchs J. Multipath Time-delay Detection and Estimation. *IEEE Trans on Signal Processing*, 47(1):237-243, January 1999.

[15] Luenberger D. *Introduction to Linear and Nonlinear Programming.* Addison-Wesley, Reading, 1973.

[16] Rissanen J. Modeling By Shortest Data Description. *Automatica*, Vol. 14, pp. 465-471, 1978.

[17] Saarnisaari, H. Estimation of Numbers of Multipaths in DS-CDMA by the MDL Principle. *Proceedings of the IEEE 5th International Symposium on Spread Spectrum Techniques and Applications*, Vol. 1, pp. 258-261, 1998.

[18] Saarnisaari, H. ML Time Delay Estimation in a Multipath Channel. *Proceedings of the IEEE 4th International Symposium on Spread Spectrum Techniques and Applications*, Vol. 3, pp. 1007-1011, 1996.

[19] Dixon R. *Spread Spectrum Systems.* John Wiley & Sons, New York, 1984.

[20] Browne, D. *EV-4014 Quad Receiver Board Documentation Set & Support Files.* I.P.S. Wireless Lab, Department of Electrical Engineering, The Ohio State University, 2000.

[21] Zhang, J. *Link Budget Report for Wideband Testbed.* I.P.S. Wireless Lab, Department of Electrical Engineering, The Ohio State University, 2000.